2017

Analytical-based methodologies to examine In vitro nanokinetics of silver nanoparticles

Sesha Lakshmi Arathi Paluri
Wright State University

ANALYTICAL-BASED METHODOLOGIES TO EXAMINE *IN VITRO* NANOKINETICS OF SILVER NANOPARTICLES

A dissertation submitted in partial fulfillment of the
requirements for the degree of
Doctor of Philosophy

By

SESHA LAKSHMI ARATHI PALURI
M.S., Wright State University, 2011
B.PHARM, Andhra University, 2009

2017
Wright State University

WRIGHT STATE UNIVERSITY

GRADUATE SCHOOL

April 22, 2017

I HEREBY RECOMMEND THAT THE DISSERTATION PREPARED UNDER MY SUPERVISION BY Sesha Lakshmi Arathi Paluri, ENTITLED Analytical-based methodologies to examine *in vitro* nanokinetics of silver nanoparticles BE ACCEPTED IN PARTIAL FULFILLMENT OF THE REQUIREMENTS FOR THE DEGREE OF Doctor of Philosophy.

_____

Ioana E. Sizemore, Ph.D.
Dissertation Director

_____

Mill W. Miller, Ph.D.
Director, Biomedical Sciences
Ph.D. Program

_____

Robert E. W. Fyffe, Ph.D.
Vice President for Research and
Dean of the Graduate School

Committee on
Final Examination

_____

Ioana E. Sizemore, Ph.D.

_____

Mill W. Miller, Ph.D.

_____

Norma Adragna, Ph.D.

_____

David A. Dolson, Ph.D.

_____

Steven R. Higgins, Ph.D.

ABSTRACT

Paluri, Sesha Lakshmi Arathi, Ph.D., Biomedical Sciences Ph.D. Program, Wright State University, 2017. Analytical-based methodologies to examine *in vitro* nanokinetics of silver nanoparticles.

Advancements in the nanotechnology have taken a huge leap in 21st century resulting in 1814 consumer products containing nanomaterials. About 47% of these products belong to the health and fitness sector and ~24% utilize silver nanoparticles (AgNPs). Despite the promising biomedical applications of AgNPs (*e.g.* bone cements, contrasting agents, and drug-carriers), lack of standardized methods for examining their nanokinetics (*i.e.*, **A**bsorption, **D**istribution, **M**etabolism, and **E**limination (ADMEs)) limit their clinical implementation. The current work addresses this knowledge gap by developing analytical-based approaches for studying *in vitro* ADMEs of AgNPs. To demonstrate the versatility of these methodologies, two *in vitro* kidney study models (Vero 76 and HEK 293 cells) were tested under pre-determined exposure concentrations (3-300 μg mL^{-1}) and times (4-48 hr). The ADMEs of both AgNPs^{+} and AgNPs^{-} in Vero 76 cells were summarized here for illustrative purposes: [**A]**: Inductively coupled plasma optical emission spectroscopy (ICP-OES) facilitated the evaluation of critical kinetic parameters including order of reaction, rate constant and bioavailability (first-order, k_{abs}= 0.05 hr^{-1}, $C_{maximum}$ < 20.7±4% and $T_{maximum}$ > 48 hr), [**D**] CytoViva and Raman imaging outlined the uptake and cellular localization patterns (*e.g.*, Raman results of mapped cells exposed to AgNPs^{+} and AgNPs^{-} were dominated by the signals corresponding to the plasma

membrane and cytoplasm, respectively), [**M**] Cloud point extraction (CPE) followed by tangential flow filtration enhanced the separation of two Ag species from the cellular matrix (≤ 11±4% of the AgNPs were converted to Ag^{+}), and [**E**] ICP-OES also facilitated the construction of clearance-time curves to evaluate the elimination kinetics of sub-lethal AgNPs (first-order, k_{eli}=0.039 hr^{-1}). Furthermore, a new laboratory module was developed according to the five essential features laid by the National Research Council for inquiry-based teaching and learning in order to introduce undergraduate and graduate students to the fabrication and characterization of green and non-green silver and gold nanoparticles. As demonstrated by the results of the formative assessments, this hands-on laboratory was not only well-received by students from diverse backgrounds, but also stimulated their critical thinking and helped them acquire new laboratory skills.

TABLE OF CONTENTS

TABLE OF CONTENTS (Continued)

TABLE OF CONTENTS (Continued)

LIST OF FIGURES

LIST OF FIGURES (Continued)

LIST OF FIGURES (Continued)

LIST OF FIGURES (Continued)

LIST OF TABLES

LIST OF SCHEMATICS

-

ABBREVIATIONS

3-(4,5-dimethylthiazol-2-yl)-2,5-diphenyltetrazolium bromide (MTT)

10 kD retentate (10 kD ret)

Absorption (A)

Absorption rate constant (k_{abs})

Agglomerative hierarchical clustering analysis (AHCA)

Catheter-associated ventriculitis (CAV)

Cetyl trimethylammonium bromide (CTAB)

Central nervous system (CNS)

Cloud point extract (CPE)

Correlation matrix (CM)

CytoViva hyperspectral imaging (CHSI)

Distribution (D)

Dynamic light scattering (DLS)

Elimination I

Elimination rate constant (k_{eli})

Energy-dispersive X-ray spectroscopy (EDX)

Environmental Protection Agency (EPA)

Food and Drug Administration (FDA)

Glutathione (GSH)

Half-life ($t_{1/2}$)

Human embryonic kidney cells (HEK 293)

Inductively coupled plasma optical emission spectroscopy (ICP-OES

Ionic silver ($Ag^{+)}$

Raman spectroscopy hyperspectral imaging (RHSI)

Reactive oxygen species (ROS)

Medial lethal concentration (LC_{50})

Metabolism (M)

Minimum detection limit (MDL)

Minimum Information for Nanomaterial Characterization (MINChar)

National Institute for Occupational Safety and Health (NIOSH)

National Nanotechnology Initiative (NNI)

National Research Council (NRC)

Original colloid (Ori)

Nanoparticles (NPs)

Nicotinamide adenine dinucleotide phosphate (NAD(P)H)

Oxidative stress (OS)

Project on Emerging Nanotechnologies (PEN)

Relative percent difference (RPD)

Scanning electron microscopy (SEM)

Silver nanoparticles (AgNPs)

Surface-enhanced Raman scattering (SERS)

Super oxide dismutase (SOD)

Tangential flow filtration (TFF)

Transmission electron microscopy (TEM)

Uv-Vis absorption spectroscopy (UV-VIS)

ACKNOWLEDGEMENTS

I would like to thank Dr. Ioana E. Sizemore, my advisor, who has given me tremendous support over the years. Besides being a mentor, she has been a good friend. I appreciate her personal attention, care and advice during rough times. It was great working with her. I will always cherish my professional and personal time spent with her.

I would also like to thank Dr. Miller for his suggestions and guidance during my time in the program. I really appreciate all the time he spent talking to me about my work. Those little talks and often long discussions helped me advance my way of thinking and let me tackle situations in a better way. I was so fortunate to have worked with him.

I would like to acknowledge my dissertation committee members, Dr. Adragna, Dr. Dolson, Dr. Higgins, Dr. Miller, Dr. Lauf and Dr. Mamrack. I really appreciate their invaluable time, advice, support and fruitful discussions.

I would like to thank Dr. Prabhakhara Marsanapalle, my undergraduate mentor. His lectures, special attention and intriguing questions were one of the main reasons that sparked my interest in research. I also thank Dr. Engisch for her guidance during my Masters program that led me to doctoral studies.

I was lucky to be surrounded by friendly people at work and outside. I would like to thank Seth Brittle, Daniel Foose, Kevin O'Neil, John Ryan, Nhi Lam, and Kevin Dorney. They have been great friends to work with and made my time in lab enjoyable. Special thanks to my wonderful friends: Pavani Beesetty, Marjorie Markopoulos,

Khadijeh Alnajjar, Michelle Newsome, Raghuram Katreddi, Neelima Sharma, Nagendra Ravilla, Sridevi Gutta, and Praveen Alla for their continuous care and encouragement.

Finally, I would like to specially thank all my family, who has shown extraordinary love and support over the years. I thank my mother Satya Vimala and my father Sivarao and my wonderful sibling Radhasai, who always cheered me and made my life great. I would also like to thank my grand parents Ramamurthy, Sesha Bharathi for their encouragement to pursue my studies. Special love and thanks to my grand father Seshagiri rao for pushing me to pursue doctoral studies and my friend-mentor Mr. Appalaraju for his invaluable advice and guidance throughout the years.

CHAPTER 1

INTRODUCTION

Nanotechnology

As of 2013, the global revenue from the nano-products exceeded $1 trillion, $318 billion of which came from the Unites States alone.[1] It is predicted that by 2020, the global nanotechnology market growth will reach as high as $75.8 billion.[2] In the past decade, advancements in nanotechnology have led to a 30-fold increase in the number of nanomaterial-based consumer products from 54 to 1814 products in 2005 and 2015, respectively.[3] Although nanotechnology gained momentum only in recent years, the very concept of 'nano' has been in-use since 4th century. One such classical example is the color-changing feature of the Roman vessel, Lycurgus cup.[4] The optical properties of silver and gold nanomaterials (50-100 nm diameters) coated on the glass cup contributed to the color change from green to red upon illumination (from outside and inside, respectively).[4] Likewise, M.C. Lea synthesized citrate-stabilized silver nanoparticles (AgNPs) in 1889, which was the first recorded synthesis of colloidal silver.[5] According to the 2015 nanotechnology consumer product inventory (Figure 1.1), majority of the registered products belong to the health and fitness sector (47%), while silver was found to be the most frequently used nanomaterial (24%).[3]

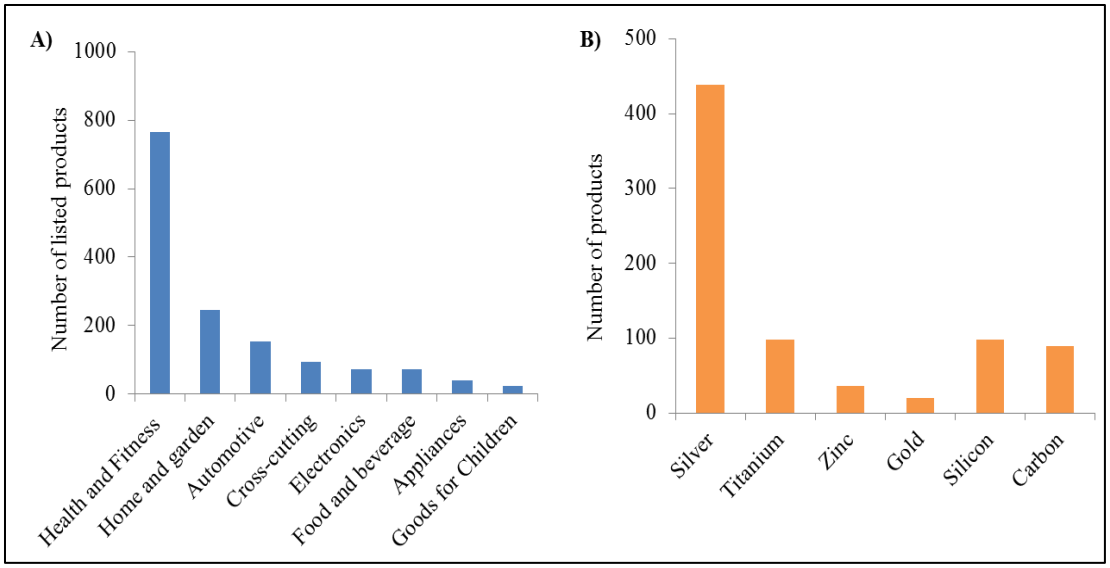

Figure 1.1: Total numbers of nanomaterial-based consumer products in 2014 excluding archived products: A) Categorical-wise B) Type of nanomaterial (charts constructed by Sesha L.A. Paluri using data from Vance *et.al,* 2015).[3].

Silver nanoparticles (AgNPs)

a) Biomedical potential

The diverse range of existing applications of AgNPs (*e.g.*, children toys, textiles, surgical implants, wound dressings, disinfectants, bone cements, *etc.*,) are mainly due to their antimicrobial properties.[6-8] In addition, they were shown exhibit anti-inflammatory, anti-thrombotic and antiviral activities.[8-10] Due to their unique optical properties, AgNPs are used as biosensors in medical diagnostic imaging.[11] For example, AgNPs were shown to be effective in the detection of cardiac troponin I, a biomarker for myocardial infarction.[12] Assemblies from diamond-like carbon-silver (4 nm) composites were proven to be hemocompatible for their potential use in cardiovascular implants.[13] Furthermore,

nanosilver-impregnated central nervous system (CNS) catheters were shown to inhibit biofilm growth. A related pilot study (stage IV clinical trials) revealed the catheters to be beneficial in preventing catheter-associated ventriculitis (CAV).[8] Despite of these impressive discoveries, their real-life clinical use is limited due to the associated toxicities.[8]

b) Toxicities

The enormous increase in the multifaceted applications of AgNPs led to an even more urgent need to examine their down-stream effects in the biological environment. It is generally accepted that AgNP toxicities are mainly due to their ability to release silver ions (Ag^{+}), which further cause production of reactive oxygen species (ROS) and induction of oxidative stress (OS).[14,15] However, AgNPs by themselves, were also shown to localize in sub-cellular compartments (*e.g.* lysosomes, mitochondria) causing: oxidative damage, DNA mutations, membrane disruption, and interference with cell cycle growth phase (G2/M) phase.[15,16] Furthermore, activation of intrinsic apoptosis pathway in AgNP-treated cells was studied in detail in human lung carcinoma cell line (A549). Specifically, cells were shown to exhibit: mitochondrial depolarization, decreased ATP levels, increased Bax expression along with formation of apoptotic regulators (smoc/DIABLO).[15,17,18] At higher concentrations (6.25-50 μg mL^{-1}), AgNPs (diameter of 7-20 nm) were reported to induce morphological changes in epithelial cells making them shrunken and fusiform.[19] The authors correlated these changes to the depletion of antioxidant machinery (*e.g.*, glutathione, GSH and superoxide dismutase, SOD), activation of caspases 3 and fragmentation of DNA. In addition, binding of Ag^{+}

and AgNPs to selenide moieties of the antioxidant machinery, and thiol-containing biomolecules in plasma membrane and mitochondria also disrupt membrane integrity [15,16]

c) Physicochemical Properties

Unlike regular chemicals, NPs are heterogeneous and thus, besides concentration, there has to be extensive characterization. In addition, the cellular uptake and the subsequent toxicities have already been shown to vary with surface chemistry (*e.g.*, size, shape, and surface charge) of AgNPs.[15,16] For instance, smaller AgNPs (5-28 nm) produced increasing amounts of ROS (hydrogen peroxide (H_2O_2) and superoxide free radicals (O_2^-)) and subjected intracellular components to OS.[15] In human lung epithelial cells, silver nanowires (length of 1.5-25 μm and diameter of 100-160 nm) exhibited increase in: lactate dehydrogenase leakage, calcium influx and immune responses (cytokine production and NF-*k*B activation). Contrarily, negligible effects were observed with spherical AgNPs (30 nm in diameter).[20] The authors inferred that the observed effects were due to the enhanced ability of nanowires to access cell surfaces without the need of internalization (like spherical AgNPs). Furthermore, incubation times and toxicity AgNPs were shown to be directly correlated but the trends varied with the study models.[7,15] It is widely-accepted that positively charged AgNPs internalize better than negatively charged or neutral AgNPs due to the electrostatic interactions with the negatively charged phospholipid head groups of the cellular membranes.[15] Although there has been deeper understanding on the ultimate adverse effects, most of these nanotoxicity studies either used non-standardized methods or did not characterize the aforementioned special properties, thus, the source of AgNP toxicity remains ambiguous.

In addition, NPs tends to interact with biological media contents (proteins, ions) leading to aggregation/agglomeration and/or dissolution. Although synthesis of NPs have been performed carefully over the years, it was only recently that these nano-media interactions were accounted in nanotoxicity research.[21] For instance, it was recommended previously that dilution of standard aquatic media (daphnia) might improve the AgNP stability without causing lethality to the study organism.[22,23] Later on, it was argued by other researchers that this might lead to alterations in vulnerability of the test model to NPs, leading to an unpredictable outcome.[22,23] In several such scenarios, inadequate emphasis on the complete physicochemical profile of nanoparticles led to overall inconsistent conclusions leading to the need of case-by-case analysis.[15,21,23]

d) Fate and transformation

The active surface of AgNPs generates free radicals under acidic conditions (*e.g.,* endosomes and lysosomes), which could trigger the release of Ag^+ and hydroxyl radicals.[24] Electron spin resonance studies revealed that AgNPs can initiate Fenton like reactions in presence of low H_2O_2 concentrations ($\leq$ 1 mM) and acidic pH. In contrast, Ag^+ can be reverted back to AgNPs at basic pH.[24] This suggests that depending on the surrounding environment, not only AgNPs alone have the propensity to generate ROS but both the species might actually co-exist. In general circumstances, like pharmaceuticals, not entire amount of administered AgNPs will be delivered to targeted tissues or cells. AgNPs might interact with surrounding proteins or thiol moieties and/or release Ag^+. In addition, this whole scenario depends on the AgNPs' surface chemistry. It should also be noted that most of the nanotoxicity studies focused on AgNP toxicities rather than their fate and

transformation.[15,21,25] Given there is little information that can be extracted from a nanotoxicity study, it is complicated to predict the fate and the existence of AgNPs and Ag^+ species in biological matrices. Nevertheless, there is infinitesimal information on the standardized methods to study the actual amount of AgNPs bioavailable, transformed (to Ag^+) and cleared by the system.[21] To improve therapeutic potential of AgNPs, basic knowledge of these aspects is crucial. National agencies like the National Nanotechnology Initiative (NNI, 2011) and the National Institute for Occupational Safety and Health (NIOSH, 2011) also stressed the need to develop accurate and reliable measurement tools to improve the existing knowledge regarding *in vitro* and *in vivo* nanokinetics (*i.e.,* Absorption, Distribution, Metabolism and Elimination, **ADME**s) prior to their nanomedical application.[25,26]

Chapter 2 of this dissertation describes the development of a suite of spectroscopic-, filtration-, and microscopic-based approaches to examine ADMEs of AgNPs in cells. This was achieved by sequentially determining each aspect of the ADMEs in the AgNP-exposed cells as follows: **[A]** ICP-OES was employed to construct absorption-time curves and to further reveal absorption kinetics **[D]** Hyperspectral data from CytoViva together with Raman imaging were used to demonstrate the uptake and predict the cellular regions of the internalized AgNPs. **[M]** CPE was coupled with TFF to facilitate the extraction of AgNPs and Ag^+. **[E]** ICP-OES was further utilized to evaluate the clearance kinetics.

As outlined earlier, the rapid increase in global trends of nanotechnology also demands greater workforce. Besides understanding its toxicokinetics, providing basic knowledge regarding nanoscale behavior to younger generation is of paramount

importance. Chapter 3 introduces some of the above discussed concepts to undergraduate and graduate students through the development of a new guided inquiry-based teaching nano-laboratory dedicated to the synthesis and characterization of green and non-green silver and gold nanoparticles. Briefly, this was achieved by a) in-class activities that correlated several day-to-day ‘macro’ examples to ‘nano’ scale (such as comparing bulk gold material vs gold nanoparticles) b) hands-on laboratory sessions that comprised of student-driven nanoparticle synthesis and characterization.

CHAPTER 2

ANALYTICAL-BASED METHODOLOGIES FOR EXAMINING THE *IN VITRO* ABSORPTION, DISTRIBUTION, METABOLISM, AND ELIMINATION (ADME) OF SILVER NANOPARTICLES

Sesha L. A. Paluri[a,b], John D. Ryan[a], Nhi H. Lam[a], Dhriti Nepal[c], and Ioana E. Sizemore[a,b]*

a. Department of Chemistry, Wright State University, 3640 Colonel Glenn Hwy., Dayton, OH 45435-0001, U.S.A.

b. Biomedical Sciences Ph.D. program, Wright State University, 3640 Colonel Glenn Hwy., Dayton, OH 45435-0001, U.S.A.

c. *Air Force Research Laboratory, 2941 Hobson Way, Wright Patterson Air Force Base, OH 45433, U.S.A.*

COPYRIGHT PEMISSION

SUMMARY OF INVOLVEMENT

Sesha L A Paluri was primarily responsible for the cell culture, obtaining necessary institutional approvals/protocols, characterization and filtration of AgNPs, design, execution of experiments and data analysis. Additionally, she drafted, edited and prepared the manuscript along with preparing graphical elements. She was also involved in the data analysis and construction of figures for CytoViva, DLS and Zeta measurements.

GRAPHICAL ABSTRACT

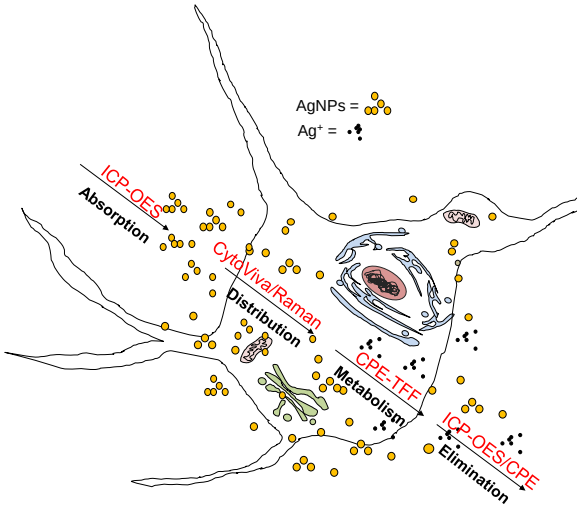

ABSTRACT

Silver nanoparticles (AgNPs) have numerous consumer product and biomedical applications but their clinical implications remain limited due to the lack of well-established methodologies for studying their nanokinetics. The primary goal of this research is to adapt a suite of analytical-based methodologies for examining the *in vitro* Absorption, Distribution, Metabolism, and Elimination of AgNPs. To achieve this, Vero 76 and HEK 293 cells were exposed to ~10 nm spherical $AgNPs^{+}$ and $AgNPs^{-}$ at relevant concentrations (0-300 µg mL^{-1}) and times (4-48 hr). Absorption: Inductively coupled plasma optical emission spectroscopy (ICP-OES) together with quality control methods demonstrated that the two AgNP formulations were not bioequivalent. For example, different bioavailable concentrations ($C_{maximum}$ < 20.7±4% and 6.8±0.4%), absorption times ($T_{maximum}$ > 48 hr and ~24 hr) and absorption rate laws (first- and zeroth-order at 300 µg mL^{-1}) were determined in Vero 76 cells for $AgNPs^{+}$ and $AgNPs^{-}$, respectively. Distribution: Raman and CytoViva hyperspectral imaging confirmed the AgNP uptake

and showed different cellular localizations for $AgNPs^{+}$ and $AgNPs^{-}$. Metabolism: Cloud point extraction (CPE) and tangential flow filtration (TFF) revealed that ≤ 11±4% of the administered, sub-lethal AgNPs were oxidized to Ag^{+} within the cellular matrix and contributed to the observed cytotoxicity. Elimination: ICP-OES and CPE suggested that AgNPs were cleared *via* exocytosis.

INTRODUCTION

The versatile applications of nanomaterials, in particular those of silver nanoparticles (AgNPs), generated a great need for understanding their impact on human health and the surrounding environment. In 2013, the Project on Emerging Nanotechnologies (PEN) indicated that 383 out of the 1,628 nano-based consumer products incorporated AgNPs mainly as antimicrobials.[27] The optical, mechanical and electrochemical properties of AgNPs have also been exploited in multidisciplinary applications including biosensors, catalysts, and electronics.[28-32] However, AgNPs were found to exert harmful effects both *in vitro* and *in vivo* mostly by producing Ag^{+} ions and causing oxidative stress.[28,32-34] In addition, recent studies indicated that AgNPs by themselves exhibit multifaceted toxicities such as DNA mutations, lipid peroxidation, disruption of respiratory chain, necrosis, and apoptosis.[7,8] The two Ag species (AgNPs and Ag^{+}) were reported to follow different uptake pathways and undergo possible interconversions within the cellular matrix.[35] Nevertheless, the lack of well-established methodologies for examining the cellular translocation and possible transformations of AgNPs limits their applications.[33,36] This knowledge gap was also emphasized by several U.S. programs (National Nanotechnology Initiative) and regulatory agencies (National Institute for Occupational Safety and Health).[36,37]Thus, the main goal of this project was

to adapt a suite of analytical-based methods for examining the *in vitro* absorption, distribution, metabolism, and elimination (ADME) of AgNPs. The measurement tools include inductively coupled plasma optical emission spectroscopy (ICP-OES) coupled with two quality control methods, CytoViva (CHSI) and Raman hyperspectral imaging (RHSI), cloud point extraction (CPE) and tangential flow filtration (TFF). To demonstrate the feasibility of the proposed methods, animal and human kidney cells were exposed to spherical AgNPs of both positive ($AgNPs^{+}$) and negative charge ($AgNPs^{-}$) at relevant concentrations (0-300 μg mL^{-1}) and time periods (0-48 hr), and the following ADME aspects were addressed: the total amount of AgNPs (A) bioavailable to, (D) distributed in, (M) transformed in, and I cleared by cells. African green monkey kidney cells (Vero 76) were selected as an *in vitro* model because of their routine use as viral hosts and in the development of vaccines.[38] This is an area of actively growing interest due to the recent, global viral outbreaks and the potential use of AgNPs as broad-spectrum antiviral agents.[39-44] Human embryonic kidney cells (HEK 293) were chosen due to their well-characterized nature and extensive use in biological and nanotoxicity research.[45-47]

Absorption (A): ICP-OES is a U.S. Environmental Protection Agency (EPA)-endorsed analytical technique that can facilitate the quantification of Ag down to the low μg L^{-1} level in biological matrices. For instance, ICP-OES and ICP-MS were reported to detect Ag in cell lysates,[48] tissues,[49] textile wastewaters,[50] and antibacterial products.[51] However, the EPA recommendations for quality control such as the determination of matrix effects and the validation of the minimum detection limit (MDL) were not entirely met.[31,36-39] Hereby, two calibration methods and two main emission lines for Ag were

employed to establish an EPA-endorsed quality control for the Ag quantification in biological matrices with experimentally determined MDL values. The standard additions method was performed in comparison with the routinely used external calibration method, and the relative percent difference (RPD) in Ag concentrations was calculated to account for possible matrix interferences leading to false positives.[52,53] To confirm the results obtained with the main emission wavelength of Ag(I) ion at 328.068 nm and to eliminate possible spectral overlaps, the second emission line of Ag at 338.289 nm was also employed in both calibrations.[52]

Distribution (D): High-resolution microscopies such as transmission electron microscopy (TEM) and scanning electron microscopy (SEM) are traditionally employed for the visualization of nanomaterials within cells, while the energy-dispersive X-ray spectroscopy (EDX) capabilities of these systems can confirm the elemental composition of the imaged nanomaterials and their surroundings.[54,55] However, these techniques are either invasive, require staining or involve tedious sample preparation.[55,56] Furthermore, an overall picture of the biochemical profile of non-fluorescent nanomaterials within the cellular matrix are not easily achievable. In recent years, two hyperspectral imaging techniques, namely enhanced dark-field CytoViva optical microscopy[54,55,56] and confocal Raman spectroscopy,[57,58] overcame some of these limitations. Hereby, it is shown that these techniques can facilitate the non-invasive hyperspectral imaging of live or fixed single cells with nano- or micro-spatial resolution and little-to-no sample preparation thereby further boosting overall time- and cost-efficiency. While CHSI enables the direct observation and spectral identification of AgNPs in the cellular environment, RHSI can chemically fingerprint the regions located in the close proximity or directly interacting

with AgNPs, thereby validating and complementing CHSI. While the above mentioned works have already demonstrated RHSI's potential on cells exposed to labeled AgNPs, this study offers a brief demonstration of how large volumes of RHSI data can be rapidly evaluated with chemometric methods so as to offer a survey picture of the cellular distribution of AgNPs in a label-and stain-free manner.

Metabolism (M): Recently, CPE was shown to facilitate the rapid differentiation of the two Ag species within biological (HepG2 cells) and environmental (solid waste waters) matrices.[48,59-61] This phase separation method is based on the selective abilities of: a) triton X-114 (TX-114) to form micelles with AgNPs above its cloud point (the detergent phase) and b) salts like sodium thiosulfate ($Na_2S_2O_3$) or EDTA to chelate Ag^+ and form hydrophilic complexes (the aqueous phase). However, the reported extraction efficiencies of AgNPs[48] were not normalized with respect to the actual amount of Ag absorbed by cells and led to possible overestimates for *in vitro* models. To address this aspect and to further improve the *in vitro* extraction, we added a one-step TFF after CPE. In our previous work, TFF was proven to size-select, concentrate, and purify either small or large volumes of colloidal AgNPs.[62-64] TFF is a "green" isolation method, which tangentially pumps the liquid sample containing dissolved (Ag^+) or suspended (AgNPs) particulates through a porous membrane filter of a desired size (1-1,000 kD).[62,64] The unique flow direction results in a gradual build-up of transmembrane pressure, which forces small particulates to pass through the filter (the permeate), while particulates larger than the membrane pores are swept along and recirculated until the desired volume reduction is attained (the retentate).

Elimination I: Quantitative information on the elimination profile and speciation of AgNPs *in vitro* is scarce.[31,65] For example, atomic absorption spectroscopy and single particle ICP-MS were used to quantify total amount of Ag eliminated from liver and kidneys of rats exposed to AgNPs.[65] Hereby, it is demonstrated that the aforementioned ICP-OES and CPE methodologies can not only quantify the total Ag cleared by cells but can also distinguish between the eliminated Ag species.

MATERIALS AND METHODS

All chemicals employed in the AgNP synthesis, characterization, and manipulations were purchased as high-grade reagents from Fisher Scientific. All cell culture supplies including Lab-Tek glass chamber slides were obtained from Nunc, Inc., while reagents for the routine maintenance of Vero 76 cells were from Hyclone. RPMI media used for HEK 293 cells were obtained from Corning. Total cellular protein content was measured using a BCA kit from Thermo Scientific Pierce. Oxidative stress of cells was determined with a GSH assay kit from Cayman Chemical. An ICP-OES grade Ag^+ standard (1,000±5 mg L^{-1}) was acquired from SPEX CertiPrep. Vero 76 mammalian cells were obtained from ATCC (CRL # 1587). HEK 293 cells were generously donated by Dr. Ashot Kozak, Wright State University, Dayton, OH. High quality (HQ) water (resistivity > 18 MΩ cm) was used as vehicle throughout the study unless otherwise specified.

Synthesis of colloidal AgNPs

Positively charged AgNPs$^+$ were synthesized through the reduction of 300 mL of silver nitrate ($AgNO_3$, 5 x 10^{-3} M) with 20 mL of aqueous cetyl trimethylammonium bromide

(CTAB, 2 x 10^{-2} M) and 0.2 mL of freshly prepared sodium borohydride ($NaBH_4$, 1% (w/v)) aqueous solutions at room-temperature, under constant mixing on a stir plate (~3200 rpm, Fisher scientific) for 30 min.[66] Solubility of CTAB was stimulated by heating the solution in a water bath at 30 °C for 30 min. *Negatively charged AgNPs*$^-$ were prepared through the aqueous reduction of 50 mL of $AgNO_3$ (1 x 10^{-3} M) with 300 mL of ice-cold $NaBH_4$ (2 x 10^{-3} M).[67] The reaction was carried out in an ice-bath under dark conditions, with constant stirring (~ 320 rpm) for 90-135 min.

AgNP characterization

UV-Vis absorption spectroscopy (Cary Bio 50, Varian Inc.): The extinction spectra of the colloidal AgNP samples were collected at a scan rate of 1200 nm min^{-1} in disposable 1-cm cuvettes.

Raman spectroscopy (LabRam HR-800, Horiba Jobin Yvon, Inc.): Raman spectra of the colloidal AgNP samples (100-4000 cm^{-1}) were collected in 2-mL quartz cuvettes. The acquisition setup was as follows: a confocal Raman BX41 microscope, an internal HeNe laser of 632.8 nm (15 mW output), Olympus 100x and 50X objectives, a holographic grating of 600 grooves mm^{-1}, acquisition times of 30 s, 5 cycles, a confocal hole of 300 μm, and a thermoelectrically cooled Andor CCD camera of 1024 x 256 pixels. Under these experimental conditions, a spectral resolution of ~ 1 cm^{-1} was achieved. The spectra were collected using the LabSpec v.5 software and were processed in Origin 8 software.

Transmission electron microscopy (TEM, Philips EM 208S): AgNP images were collected on carbon-coated copper grids using a high resolution Gatan Bioscan camera at

70 KV and were processed in ImageJ 1.46R and Origin 8 software. Details are given in Supporting Information.

TFF (Spectrum Labs, Inc.): The original colloidal AgNPs were size-selected, purified and concentrated through a KrosFlo Research Iii system equipped with modified polyether ether sulfone (mPES) Midi Kros filter modules (Schematic 2.S1). Detailed TFF procedures are provided in our previously published work[62-64]. Briefly, 3 L of colloidal $AgNPs^-$ were first passed through a 500 kD (790 cm^2, ~ 50 nm pore size[68]) membrane filter. The resulting 500 kD permeate was then pumped through a 10 kD (790 cm^2, ~ 5 nm pore size[68]) membrane filter. The final 10 kD retentate (10 kD ret) was used as $AgNP^-$ stock (~10 nm in average diameter) for cell culture experiments. Because the original colloid of $AgNPs^+$ already consisted of particles smaller than 40 nm in diameter, only one-step filtration (10 kD, 790 cm^2) was implemented to purify and concentrate 0.350 L of colloid.

Salt experiments: Inorganic salts that predominate in DMEM (0.2 mM of $CaCl_2$, 0.4 mM of KCl, 0.0097 mM of $MgSO_4$, 6.5 mM of NaCl, and 0.125 mM of NaH_2PO_4 H_20) and RPMI (0.4 mM of KCl, 0.048 mM of $MgSO_4$, 6 mM of NaCl, 2 mM of $NaHCO_3$, and 0.8 mM of Na_2HPO_4) were prepared in HQ water and were mixed with AgNPs at 1x or 0.5x the salt concentratios in media. The final concentration of AgNPs in the samples was 10 μg mL^{-1} and the resultant samples were incubated at 37 ºC and in 5% CO_2 for 0, 4, 12, 24, and 48 hr. UV-Vis absorption spectra were collected following the above protocols at each time point.

Zeta potential and DLS (Malvern Zetasizer Nano ZS): Zeta potential and DLS measurements were carried out N = 3 independent times in folded capillary cells (0.75

mL) at 90º scattering angle and 25 ºC immediately after preparation. Zeta potential: An average of *N* = 100 spectra were acquired in the -150 to +150 mV range. DLS: *N* = 100 scans were performed per each measurement.

TEM-EDX (FEI/Philips CM-200 LaB_6): Samples were prepared by separately incubating $AgNPs^+$ or $AgNPs^-$ in DMEM and RPMI for 1 hr, at a final concentration of 10 µg mL^{-1}, at 37 ºC and in 5% CO_2. TEM grids were prepared by depositing 10 µL of samples on carbon-coated copper grids (Electron Microscopy Sciences) and dried in a desiccator. Data was collected using a high resolution Gatan Bioscan camera at 200 kV and was processed in the Origin 8 software.

Inductively coupled plasma optical emission spectroscopy (ICP-OES, Varian 710-ES)

ICP-OES sample preparation: Each AgNP sample was subjected to "cold and hot" digestions. In the first step, a cold digestion was performed in glass beakers at room-temperature for 15 min using 5 mL of HNO_3. In the second step, a hot digestion was carried out with 5 mL of HNO_3 at ~220 °C until the volume of the liquid was reduced to ~$1/4^{th}$ of its initial value. In the last step, beakers were cooled down, rinsed five times with water and transferred to 10- or 25-mL volumetric flasks for dilutions in 2% HNO_3.

ICP-OES analysis: Samples were aspirated into the ICP-OES instrument with an autosampler (Varian SPS 3) at a peristaltic pump rate of 2 mL min^{-1}, nebulized and further pumped to the axially positioned quartz torch. The instrument response was obtained in triplicates at the two main emission lines of Ag (328.068 nm and 338.289 nm). The ICP-OES operating conditions were: nebulizer pressure of 200 kPa, plasma flow of 15.0 L min^{-1}, auxiliary flow of 1.50 L min^{-1}, radio-frequency power of 1.20 kW,

replicate read time of 15 s, internal stabilization delay of 45 s, sample uptake delay of 40 s, and rinse time of 15 s.

External calibration method: Ag^+ working standards (0-800 μg L^{-1}) were prepared from the stock Ag^+ standard (1,000 mg L^{-1}) by quantitative dilutions in 2% (v/v) HNO_3 aqueous matrix. An external calibration curve was constructed by plotting the emission intensity of the standards as a function of the Ag^+ standard concentrations. The total amount of Ag in each sample was determined by interpolation from the curve.

Standard additions method: Standard additions were performed on the digested samples at the highest AgNP exposure. For this, known concentrations of the Ag^+ standard (800 μg L^{-1}) were added to equal volumes of sample (0.500 mL for cells and 1 mL for media) in gradual volume increments of 0.100 mL, in the 0-0.500 mL range. A standard additions curve was constructed by plotting the emission intensity of the standards as a function of the Ag^+ standard concentrations. The total amount of Ag in each sample was extrapolated from the curve.

The two calibrations methods were compared by calculating the relative percent difference (RPD) in the Ag concentrations (Supporting information).

Cell lines

African green monkey kidney (Vero 76) and Human embryonic kidney (HEK 293) cells were grown in DMEM and RPMI substituted with 10% fetal bovine serum (FBS) and 1% penicillin-streptomycin (pen-strep), respectively. Both cell lines were maintained in an incubator with 5% CO_2 at 37 °C.

ADME of AgNPs

Absorption (A)

Exposure to AgNPs: Vero 76 cells and HEK 293 cells were seeded in 35-mm culture dishes at a density of 2.5 x 10^4 and 2 x 10^5 cells mL^{-1}, respectively. The following day, cells were exposed to fresh media containing TFF-processed $AgNPs^+$ or $AgNPs^-$ for 4, 12, 24, and 48 hr. The dilutions of the AgNP stock were done in media to minimize the total volume of water added to cells (< 50 µL of water per plate). For Vero 76 cell exposure, the final concentrations of AgNPs in the 2 mL of vehicle (media plus insignificant amounts of water) were 3, 15, 30, 100, 150, and 300 µg mL^{-1}. For HEK 293 cells, the final concentrations of $AgNPs^+$ were 20 µg mL^{-1}. Controls included vehicle, vehicle and AgNPs, and cells in vehicle.

Sample preparation for ICP-OES: Following the collection of media portions, the culture plates were washed thrice with PBS and the adherent cells were gently harvested with a cell scraper. In order to maximize the harvest, a "cold" digestion of scraped cells was performed directly in each of the culture plates and all cell contents were transferred to glass beakers for a "hot" digestion following the two-step digestion procedure for colloidal AgNPs. In addition, a hot digestion was performed with concentrated H_2O_2 to bleach the cellular and media matrices. Briefly, the HNO_3-digested samples were cooled down to ~80 ˚C, 1 mL of H_2O_2 was added to each beaker, and the contents were heated at 180 ˚C until ~200 µL of sample was left. Finally, the beakers were rinsed five times with water and the digested samples were subsequently diluted in 10-mL volumetric flasks containing 2% aqueous HNO_3 for ICP-OES measurements. The resulting Ag

concentrations were normalized to the corresponding cell proteins (*i.e.*, µg of Ag per mg protein in cells without AgNPs) under each condition.

Distribution (D)

CHSI: Live Vero 76 cells were grown in 8-well glass chamber slides (0.5×10^3 cells per well) and exposed next day to the highest, sub-lethal concentration of $AgNPs^+$ (30 µg mL^{-1}) and $AgNPs^-$ (100 µg mL^{-1}) for 4 hr. CHSI was also performed on formaldehyde-fixed cells. For this, Vero 76 cells were seeded in 6-well plates containing glass coverslips (2.5×10^4 cells per well) and were similarly exposed to AgNPs for 4 hr. Cells were fixed with formaldehyde (~3.7 % v/v in PBS), washed thrice, and stored in fresh PBS at 4 ºC until use. HEK 293 cells at a density of 1×10^5 cells mL^{-1}were similarly exposed to 10 µg mL^{-1} of $AgNPs^+$ for 4 hr and 24 hr. Following this, cells were detached and pelleted by centrifuging at 100 g for 10 min. The resultant cell pellets were fixed by addition of 1 mL of formaldehyde in Eppendorf tubes for 15 min. In order to remove excess reagents, fixed pellets were washed thrice with 1 mL of PBS by centrifugation (100 g for 2 min) and finally suspended in 0.2 mL of fresh PBS and stored at 4 ºC until use. Images were collected in real-time using an Olympus research grade optical microscope equipped with CytoViva (Auburn, AL) patented enhanced darkfield illumination optics and full spectrum aluminum halogen source illumination. The corresponding hyperspectral data were acquired in the 400-1000 nm region, at 2 nm spectral resolution, with the help of the integrated hyperspectral imaging system. Prior to the data acquisition, spectra of dark current images were also collected for background correction and normalization with respect to the lamp spectrum was carried out. The spectral response of the sample was analyzed using a customized version of ENVI

hyperspectral image analysis software. Specifically, spectral libraries of the controls samples (cells alone and AgNPs alone) were constructed and the acquired sample images (cells exposed to AgNPs) were filtered against these libraries to ensure no false positives.

RHSI: Cell density and sample preparation of Vero 76 and HEK 293 cells were similar to CHSI. Raman maps of fixed, single cells (N = 3 cells for each condition, areas of 10 x 10 µm to 15 x 15 µm) with and without AgNP exposure were acquired in 100-2000 cm^{-1} spectral region, at 1 µm step size, using the same LabRam HR-800 system (3 s exposure time and 2 accumulation cycles). Cells were imaged with a confocal Raman microscope (100x Olympus objective) and irradiated with a He:Ne laser (632.8 nm and 15 mW output). All other instrument parameters were similar to the ones in the Raman measurements of AgNP colloids.

Clustering analysis of Raman spectral maps: In-house written Matlab (v.7.11.0.584, R2010b) codes were employed for the evaluation of Raman maps, while the Origin 8 software was used to plot representative spectra. Spectral maps were first pre-processed using the low pass Savitzky-Golay filter (2^{nd} order derivative, 4^{th} degree polynomial with a frame size of 11) in order to smooth the possible background noise from cosmic rays and glass coverslip.[69] The resultant data was further normalized using the Z-scores. Agglomerative hierarchical clustering analysis (AHCA) using the Ward's merging algorithm was employed on the processed data in order to identify 10 representative clusters (n = 10)[54.55] Briefly, a correlation matrix (CM) containing N^2 initial input values (N = total number of spectra) was first created and correlation coefficients were assigned based on spectral similarities (CM = 1 for similar spectra and CM = 0 for spectral overlaps). Ward's algorithm was then employed to pick the identical

spectra from this CM, which were then grouped as new cluster objects. Finally, a pseudo-color image was constructed using these colors and means of the spectra present in each cluster were generated to illustrate spectral differences among clusters.

Metabolism (M)

Cloud point extraction (CPE) of cellular AgNPs and Ag^+: Vero 76 cells and HEK 293 cells were seeded at the density mentioned above and exposed next day to sub-lethal concentrations of $AgNPs^-$ (30 µg mL^{-1}) and $AgNPs^+$ (10 µg mL^{-1}), respectively for 24 hr. After exposure, cells were washed thrice with PBS, trypsinzed, and counted. CPE was then performed following established protocols[45] with minor modifications (Schematic 1). Briefly, ~10^4 cells were added to each sample or control vial, and the final volume was brought up to 1 mL using 10% TX-114. Afterward, 0.2 mL of 1 M of $Na_2S_2O_3$ was sequentially added to each vial, whose contents were mixed and heated in a water bath at 40 ˚C for 30 min. The vials were then centrifuged at 5,000 g for 5 min to facilitate phase separation and the resulting aqueous and detergent-rich phases were collected and stored at 4 ºC for further analysis.

TFF processing of aqueous CPE phase: The upper aqueous phase of CPE was immediately subjected to TFF using a 1 kD mPES MicroKros (110 cm^2) filter module to further extract AgNPs. A feed rate of 20 mL min^{-1} and a feed volume of 10 mL were applied.

Control CPE-TFF experiments on AgNP stocks (10 kD retentate): Control CPE-TFF experiments were performed similarly on the concentrated stocks of $AgNPs^+$ and $AgNPs^-$ alone. Aliquots collected at each CPE-TFF step were digested and analyzed using ICP-

OES. In order to validate the effectiveness of the CPE-TFF approach in extracting Ag species, additional experiments were performed on the AgNP stocks by ultracentrifugation at 10,000 g for 60 min. The resultant supernatants and pellets were digested similarly and analyzed by ICP-OES for their total Ag^+ and AgNP content, respectively.

Schematic 2.1: Enhanced extraction of Ag species *via* CPE followed by one-step TFF.

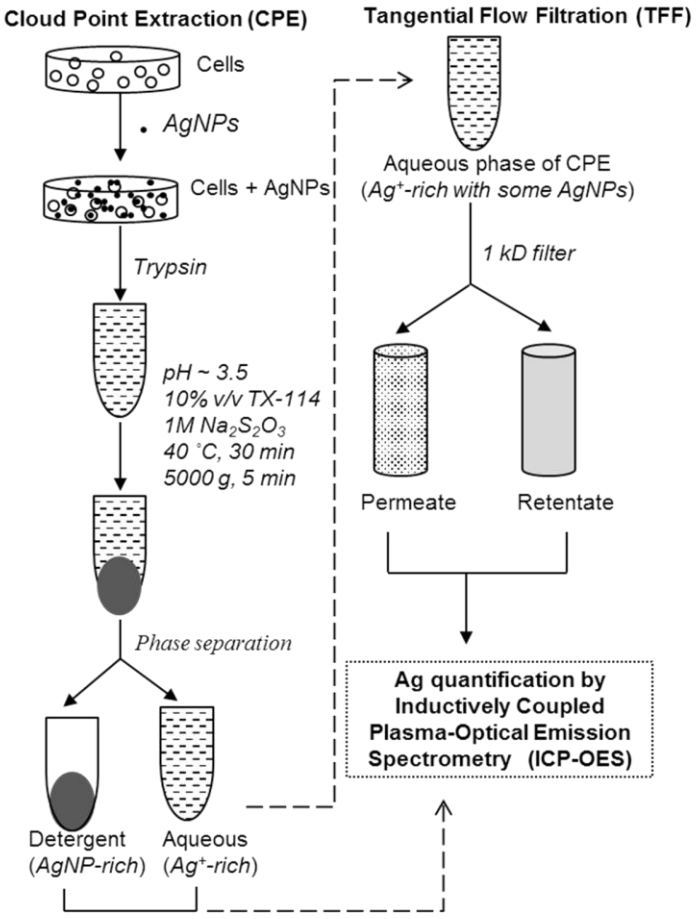

The final step of CPE results in AgNP-rich and Ag^+-rich phases. TFF further extracts AgNPs present in the Ag^+-rich phase of CPE. AgNPs and cells are drawn out of scale for illustrative purposes.

ICP-OES quantification of AgNPs and Ag^+: In order to obtain the total Ag bioavailable to cells, a sample of cells exposed to AgNPs was digested prior to the CPE and quantified by ICP-OES for each experimental condition. Finally, both the aqueous (1 kD permeate and retentate) and detergent-rich phases were analyzed on the same day *via* ICP-OES following the above described procedures.

The *BCA, MTT and GSH assays* are described in the Supporting Information.

Elimination I

Vero 76 cells were seeded in 35-mm culture dishes (2.5×10^4 cells mL^{-1}) and were exposed to 30 and 100 μg mL^{-1} of $AgNPs^+$ and $AgNPs^-$ the following day for 24 hr. HEK 293 cells were seeded in 35-mm culture dishes (1×10^5 cells mL^{-1}) and were similarly exposed to 20 μg $mL^{-1}$of $AgNPs^+$ for 24 hr. Following this, media was removed, cells were washed thrice with PBS, and 2 mL of fresh media was added to the plates. To obtain the amounts of AgNPs cleared from cells with time, 50 μL of media was collected from each of the cells at 1, 4, 12, and 24 hr and analyzed by the ICP-OES- and CPE-based methodologies described above. Elimination kinetics of AgNPs was explored and rate constants (k_{eli}) were obtained by plotting the natural logarithmic of the protein-normalized concentrations as a function of time.[70]

Statistics

Statistical analysis was performed using the SigmaPlot 12.0 package. A two factorial analysis of variances (2-wayANOVA) in combination with the Holm-Sidak multiple comparison method (post-hoc test, $p \leq 0.05$) determined significant differences in the cellular uptake of AgNPs with respect to concentration and surface charge at 4, 12, and 48 hr. A *t*-test assessed significant differences in the surface charge of AgNPs at 24 hr. One factorial ANOVA (1-way-ANOVA) on ranks determined significant differences in concentration within a specific exposure condition. 1-way ANOVA was employed for the GSH assay to determine the significance within concentrations ($p \leq 0.05$).

RESULTS AND DISCUSSION

Nano-sized materials exhibit unique physicochemical properties that are distinct from those of their bulk counterparts. These properties are not only responsible for their multifarious applications, but also govern their ADMEs *in vitro* and *in vivo*.[36,65] The Minimum Information for Nanomaterial Characterization (MINChar) Initiative[71] recommended a set of minimum nine parameters (average size/size distribution, agglomeration/aggregation, shape, overall composition, surface composition, purity, surface area, surface chemistry, and surface charge) to be considered while performing toxicity studies or developing new methodologies for measuring their fate and transformations in biological environments.[71,72] In view of these recommendations, the properties of the AgNPs utilized in this study are described below.

The UV-VIS absorption spectra of the colloidal samples confirmed the presence of AgNPs pre- and post-TFF processing through a localized surface plasmon resonance (LSPR) peak at ~400 nm (Figure 2.S1). The TEM micrographs and size histograms of the original $AgNPs^{-}$ showed that they were spherical and moderately distributed in size (1-

100 nm) (Figure 2.1). After the two-step TFF processing (Schematic 2.S1), the larger $AgNPs^-$ and $AgNP^-$aggregates (> 35 nm in diameter, Ori) were eliminated, thus attaining a narrower size distribution with little to no aggregation and suitable for cell culture studies (10 kD ret). The analysis of N = 600 $AgNPs^-$ indicated an average diameter of ~10 nm in the 10 kD ret. $AgNPs^+$ were also spherical but had a narrower size distribution (1-40 nm) in the original colloid. Thus, only one-step TFF processing was employed to concentrate $AgNPs^+$ of a similar average diameter of ~10 nm in the 10 kD ret (N = 600 $AgNPs^+$). DLS measurements confirmed the TEM trends, but as expected, the hydrodynamic diameters of the original AgNPs had a larger size distribution (1-300 nm). The AgNP concentrations of all colloidal samples were quantified by ICP-OES (Table 2.S1 and Figure 2.S2). The surface area (SA) of a single spherical AgNP was estimated to be 314 nm^2 based off the TEM data. TFF also facilitated the purification of both original colloids by eliminating excess reagents and byproducts together with the solvent (Figure 2.S3).[62,64] The colloidal $AgNPs^+$ and $AgNPs^-$ were found to have a Zeta potential of +34±2 mV (pH of 6.9) and -28±2 mV (pH of 6.8), respectively, in good agreement with the literature[64,65] and at pH values close to that of cells in the media (7.2). Literature shows these charges are the result of CTAB[73,74] and $B(OH)_3$[75] present at the surface of $AgNPs^+$ and $AgNPs^-$, respectively.

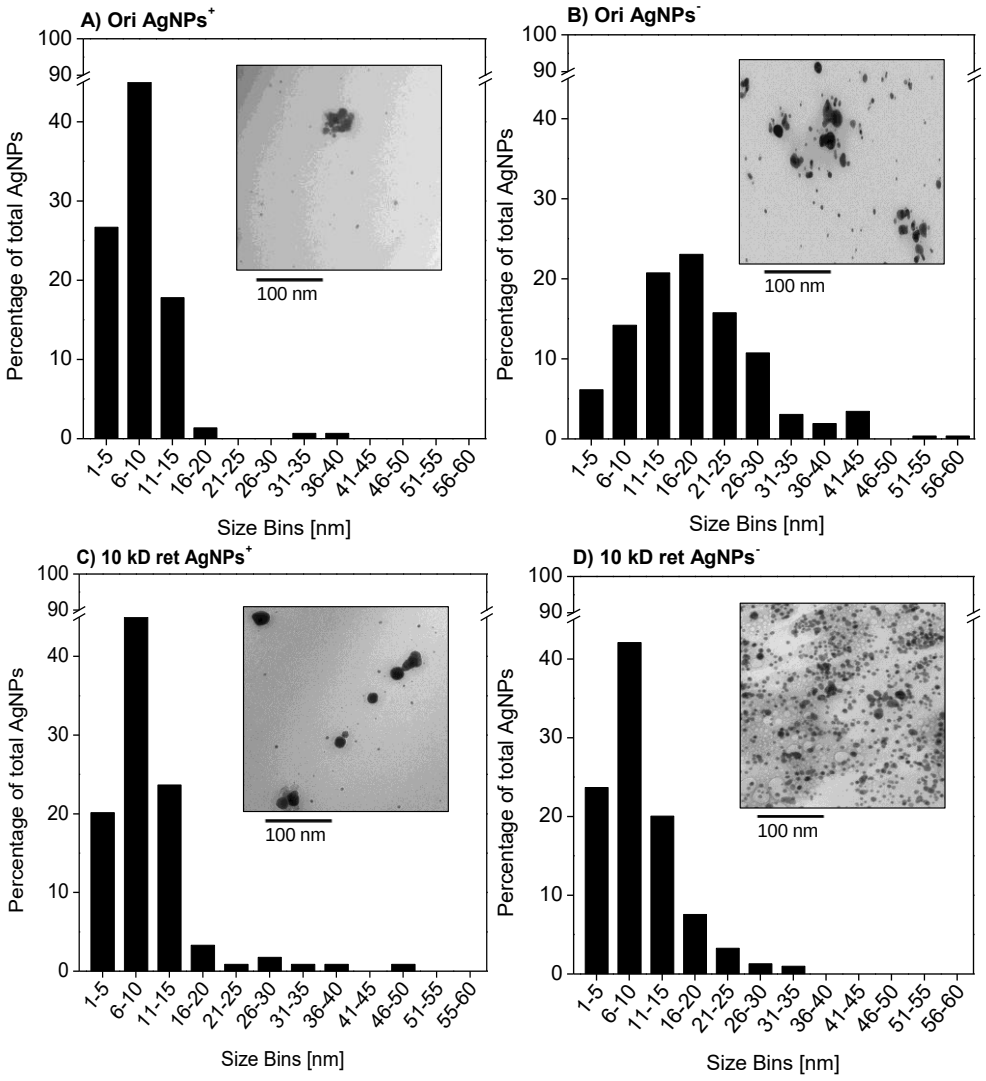

Figure 2.1: TEM micrographs and size histograms of AgNPs (N = 600) before and after TFF manipulation. A) and B) refer to the Original colloids (Ori), while C) and D) denote 10 kD retentates (10 kD ret) of $AgNPs^{+}$ and $AgNPs^{-}$, respectively. The scale bar in the insets is 100 nm.

Absorption, Distribution, Metabolism and Elimination (ADME) of AgNPs

According to the 2006 Nanomedicine, Device & Diagnostic Report released by NanoBiotech News, 130 nanotech-based drugs and delivery systems and 125 devices or diagnostic tests have entered preclinical, clinical, or commercial development.[36,76,77] A

few AgNP examples include targeted drug-delivery systems,[29,78] imaging contrast agents,[31] antimicrobials,[29,31] cancer agents,[79,80] and antivirals[39-41,43]. In response to the growing number of nano-biomedical applications, the U.S. Food and Drug Administration (US-FDA) has recently highlighted the need of characterizing their nanokinetic behavior.[81] Thus, the development of adequate methodologies for examining the ADME aspects of AgNPs becomes critical for their clinical applications. Hereafter, we will demonstrate the efficiency of the proposed analytical- based methodologies in examining *in vitro* ADME aspects of AgNPs as a function of AgNP exposure time, concentration, and surface charge.

Absorption (A): As biological matrices are chemically complex in nature, the effect of matrix interferences was first tested at higher concentrations of AgNPs and 24 hr of exposure in order to eliminate the likelihood of false positives. Throughout the experiments, an RPD value $\leq$ 6% was estimated between the two methods (Supporting Information), which is within the U.S. EPA recommended threshold of ~10%.[52,53] This demonstrated that there were no matrix interferences in this particular cellular system and validated the proposed ICP-OES quantification method. The MDL value at the main emission line of Ag was determined to 2.95±0.6 μg L^{-1} (Supporting Information). The total amount of Ag bioavailable to cells at 4, 12, 24, and 48 hr of exposure to both $AgNPs^{+}$ and $AgNPs^{-}$ was then determined by ICP-OES and normalized to the corresponding cellular protein content before plotting it as a function of AgNP surface charge, concentration, and exposure time.

The ICP-OES results on Vero 76 cells indicated that **AgNP surface charge** played a key role in their absorption at 4, 12, 24, and 48 hr (Figure 2.2). Specifically, at

any given concentration or exposure time, cells exposed to $AgNPs^{+}$ accumulated ~1- to 25-fold more Ag than cells exposed to $AgNPs^{-}$. For instance, the absorptions at 12 hr exposure to 100 μg mL^{-1} of $AgNPs^{+}$ and $AgNPs^{-}$ were 18.1±4.3 and 3.10±0.1 μg of Ag per mg of protein, respectively. AgNPs are known to enter cells mainly *via* energy-dependent endocytic pathways.[82,83] In good agreement with previous studies, both types of AgNPs were found to directly interact with culture media components facilitating their cellular internalization irrespective of surface coating.[84-87] Additionally, $AgNPs^{+}$ might have also experienced electrostatic attractions to the negatively charged components of the plasma cell membrane (-70 mV).[74,83,84] Evidence for the interaction of both $AgNPs^{+}$ and $AgNPs^{-}$ with culture media and its individual components (*e.g.*, Dulbecco's modified eagle media (DMEM) and fetal bovine serum (FBS)) was brought by UV-Vis absorption spectroscopy, which showed significant changes in the profile of the LSPR peak of AgNPs (Figure 2.S4). For example, a ~10-fold decrease in relative absorbance and a 39-nm redshift in the LSPR peak were seen after placing 300 μg mL^{-1} of $AgNPs^{+}$ in DMEM for 24 hr. The media also exhibited similar LSPR changes for $AgNPs^{+}$, *i.e.*, a 1.3-fold change in intensity and 20-nm redshift, but not as dramatic as for DMEM. Similar protein corona-induced changes in the LSPR profile have been reported for other types of AgNPs incubated with various DMEM-containing media. For example, the adsorption of bovine serum albumin (BSA) proteins were reported to cause significant red shifts in the LSPR peaks of PVP- or citrate-coated AgNPs on account of the change in the dielectric function of the surrounding medium.[85,86] Because the LSPR peak is sensitive to the AgNP morphology, LSPR shifts to lower energy may also be indicative of the formation of AgNP-agglomerates in such salt-rich media. These salt-induced changes in the LSPR

profile were confirmed via titration experiments, in which $AgNPs^{+}$ or $AgNPs^{-}$ were exposed to the media salts alone as a function of time (0-48 hr) and salt concentration (1x and 0.5x), and were subsequently measured by UV-Vis absorption spectroscopy (Figure 2.S5 and 2.S6). The absorption data showed that the protein corona formed around AgNPs prevented the dissolution and salt-induced precipitation of AgNPs, which were observed in media salts alone at long incubation times (24 hr) and high salt concentrations (1x) (Supporting Information). Furthermore, the formation of protein corona and the increase in AgNPs' size were confirmed by DLS and TEM-EDX measurements (Supporting Information). For example, a 4-fold increase in the hydrodynamic diameters of $AgNPs^{-}$ was noticed in DMEM, while $AgNPs^{+}$ in RPMI exhibited the appearance of a second, broad DLS peak in the 130-1290 nm size range (Figure 2.S7). In addition, TEM-EDX data confirmed the existence of AgNP-agglomerates in the immediate vicinity of salt crystals (*e.g.*, Ag, Na, K, Cl, and Ca peaks) and the formation of protein corona around AgNPs in media (*e.g.*, Ag, C, and O peaks) (Figure 2.S8).

The total absorption of **AgNP**s in Vero 76 cells was found to be **concentration**-dependent within a specific time frame. In general, it increased with the increase in the added AgNP amounts (3-300 μg mL^{-1}) and was significant above 100 μg mL^{-1} (Figure 2.2). For example, cells exposed to 300 μg mL^{-1} of $AgNPs^{+}$ and $AgNPs^{-}$ for 4 hr (t_4) accumulated over 5-fold and 2-fold more Ag, respectively, than in all other exposures at t_4. In order to gain further understanding on these trends, absorption versus time curves were constructed for both $AgNPs^{+}$ and $AgNPs^{-}$ (Figure 2.3). Overall, less than 20.7±4% and 6.82±0.4% of the added $AgNPs^{+}$ and $AgNPs^{-}$, respectively, interacted with the cells

across all exposure times and concentrations. ICP-OES measurements on the extracellular matrix (Figure 2.S9) revealed that 45-90% and 20-95% of the administered $AgNPs^{+}$ and $AgNPs^{-}$, respectively, were still present in the media after the cell harvest. The remaining portion of AgNPs probably adsorbed on the walls of the cell plates as suggested by an SEM-EDX analysis (Figure 2.S10). Clearly, this aspect plays a critical role in the absorption and distribution mechanisms of AgNPs or other types of metallic NPs. However, it was often overlooked in previous nano-toxicity and –medical studies and might have led to the overestimation of reported lethal concentrations (LC_{50}) and bioavailable levels of AgNPs.[34,65,87-90]

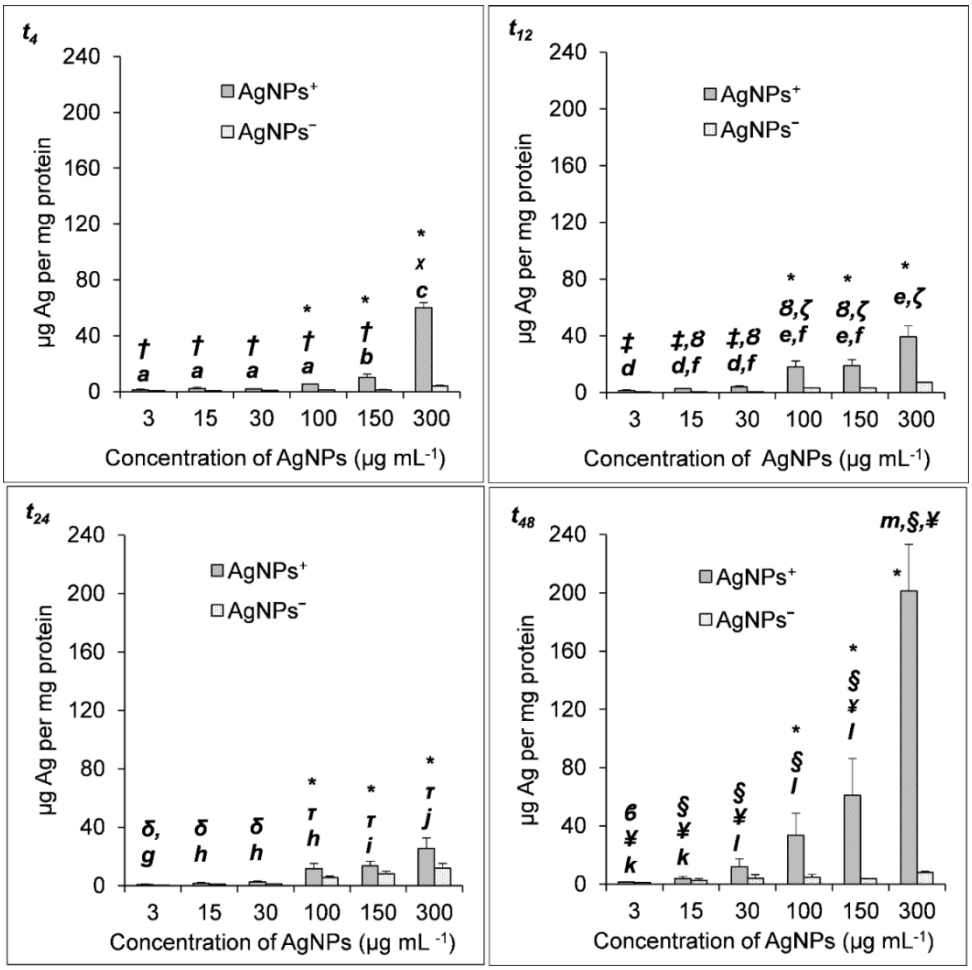

Figure 2.2: Accumulation of Ag in Vero 76 cells as a function of AgNP surface charge and concentration as determined by ICP-OES. *T* denotes the exposure time of 4, 12, 24, and 48 hr. '*' marks the concentrations at which surface charge led to statistically significant absorption of Ag ($p < 0.05$ for 2-way ANOVA at 4, 12, and 48 hr and *t*-test at 24 hr). Lowercase letters and symbols were employed to represent the statistical differences in the concentration for each exposure time of $AgNPs^{+}$ and $AgNPs^{-}$, respectively. At any exposure time in the graph, same letters (*a*, *b*, *c*, *d*, *e*, *f*, *g*, *h*, *i*, *j*, *k*, *l* and *m*) or symbols (†, χ, ‡, ℬ, ζ, δ, *T*, ℴ, ¥, and §) indicate that the Ag concentrations were not statistically significant from each other (1-way ANOVA on ranks). The error bars represent standard error of $N = 3$ independent trials for each AgNP treatment at a specific exposure time except for t_{24} of $AgNPs^{+}$ exposure, where $N = 6$ in order to increase confidence in the collected data of larger experimental deviations than in the other exposure data. The error bars for some concentrations are too small in values to be clearly visible.

The total Ag accumulated by Vero 76 cells versus **time profiles** are shown in Figure 2.3 for all administered $AgNP^{+}$ and $AgNP^{-}$ concentrations. The maximum cellular uptake of Ag ($C_{maximum}$) was observed at the highest exposed concentration of 300 μg mL^{-1}, when $C_{maximum}$ reached 201±32 and 11.9±3.1 μg of Ag per mg of protein for $AgNPs^{+}$ and $AgNPs^{-}$, respectively. However, care should be exercised above sub-lethal AgNP concentrations when other possible uptake mechanisms (besides endocytosis) may come into play due to the damage or death of cells. In such cases, the normalization of the absorption data with respect to the cellular protein content or other discriminant factors

becomes critical. **Above sub-lethal concentration ranges** (LC_{50} = 25-30 μg $mL^{-1}$and 100-125 μg mL^{-1} of $AgNPs^{+}$ and $AgNPs^{-}$, respectively – see Metabolism section), the time needed to reach the maximum cellular uptake ($T_{maximum}$) was around 24 hr for $AgNPs^{-}$ suggesting the entrance of the post-absorption phase. As expected, $T_{maximum}$ for $AgNPs^{+}$ was longer than $T_{maximum}$ for $AgNPs^{-}$ due to the favorable electrostatic interactions enhancing cellular absorption. Specifically, the absorption of $AgNPs^{+}$ continued to increase after 24 hr, with a relative $T_{maximum}$ > 48 hr within the monitored time interval. $T_{maximum}$ for $AgNPs^{+}$ might be more precisely determined under experimental conditions where longer exposure times become feasible. The ratio of the areas under the Ag absorption-time curves ($AUC_{AgNPs^{+}} / AUC_{AgNPs^{-}}$) were 4.90 and 10.1 at 150 μg mL^{-1} and 300 μg mL^{-1} exposure, respectively (Figure 2.3). These ratios offer more accurate estimates of the overall Ag bioavailability than the corresponding absorption ratios obtained from the average Ag accumulation values ($A_{AgNPs^{+}} / A_{AgNPs^{-}}$) of all individual time points, namely 8.10 and 12.5 at 150 μg mL^{-1} and 300 μg mL^{-1} exposure, respectively (Figure 2.2). A closer examination of the absorption portion of the curve ($\leq T_{maximum}$) indicates a zeroth-order rate law for the 300 μg mL^{-1} of $AgNPs^{-}$ exposure in the 4-24 hr time period, with a cellular absorption rate of k_{abs} = 0.4 μg of $AgNPs^{-}$ hr^{-1}. This means that the cellular absorption of $AgNPs^{-}$ is concentration-independent probably due to the protein-corona regulated uptake, which may be a main entry route for $AgNPs^{-}$. In contrast, the absorption for the 300 μg mL^{-1} of $AgNPs^{+}$ exposure was identified as a first-order process with k_{abs} = 0.05 hr^{-1} in the 12-48 hr time period. In this case, the cellular absorption of $AgNPs^{+}$ could be the result of the favorable electrostatic interactions with the plasma membrane. **At sub-lethal concentration**

ranges, the absorption of both types of AgNPs increased with exposure time, but $T_{maximum}$ was not yet reached.

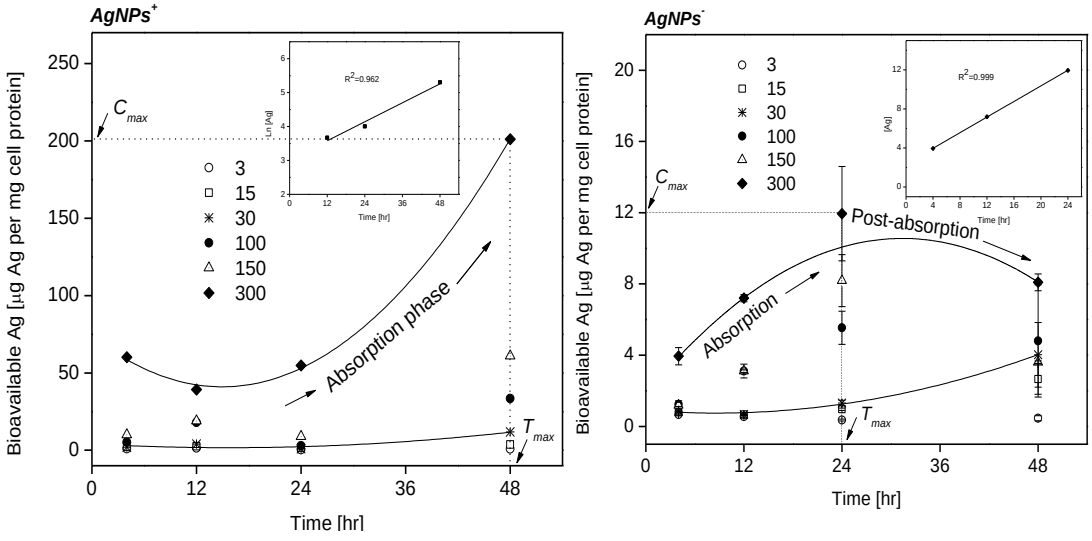

Figure 2.3: Bioavailability of Ag in Vero 76 cells exposed to $AgNPs^{+}$ and $AgNPs^{-}$ (3-300 µg mL^{-1}) for 4, 12, 24, and 48 hr. The error bars represent the standard error of N = 3 independent trials for each AgNP concentration and exposure time. For clarity purposes, absorption-time spline curves were shown for two representative sub-lethal and lethal concentrations (*i.e.,* 30 and 300 µg mL^{-1}). Insets show the ln [Ag] and [Ag] bioavailable concentration dependence on time for the absorption portion of the curves at 300 µg mL^{-1} of $AgNPs^{+}$ and $AgNPs^{-}$ exposure, respectively. $C_{maximum}$ and $T_{maximum}$ represent the concentration and time at which the maximum bioavailability was observed in cells in the measured time periods. The absorption and post-absorption phases of AgNPs are delineated by $T_{maximum}$.

To demonstrate the applicability of the ICP-OES-based methodology to different cell lines, we also investigated the uptake of $AgNPs^{+}$ at 20 µg mL^{-1} (< LC_{50}) in HEK293

cells after 4, 12, 24 and 48 hr of exposure (Figure 2.S11). HEK 293 cells followed a non-linear absorption of $AgNPs^{+}$, with a $C_{maximum}$ of 432±27 µg of Ag per mg of protein and a $T_{maximum}$ of 48 hr during the monitored time periods.

Overall, the results derived from the absorption-time curves demonstrate that the proposed ICP-OES-based methodology can be successfully applied to evaluate the efficacy of nanomaterial formulations in various biomedical applications (*e.g.*, drug delivery and imaging). Because both C_{maximum} and $T_{maximum}$ were different for $AgNPs^{+}$ and $AgNPs^{-}$, the two **AgNP formulations** were **not** deemed **bioequivalent** in Vero 76 cells. It is important to note that these parameters play a critical role in establishing the pharmacokinetic profile and the potency of drugs. Thus, results obtained through the ICP-OES-based methodology can shed further light on the biokinetic profile of nanomaterials.[91,92]

Distribution (D)

***CHSI*:** The enhanced dark-field optical images that were collected from live Vero 76 cells along with the hyperspectral profile of extracellular and intracellular AgNPs are shown in Figure 2.4. CHSI measurements may also be carried out on formaldehyde-fixed cells for longer, more detailed investigations (Figure 2.S12). Because AgNPs are in general better light scatterers than cells, sufficient contrast was obtained to demonstrate their cellular internalization. The cellular environment appeared as greyish-white, bright areas on a black background (Figure 2.4A and 2.4C). Bright, spherical spots were identified as extracellular AgNPs (mostly golden yellow –Figure 2.4A and2. 4B) or AgNPs alone controls (red-white, golden yellow, or green – Figure 2.4D), while the intracellular $AgNPs^{-}$ looked more faded in color, in general reddish-brown (Figure 2.4B).

In order to confirm the internalization of $AgNPs^-$, mean hyperspectral signatures were collected from the aforementioned spots on the sample and the corresponding controls (Figure 2.4E). These measurements also discarded the presence of false positive related to subtle color and shade variations. A significant change was noticed in between the spectral profiles of extracellular and intracellular AgNPs (Figure 2.4E). Extracellular AgNPs exhibited a strong scattering intensity, which dropped over 2.3-fold after cellular internalization. The scattering peak of extracellular AgNPs was located at about 600 nm, which is indicative of larger AgNPs probably comprising a protein corona and/or AgNP-aggregates [93] as also revealed by the UV-Vis absorption spectroscopy, DLS, TEM-EDX and Raman spectroscopy measurements.

The survey hyperspectral images also indicated that $AgNPs^-$ were broadly distributed both extracellularly and intracellularly. It is evident that 4 hr of exposure gave ample time to these $AgNPs^-$ to enter cells. In fact, the survey optical images showed that $AgNPs^-$ were spread throughout the live cellular environment at 4 hr. These observations are in good agreement with previous studies that indicated similar cellular entry and distribution trends of $AgNPs^-$ during the first 4 hr of exposure.[33,83] As expected, longer exposure times and the fixation of live cells led to the acquisition of CytoViva dark-field image images of higher quality and offered further details about AgNP distribution within cells. For example, HEK 293 cells exposed to 10 μg mL^{-1} of $AgNPs^+$ for ~ 24 hr showed that $AgNPs^+$ were widely distributed across the cells with distinct patterns of cellular entry/exit and sub-cellular localization (Figure 2.S13).

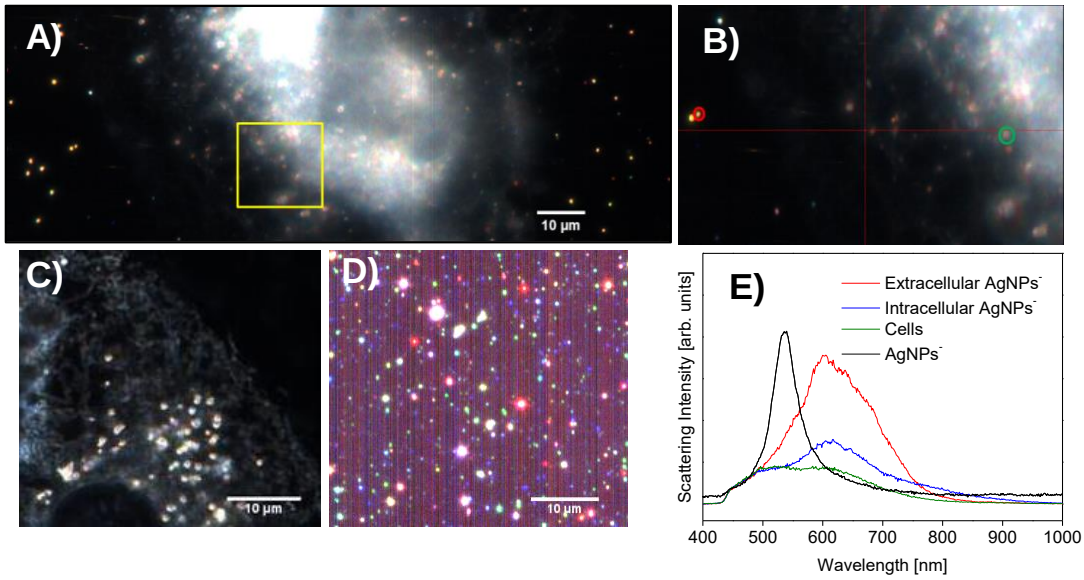

Figure 2.4: A) Enhanced dark-field image (60x magnification) of a single, live Vero 76 cell exposed to 100 µg mL^{-1} of $AgNPs^-$ for ~ 4 hr. Yellow square encloses a cellular area that was further zoomed in. B) Magnified optical image of the marked cytosolic area (yellow square, zoomed in 4x) showing the presence of extracellular (red circle) and intracellular (green circle) $AgNPs^-$ in cells. Control images (100x) of C) a fixed cell alone and D) AgNPs alone. E) Corresponding hyperspectral signatures of the circled areas along with controls indicating the internalization of $AgNPs^-$.

RHSI: Agglomerative hierarchical clustering analysis (AHCA) was performed on all Raman maps of single cells. Figure 2.5A and 2.5B displays the optical image of a Vero 76 cell, which was exposed to 100 µg mL^{-1} of $AgNPs^-$ for ~ 4 hr, and the pseudo-color cluster image (N =10 clusters) constructed from the Raman map of this cell. Equivalent images and Raman spectra for $AgNPs^+$ (Figure 2.S14) are given in Supporting Information together with the assignment of hierarchical clusters for both AgNPs (Table

2.S2). Control Raman spectra of cells without AgNPs or AgNPs alone on the coverslip exhibited only two broad bands characteristic to the glass coverslip (~1100 cm^{-1}) and phosphate buffer saline (PBS, ~1600 cm^{-1}) (Table 2.S2). In contrast, the Raman maps of cells exposed to AgNPs exhibited rich spectra of sharp, well-defined peaks as a result of the surface-enhanced Raman scattering (SERS) effect associated with internalized AgNPs. In SERS, molecules located nearby AgNPs or in the crevices of AgNP-aggregates are known to experience significant increases in Raman signal mainly due the increase in the magnitude of both the incident and the scattered electromagnetic fields resulting from the excitation of LSPR.[75,94-96] Thus, RHSI of single-cells comprising AgNPs can fingerprint molecules present in their immediate vicinity. AHCA of the Raman maps of Vero 76 cells exposed to AgNPs indicated that 10 distinct clusters accounted for more than 90% SERS data variance. The spectra associated with two representative clusters for $AgNPs^-$ (cluster 1 and 10) are also shown for illustrative purposes (Figure 2.5C and 2.5D). Each cluster is comprised of spectra groups of similar Raman peak signatures. Although the representative clusters of $AgNPs^+$ and $AgNPs^-$ shared similar Raman features, additional Raman peaks were noticed in the $AgNP^+$ clusters suggesting distinct sub-cellular distribution patterns. After 4 hr exposure, both AgNPs were present in the cytoplasmic matrix as confirmed by the similar Raman signatures characteristic to phosphodiesterases/RNA (811-813 cm^{-1}) and lipid droplets (1264, 1447 and 1657 cm^{-1}) (Table 2.S2). However, $AgNPs^+$ seemed to have accumulated to a larger degree at the plasma membrane than $AgNPs^-$. This preferential distribution of $AgNPs^+$ to the negatively charged cellular membrane was pointed out by the appearance of additional Raman peaks specific to phospholipids at 699, 957-960, 970,

1250-1350, and 1425-1475 cm^{-1} (Table 2.S2). This is not a surprising result taking into account the higher absorption levels of $AgNPs^{+}$ than $AgNPs^{-}$ at 4 hr exposure. Furthermore, Raman spectra associated with the $AgNP^{+}$ exposure had less noticeable sharp peaks beyond cluster 3. In contrast, even cluster 10 resulting from $AgNP^{-}$ exposure had clearly defined Raman peaks suggesting a wide distribution of $AgNPs^{-}$ throughout the cell as also revealed by CHSI.

The RHSI of HEK 293 cells exposed to 10 μg mL^{-1} of $AgNPs^{+}$ for 24 hr exhibited abundant phospholipid peaks at 693, 970, 1200-1350 cm^{-1} similarly to Vero 76 cells (Figure 2.S15). However, additional peaks at ~1369, 1500 and 1500-1550 cm^{-1} were also detected. These were attributed to sub-celluar regions such as the endoplasmic or golgi regions according to the literature.[57,58] This broader distribution was also seen in the CHSI of HEK 293 cells, most likely due to the longer exposure time (24 hr). The overall results indicate that the RHSI of single cells in conjunction with Matlab-based cluster analysis have the potential of examining the distribution of internalized AgNPs at the molecular level.

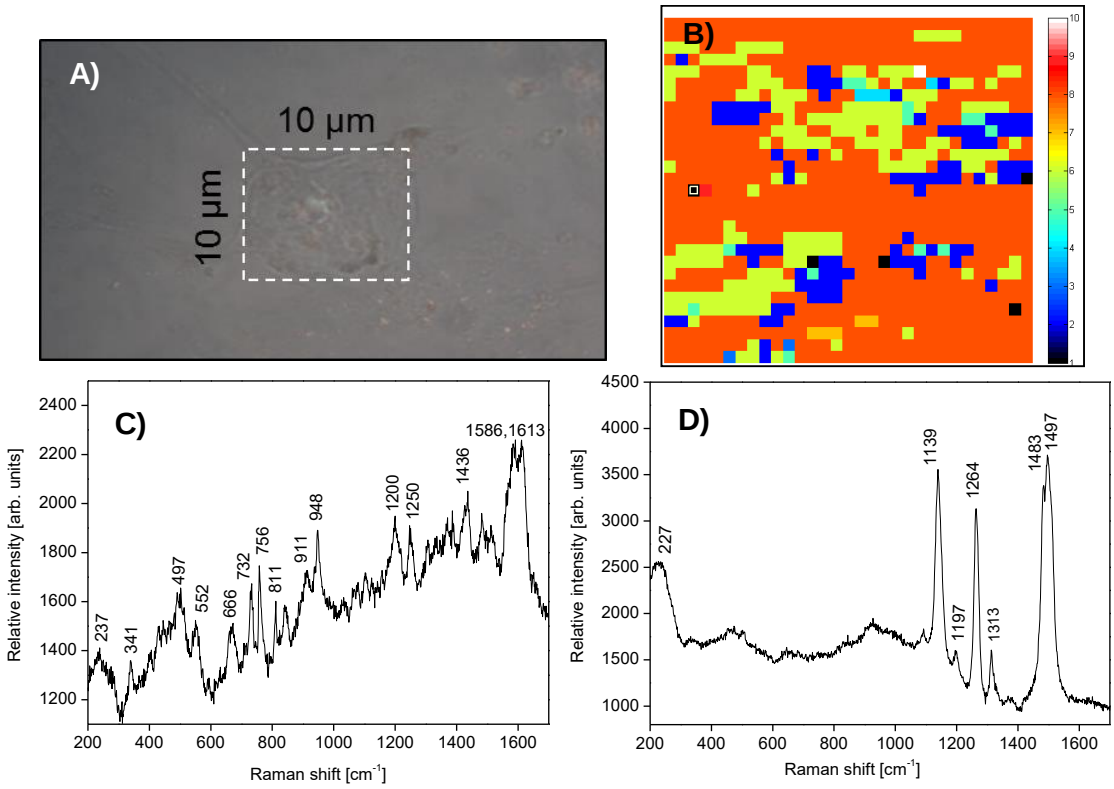

Figure 2.5: (A) Optical microscopic image of a single, fixed Vero 76 cell that was exposed to 100 µg mL^{-1} of $AgNPs^{-}$ for ~ 4 hr. Dotted white square encloses a cellular area that was mapped by Raman spectroscopy. (B) Pseudo-colored image that corresponds to the cluster distribution of the mapped area. C) and D) Raman signatures of cluster 1 and cluster 10, respectively, demonstrating the distribution of $AgNPs^{-}$.

Metabolism (M): In this section, we will demonstrate the efficiency of the CPE-TFF combination in separating the two metabolically active Ag species, namely AgNPs and Ag^{+}, from cellular matrices (Vero 76 and HEK 293 cells). For example, the CPE process that was performed alone on Vero 76 cells exposed to 30 µg $mL^{-1}$of $AgNPs^{-}$ for 24 hr had an efficiency of 52±9 %. This percentage was determined via ICP-OES measurements of

the TX-114 detergent phase rich in $AgNPs^-$ (Figure 2.6A) and corresponds to 149 ±5 ng of $AgNPs^-$ per 10^4 Vero 76 cells. The previously reported CPE value for HepG2 cells was 67.8 ng of PVP-coated $AgNPs^-$ per 10^4 cells exposed to 10 μg mL^{-1} for 24 hr.[48] The difference in the bioaccumulation levels in Vero76 and HepG2 cells is not surprising taking into account that different AgNPs, cell line types and administered AgNP concentrations were employed. It also should be noted that the total amount of Ag uptaken by HepG2 cells before CPE was calculated "as the sum of the Ag contents of the upper aqueous phase and the TX-114-rich phase"[48] obtained after CPE, which might have led to possible overestimations. In this study, the percentages of AgNPs and Ag^+ extracted from cells were normalized with respect to the actual amounts of Ag absorbed by cells that were measured by ICP-OES prior to performing CPE. Thus, Ag losses occurring during the extraction process were carefully considered by the difference between the actual amount of Ag uptaken by cells and the total amount of Ag retrieved in the extraction samples *via* ICP-OES. Furthermore, the addition of one 1-kD filtration step to CPE (Schematic 2.1) confirmed that the $Na_2S_2O_3$ aqueous phase rich in Ag^+ also contained a considerable amount of $AgNPs^-$. TFF further recovered 19±4% of the uptaken $AgNPs^-$ from the aqueous phase of CPE, thereby improving the overall extraction efficacy of AgNPs from 52±9% for CPE alone to 71±7% for CPE-TFF. TEM measurements also confirmed the physical presence of $AgNPs^-$ in the final 1 kD retentate resulting from the TFF-processing of the CPE aqueous phase (Figure 6B). It is important to note that 11±4% of the administered $AgNPs^-$ was oxidized to Ag^+ in the cellular environment (Figure 2.6A) and may have contributed to the cytotoxicity effects described below. Control experiments on both AgNPs alone showed that a) relatively small

amounts of Ag^+ (< 10%) were present in the concentrated stock colloid utilized in the cell culture experiments (10 kD retentate), and b) the CPE-TFF process did not induce significant ($p < 0.05$) transformations of AgNPs to Ag^+. By difference, a loss of 18±1% of Ag was estimated throughout the course of the CPE-TFF experiment, probably due to the interaction of $AgNPs^-$ with the extraction vessels, the filter membrane and/or the tubing of the TFF system.[58-60]

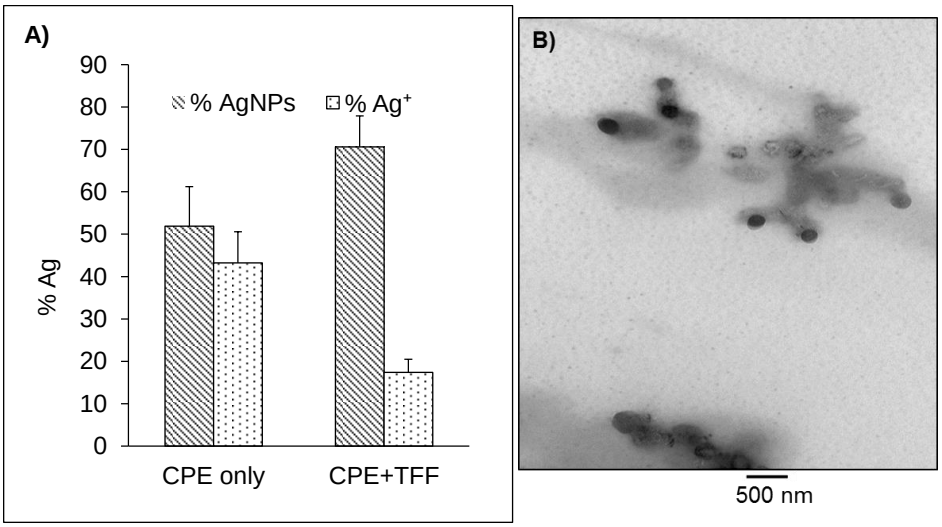

Figure 2.6: A) Percentages of the two Ag species ($AgNPs^-$ and Ag^+) isolated *via* CPE alone and CPE in combination with a one-step TFF (1 kD filter) as quantified by ICP-OES. All values were normalized to the total amount of Ag absorbed by cells prior to CPE. Error bars indicate the standard error of $N = 3$ independent trials. B) TEM micrograph of the 1 kD retentate depicting spherical $AgNPs^-$ (black) surrounded by TX-114 micelles in the detergent phase (greyish matrix) of the CPE-TFF process. The scale bar is 500 nm.

Similar CPE experiments conducted in HEK 293 cells exposed to 10 µg $mL^{-1}$of $AgNPs^{+}$ for 24 hr resulted in an extraction efficiency of 53±7 % (Figure 2.S16), which corresponds to 75.2 ±5 ng of $AgNPs^{+}$ per 10^{4} HEK 293 cells. As expected, the incorporation of a one-step TFF boosted the extraction efficiency to 83.1±5 % of $AgNPs^{+}$ and 8±1 % of Ag^{+}. It should be noted that the overall recovery was improved in HEK 293 cells compared to Vero 76 cells. This could be attributed to the presence of the additional CTAB-coating on the $AgNPs^{+}$, which might act like a surfactant and help extract further AgNPs from the aqueous phase. As a result, the overall Ag loss of the CPE-TFF process in HEK 293 cells (10±2 %) was also lower than in Vero 76 cells.

Cytotoxicity: A large variety of AgNPs were previously shown to interfere with the cellular metabolism due to their pronounced reactions with glutathione (GSH) and the antioxidant machinary[33]. Additionally, the cytotoxicity of AgNPs was commonly attributed to their interferences with several stages of the mitochondrial electron transport chain[33]. Hence, the *in vitro* metabolism of AgNPs was tested in this work using 3-[4,5-Dimethylthiazol-2-yl]-2,5- diphenyl tetrazolium bromide (MTT) and GSH assays in Vero 76 and HEK 293 cells (Figure 2.7 and Figure 2.S17, respectively).

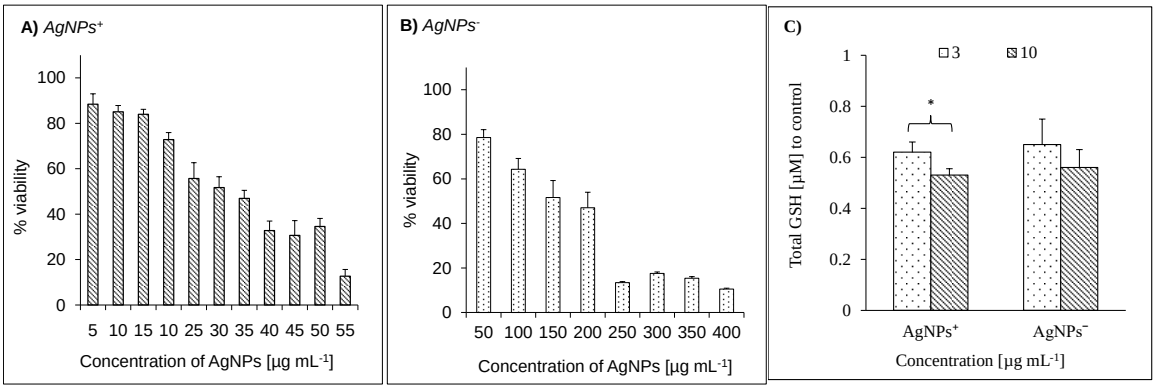

Figure 2.7: Percentage viability of Vero 76 cells (~10^4 cells per well) exposed to various concentrations of A) $AgNPs^+$ and B) $AgNPs^-$ for 24 hr *via* MTT assay. All results were plotted after subtracting the corresponding absorbance values of the blanks (media + AgNPs) and then normalizing to the absorbance of untreated cells. C) Total GSH levels in Vero 76 cells exposed to both types of AgNPs at 3 and 10 μg mL^{-1} for 24 hr. All GSH results (μM) were normalized to the corresponding control cell values (untreated cells). '*' indicates the presence of statistical significance among the two $AgNPs^+$ concentrations ($p < 0.05$, 1-way ANOVA). In all plots, error bars indicate the standard error of $N = 3$ independent trials. The error bars for some AgNP concentrations are too small in values to be clearly visible.

Although it is a common practice to measure % viability of cells by MTT, the cellular reduction of the tetrazolium salt also depends on the presence of nicotinamide adenine dinucleotide phosphate (NAD(P)H), which is an important cofactor in several oxidation-reduction (*e.g.,* electron transport chain and GSH regeneration) and biosynthetic reactions (*e.g.,* lipid synthesis).[97] Thus, this colorimetric assay also serves as an indirect indicator of the metabolic activity of cells.[97,98] The MTT assay results suggest that the metabolic activity of Vero 76 cells was influenced by the AgNP surface charge (Figure 2.7A and 2.7B). The 50% cell viability level was ~ 4-fold higher for $AgNPs^-$ (LC_{50} = 125 ± 4 μg mL^{-1}) than $AgNPs^+$ (LC_{50} = 32 ± 2 μg mL^{-1}). This is probably due to the larger cellular internalization of $AgNPs^+$ as a result of their pronounced electrostatic interactions with the negatively charged moieties of the plasma membrane (-70 mV) and other sub-cellular regions *(e.g.,*-120 mV of mitochondria).[58,99] The LC_{50} of $AgNPs^+$ in

HEK 293 cells was found to be 26 ±3 μg mL^{-1}, which was slightly lower than the LC_{50} value of Vero 76 cells (Figure 2.S17). This suggests that human cells could be more susceptible to the nanotoxic effects of AgNPs than murine cell lines.

AgNPs are known to induce oxidative damage to cells, which in general they combat it by deploying intracellular antioxidant. [87,100] GSH is one of the important thiol-containing tripeptides that maintains cells in a reduced environment and participates to the cellular antioxidant defensive mechanisms. [100] As shown in Figure 2.7C, both types of AgNPs depleted the total GSH content in Vero 76 cells, which indicates a possible interference with the redox state of the cell and the further induction of oxidative stress. No significant differences ($p < 0.05$) were seen between the GSH levels of all exposures to $AgNPs^-$ at a specific concentration. However, there was significant decrease ($p < 0.05$) in the GSH levels with the increase in AgNP concentration from 3 μg mL^{-1} to 10 μg mL^{-1}. For example, the total amount of normalized GSH was ~1.2-fold lower in cells exposed to 10 μg mL^{-1} than to 3 μg mL^{-1} of $AgNPs^+$. HEK 293 cells exposed to sub-lethal concentrations of $AgNPs^+$ (3 and 10 μg mL^{-1}) exhibited similar trends (Figure 2.S17). Specifically, GSH was depleted ~1.5-fold at 10 μg mL^{-1} of $AgNPs^+$ exposure compared to 3 μg mL^{-1} exposure.

Elimination I: While the cellular absorption of AgNPs is of great importance for therapeutic applications such as the development of effective drug carriers or antimicrobials, the cellular elimination of AgNPs holds tremendous value in the removal of bioimaging agents or clearable drugs after delivery and their dosing frequency.[53] In spite of its importance, the cellular elimination of AgNPs and their speciation were vaguely explored due to the limited capabilities of the existing methodologies. [36,65] In this

section, we will demonstrate how the same ICP-OES- and CPE-based methodologies, which were employed for examining the absorption behavior of AgNPs and their oxidation within cells, may also be implemented for probing their release profile. Figure 2.8 shows the elimination curves of Vero 76 cells exposed to exposed to sub-lethal concentrations of $AgNPs^{+}$ (30 μg mL^{-1}) and $AgNPs^{-}$ (100 μg mL^{-1}) for 24 hr. Sub-lethal AgNP concentrations were chosen in order to minimize possible interferences from AgNP toxicities (*e.g.*, membrane disruption and mitochondrial damage),[31] while studying their kinetic behavior. The total Ag cleared by cells was quantified after replenishing media (no AgNPs) and was normalized to the corresponding cellular protein content before plotting it as a function of time at 1, 4, 12, and 24 hr (Figure 2.8). Similar to most pharmaceuticals, both $AgNPs^{+}$ and $AgNPs^{-}$ were found to follow first-order elimination kinetics with comparable rate constants (k_{eli}) of 0.039 hr^{-1} and 0.038 hr^{-1}, respectively. This suggests that even though the absorption of AgNPs was surface charge-dependent in Vero 76 cells, their elimination may be solely dependent on the concentration of the total bioavailable Ag. In other words, the elimination rate of AgNPs decreases linearly with the decrease in the concentration of bioavailable AgNPs. As expected, the initial cleared concentration of Ag (*i.e.*, $[Ag]_0$) was larger for $AgNPs^{+}$ than $AgNPs^{-}$, for which the absorption $C_{maximum}$ was over 2-fold greater at 30 μg mL^{-1} of $AgNPs^{+}$ exposure. The corresponding half-lives ($t_{1/2}$) of $AgNPs^{+}$ and $AgNPs^{-}$ were estimated to be 17.7 hr and 18.2 hr, respectively. These values are comparable to those determined in mouse models exposed to PEG-coated nanoparticles.[101] It is in general accepted that drugs have no longer a pharmaceutical effect after 4 half-lives[92] Thus, steady-state may be attained for these AgNPs in Vero 76 cells after 71-73 hr.

In order to quantitatively distinguish the eliminated Ag species, the CPE-based isolation methodology was performed on aliquoted samples that were collected from Vero 76 cells 24 hr post AgNP-exposure. For example, in case of $AgNPs^{+}$, 11.6±6.1% and 85.6±3.6% of the total Ag eliminated was found to exist as Ag^{+} and $AgNPs^{+}$, respectively. The high $AgNPs^{+}$ percentage suggests that the elimination process might be mainly exocytosis-driven; however, diffusion-based elimination of $AgNPs^{+}$ cannot be ruled out.[84,102]

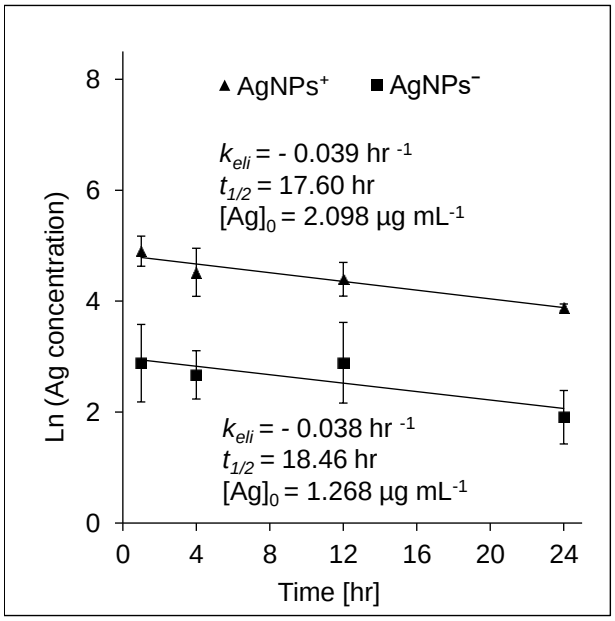

Figure 2.8: Clearance of Ag (µg Ag per mg of protein) from Vero 76 cells exposed to sub-lethal concentrations of $AgNPs^{+}$ (30 µg mL^{-1}) and $AgNPs^{-}$ (100 µg mL^{-1}) for 24 hr. The ICP-OES measurements of total Ag were carried out at 1, 4, 12, and 24 hr after replenishing the media (no AgNPs). The bars represent the standard error of N =3 independent trials for each elimination time. The error bars for some concentrations might be too small in values to be clearly visible.

In contrast to Vero 76 cells, the elimination process in HEK 293 cells exposed to 20 μg mL^{-1} of $AgNPs^{+}$ followed zeroth-order kinetics and therefore, was independent of the administered concentration (Figure 2.S18). The corresponding $t_{1/2}$ *and* k_{eli} values were 73 hr and a 0.057 μg mg $protein^{-1}$ hr^{-1}, respectively. Although it is rarely seen, the half-lives of drugs that follow zeroth-order elimination increase with the administered dose. It can be recalled that there was non-linear absorption in HEK293 cells at the same administered concentration. Thus, unlike Vero76 cells, HEK293 cells may experience Ag saturation and subsequent constant clearance at this sub-lethal concentration (20 μg $mL^{-1}$of $AgNPs^{+}$).[103]

CONCLUSIONS

This works demonstrates the capabilities of the newly adapted analytical-based methodologies in examining ADME aspects of AgNPs in *in vitro,* adherent models. Future challenges may arise when dealing with suspension of cell lines, but could be addressed through modified cell harvest procedures and rigorous characterization of the interaction between NPs and culture media. Due to the flexibility of the proposed methodologies, nanokinetics of a large variety of metallic NPs may also be investigated. More specifically, ICP-OES covers a great number of metals on the periodic table, while commercially available TFF filters and CPE chelating agents can be selected to suit most metallic NPs of interest. In addition, ICP-OES can be used for either the sequential or simultaneous detection of metals in a variety of biological or environmental matrices. While CHSI can identify and map the nano-distribution of any light scattering agents, RHSI can interrogate in a label-free manner the immediate biomolecular environment of diverse NPs (*e.g.*, Au, Cu, Zn, Si, TiO_2, and so on). For example, the proposed

methodologies could be extended to the following biological or environmental scenarios: drug-release kinetics from nano-vehicles, identification and quantification of metallic NPs and their possible ionic byproducts in consumer products (*e.g.*, wound dressings, tablet-coatings or sunscreens), transformation of metallic NPs in biological fluids (*e.g.*, urine, saliva, and blood), and so on. Overall, this study covers several fundamental knowledge gaps by demonstrating the applicability of the proposed analytical-based methodologies to the risk assessment and control associated with the heavy use of nanomaterials in biomedical and environmental settings.

ACKNOWLEDGEMENTS

The U.S. National Science Foundation Award #1438340 is highly acknowledged. The authors acknowledge A. Kozak at WSU for his generous donation of HEK 293 cell line. The authors thank N. Adragna for the use of the Multi-skan transmit reader in her research laboratory at WSU and the helpful discussions. G. Vanness and J. Solch are acknowledged for their assistance with the maintenance and operation of the Varian 710-ES ICP-OES system at WSU. B. Cheatham, S. Mills, E. V. Johnson, and R. Eby from CytoViva Inc (www.cytoviva.com) are thanked for their help with the collection and analysis of the presented CytoViva data at WSU and at CytoViva Inc. in AL. The authors thank WSU graduate students: D. Foose for his guidance in Matlab-based analysis of Raman maps and S. Brittle for the scientific discussions on the ICP-OES and CPE data analysis. The manuscript was written through contributions of all authors. All authors have given approval to the final version of the manuscript.

SUPPORTING INFORMATION

Tangential flow filtration (TFF) of AgNPs

Schematic 2.S1 illustrates the steps involved in the filtration of original colloidal $AgNPs^-$ using a Spectrum Labs system. Briefly, colloidal $AgNPs^-$ were first passed through a 500 kD membrane filter. The resulting 500 kD permeate was then pumped through a 10 kD membrane filter. The final 10 kD retentate (10 kD ret) was used as $AgNP^-$ stock for cell culture experiments.

Schematic 2.S1: Two-step TFF of $AgNPs^-$ through 500 kD and 10 kD mPES filter modules.

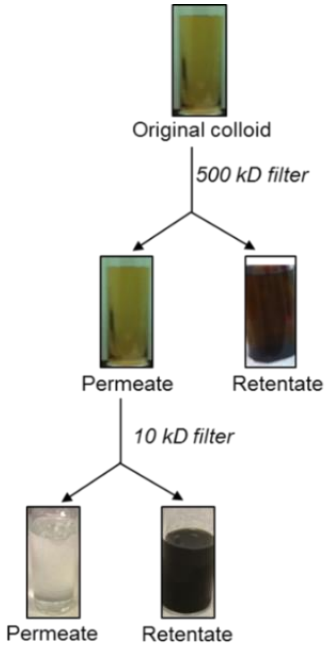

The inset vial pictures show aliquots of the corresponding permeates and retentates.

ICP-OES analysis

Method detection limit (MDL): The *MDL* of the ICP-OES instrument was determined by measuring the lowest Ag standard (5 µg L^{-1}) $N = 9$ independent times with the main emission line for Ag at 328.068 nm. The resultant *MDL* and the standard error were found to be 2.95 ± 0.6 µg L^{-1}. Thus, all the ICP-OES measurements (standards and sample dilutions) were conducted after considering the *MDL* value.

Relative percent differences (RPD): The presence of matrix effects was tested by comparing the *RPD* in the Ag concentrations obtained by the external calibration and standard additions. The resultant *RPD* was < 10%, which was within the EPA acceptable limits for quality control.[104] This suggested the use of the external calibration method for the Ag analysis in all samples. Briefly, *RPD* was calculated by dividing the absolute difference of Ag concentration derived from both methods with the average Ag concentration from the two methods (eq. 2.S1).

$$\boldsymbol{RPD} = \left| \frac{[Ag]Ext.\ cal - [Ag]Std.\ addn}{Average\ ([Ag]Ext.\ cal\ ,\ [Ag]Std.\ addn)} \right| \times 100\ \% \qquad (2.S\mathbf{1})$$

Transmission electron microscopy (TEM) analysis

AgNP samples (10 µL) were deposited on carbon-coated copper grids (Electron Microscopy Sciences) and dried in a desiccator. The highly concentrated retentates were diluted with water (1:10 v/v) prior to deposition and measurements at 70 kV using a high resolution Gatan Bioscan camera (Philips EM 208S). The collected images were imported into ImageJ 1.46R (Media Cybernetics Inc.) for further analysis. Only particles with a complete enclosed circumference were considered for counting in the construction of the TEM size histograms. To differentiate the light background from the dark AgNPs,

automated count settings were used. A minimum of N = 600 particles per sample were analyzed and the average particle diameter was estimated. The final size histograms were constructed in Origin 8 software.

Bioassays

Bicinchoninic acid assay (BCA): The total protein content in Vero 76 and HEK 293 cells was determined based on the general ability of proteins to reduce cuprous ions under alkaline conditions. Briefly, fresh reagent mix (reagent A: reagent B in 50:1 v/v) and bovine serum albumin (BSA) standards were prepared as recommended from a stock ampoule (2 mg mL^{-1}). Cells alone were used to analyze the total protein concentration at all exposure times (4, 12, 24, and 48 hr). Media from culture plates was removed and cells were washed thrice with PBS. The total protein present in the corresponding media portions were analyzed similarly. To dissolve the proteins, cells were incubated with 1 mL of sodium hydroxide (NaOH, 1 x 10^{-3} M) for 30 min at room-temperature. Following this, 1.25 x 10^{-2} mL of samples or standards were added to the 96-well plate. Then, 0.1 mL of reagent mix was added to each well and the plate was placed in incubator for 30 min. The absorbance was recorded using a Multi-skan transmit reader at 540 nm. A calibration curve was constructed by plotting the optical density (OD) values as a function of the concentration of BSA standards, and the total protein content was interpolated from the curve.

MTT assay: The percentage cell viability of cells exposed to AgNPs was measured following standard protocols. Briefly, 10^4 cells per well were seeded in 96 well plate and were exposed next day to controls, blanks, $AgNPs^+$ (0-60 µg mL^{-1}) and $AgNPs^-$ (0-400 µg mL^{-1}) for 24 hr. Negative and positive controls comprised of untreated cells and cells

treated with 1%v/v triton X, respectively. Blanks comprised of wells with similar concentrations of AgNPs in media. Following the exposure, all supernatant media was replaced with fresh media containing MTT reagent in PBS (30 µg mL^{-1}) and incubated for 4 hr. The formazan crystals were dissolved in dimethyl sulfoxide (DMSO, 100µL) and the absorbance was measured at 570 nm using a Cary 50-Multi Plate Reader (Cary 50-MPR). To obtain the % viability, the absorbance of blanks was first subtracted from that of samples. The resultant value was then divided by the absorbance of negative control (untreated cells) and multiplied by 100.

GSH assay: The metabolic state of cells was determined by measuring the total GSH of cells exposed to 3 and 10 µg $mL^{-1}$of AgNPs for 24 hr. Briefly, cells were grown in 12-well plates to 80% confluency and were exposed to $AgNPs^{+}$ or $AgNPs^{-}$ for 24 hr. Cells were then washed thrice in PBS, harvested using a cell-scraper and centrifuged at 200 g for 5 min. Cell lysates were obtained by dispersing pellets in 1 mL of 1% triton lysis buffer on ice and centrifuging at 10,000 g for 15 min. In order to remove proteins from cell lysates, 0.6 mL of 10% trichloroacetic acid was added to 0.6 mL supernatant and the mixtures were centrifuged at 2,000 g for 10 min. For the GSH analysis, 25 µL of the collected supernatants and standards were transferred to a 96-well plate, and 75 µL of freshly prepared assay cocktail mixture was added to each well. The plate content was allowed to mix on an orbital shaker in dark for 10 min and the OD values were measured using a plate reader (Cary Eclipse) at 414 nm. Total GSH in the samples (in µM) was interpolated from the external calibration curve and normalized to the control (*i.e.,* GSH of the untreated cells).

Characterization of AgNPs

Extinction spectra of AgNPs: The formation of spherical $AgNPs^{+}$ and $AgNPs^{-}$ in the original colloids (denoted Ori) was confirmed by the presence of a single localized surface plasmon resonance peak (LSPR) at ~400 nm.[66,61] The extinction spectra of the final TFF-retentate (denoted 10 kD ret) showed that the plasmonic properties of $AgNPs^{+}$ and $AgNPs^{-}$ were maintained after their TFF-manipulation for cellular experiments (Figure 2.S1). However, changes in the spectral profile of the LSPR peaks were noticed as a result of the significant increase in AgNP concentrations and the narrower size distribution. For instance, TFF-processed $AgNPs^{-}$ exhibited a 40-fold increase in LSPR maximum (from 0.8 to 3.2 arbitrary units) and the full-width-at-half-maximum (FWHM) decreased from 47 nm to 23 nm. These properties were more accurately quantified by ICP-OES and TEM.

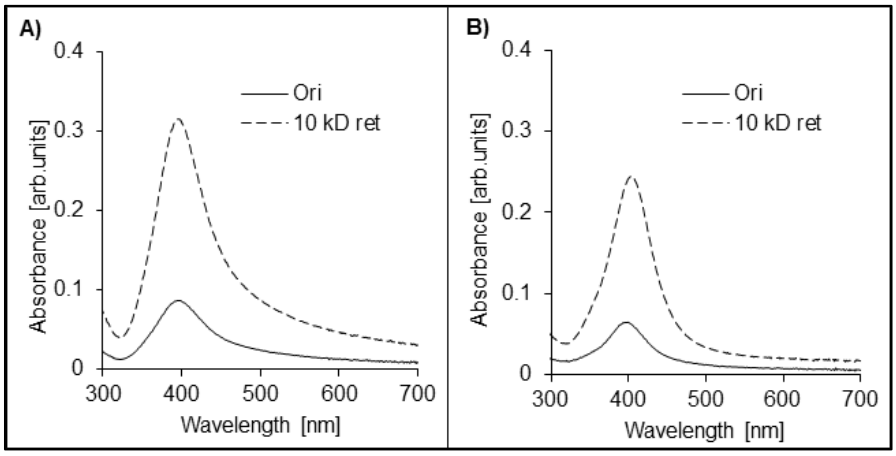

Figure 2.S1: UV-Vis absorption spectra of the colloids before (Ori) and after tangential flow (TFF) filtration processing (10 kD ret): A) $AgNPs^{+}$ and B) $AgNPs^{-}$.

ICP-OES: The total concentration of Ag in each colloidal sample was determined by ICP-OES through interpolation from the external calibration curve (Figure 2.S2), which

was constructed using six Ag^+ standards of 0, 100, 200, 400, 600 and 800 µg L^{-1} (*R^2* of 0.9996). The total Ag concentration of 10 kD ret was 2-fold and over 60-fold higher for $AgNPs^+$ (730.1 µg mL^{-1}) and $AgNPs^-$ (720.6 µg mL^{-1}), respectively, than that of Ori (Table S1). The relative percent differences for the Ag concentrations (*RPD* = 2.236±0.6 for $AgNPs^+$ and 1.687±0.4 for $AgNPs^-$) obtained by the external calibration method and the standard additions method were within the EPA recommended limits,[104,52] which confirmed the absence of matrix effects.[104] In our previous TFF work, it was demonstrated that TFF can also facilitate the elimination of byproducts and excess reagents, thereby, purifying the final retentate of AgNPs.[105] For example, the Na content of an original Creighton colloid of AgNPs decreased from 40.5±9.8 µg mL^{-1} to 18.6±1.4 µg mL^{-1} in a TFF process employing 50 nm and 30 kD retentate filters.[105] Although the Na levels of the colloidal samples in this project were negligible in comparison with those of the cell culture media (*e.g.*, > 100 mM in typical DMEM or ~3.5 g L^{-1} in the form of sodium bicarbonate), future nanotoxicity and bioimaging studies should consider minimizing the amount of detrimental excess reagents and byproducts of the stock colloids of NPs.

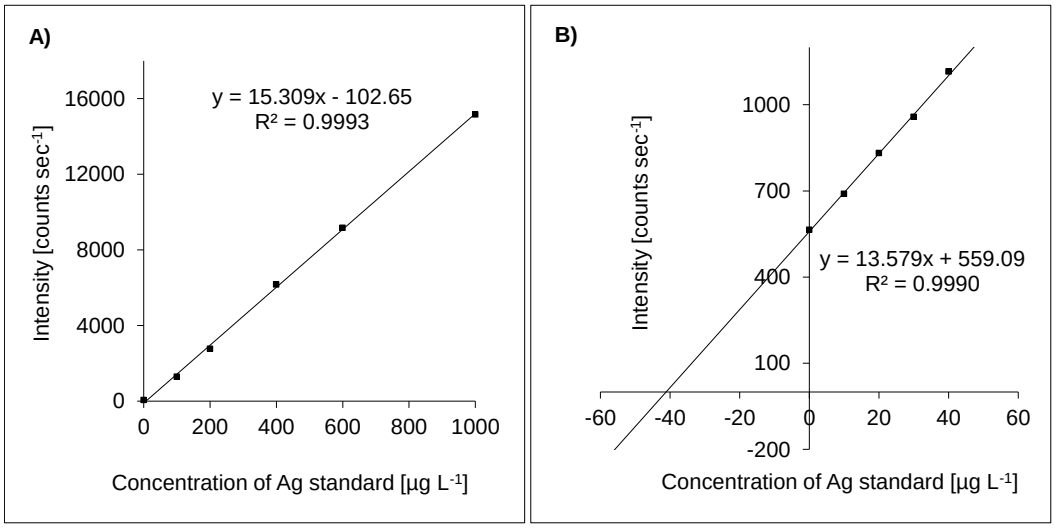

Figure 2.S2: ICP-OES quantification of total Ag in Creighton colloids of $AgNPs^-$ using the: A) external calibration and B) standard additions curves. Six standards in the 0-800 µg L^{-1} range were employed.

Table 2.S1: The total Ag concentration in the original colloid (Ori) and the final 10 kd retentate of AgNPs (10 kD ret), and the relative percent differences (*RPD*s) in between the external calibration and standard additions results as determined by ICP-OES.

Sample	**[Ag] in Ori (µg mL^{-1})**	**[Ag] in 10 kD ret (µg mL^{-1})**	***RPD* for 10 kD ret**
$AgNPs^+$	300.6	730.1	2.236±0.6
$AgNPs^-$	10.70	720.6	1.687±0.4

Raman spectroscopy: As shown in Figure S3, only three peaks characteristic to the bending (1642 cm^{-1}) and stretching (3240-3420 cm^{-1}) vibrational modes of H_2O were detected in the Raman spectra of colloidal samples.[61,62,75] Thus, the presence of any major organic impurities in the colloidal AgNPs or at their surface was dismissed.

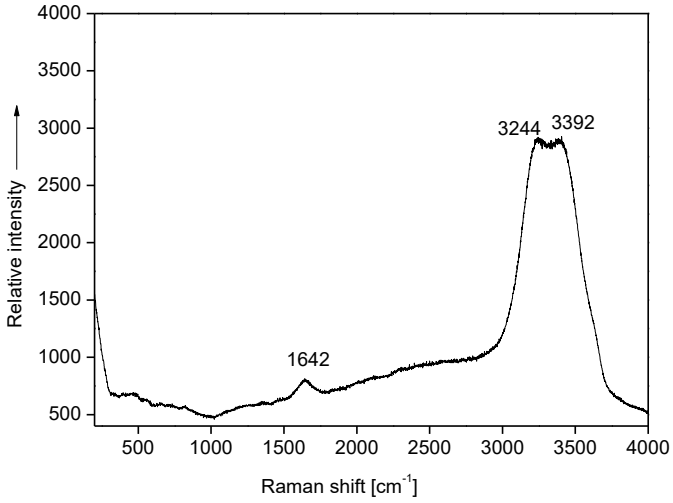

Figure 2.S3: Raman spectra of colloidal $AgNPs^-$ demonstrating colloidal purity. The three peaks at 1642 and 3244-3392 cm^{-1} mark the bending and stretching modes of water, respectively.

Absorption spectra of AgNPs in media

The pronounced interactions of AgNPs with proteins present in biological media affects their cellular entry through the formation of protein corona (PC). In a study by Shannahan *et al.*, serum albumin present in the culture media was shown to be one the most abundant proteins present on the PC of AgNPs.[86] They also revealed that hydrophobic and electrostatic interactions exist in AgNP-PC, but their dominance depends on the surface chemistry of AgNPs (*e.g.*, surface coating, shape, charge, and size). For instance, $AgNPs^-$ were found to attract more amphiphilic protein moieties than $AgNPs^+$. It was also shown that the presence of PC protects the surface of NPs, thereby decreasing the cellular toxicity.[106,107] Thus, it can be inferred that AgNPs interact with

media components, which in turn influences their fate and biological effects. $AgNPs^{+}$ have an additional layer of CTAB coating on their surface, which limits the available area for protein interactions. In contrast, $AgNPs^{-}$ have more chances to offer free surface for the proteins and facilitate the formation of PC due to the easily displaceable layer of $B(OH)_3$ present at their nanosurface. Figure 2. S4 shows changes observed in the absorption spectra upon 24 hr incubation of media components with 300 µg mL^{-1} of $AgNPs^{+}$ and $AgNPs^{-}$. In agreement with previous reports, the initially diminished LSPR peak in DMEM alone (Figure 2.S4A and 2.S4C) was recovered in the presence of serum proteins in media (Figure 2.S4B and 2.S4D), which is indicative of colloidal stability.[85] These results outline the importance of studying the distribution of AgNPs in the biological environment prior to their *in vivo* application.

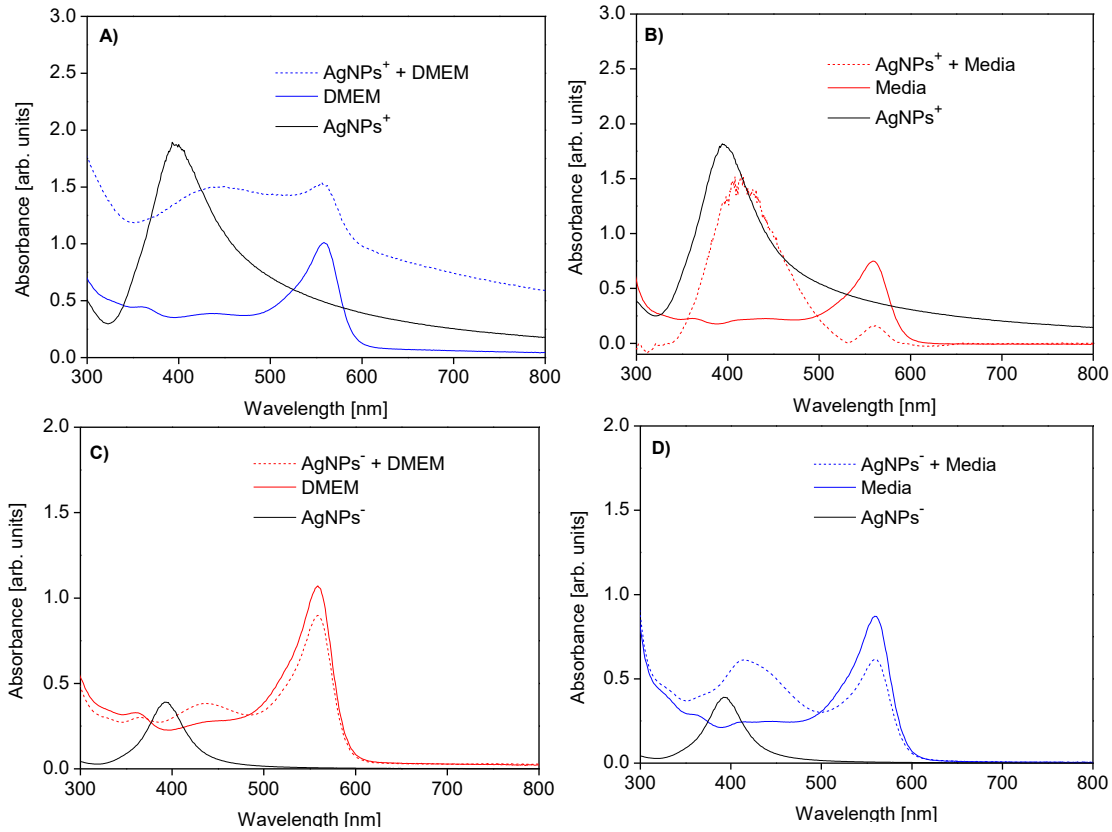

Figure 2.S4: UV-Vis absorption spectra of DMEM alone (A and C) and DMEM media (B and D) incubated with 300 μg mL^{-1} of AgNPs for 24 hr.

Figure 2.S5 and 2.S6 show the UV-VIS absorption spectra collected during the incubation of both $AgNPs^{-}$ and $AgNPs^{+}$ (10 μg mL^{-1}) with the inorganic salts present in the cell culture media (DMEM and RPMI) as a function of time (0, 4, 12, 24, and 48 hr) and salt concentrations (1x and 0.5x media concentrations). The UV-Vis absorption spectra collected during the experiments (Figures 2.S5 and 2.S6) showed significant broadening and decrease in the intensity of LSPR peaks with the increase in incubation time (from 0 to 48 hr) or salt concentration (from 0.5x to 1x). For example, 10- and 100-fold decreases in relative intensity of the LSPR peaks were observed after 24 hr exposure of $AgNPs^{+}$ and $AgNPs^{-}$, respectively, to DMEM salts (1x) (Figure 2.S5). Also, the LSPR intensity changes were 2-fold and 20-fold lower at 1x than 0.5x DMEM salt concentrations for $AgNPs^{+}$ and $AgNPs^{-}$, respectively (Figure 2.S6). Furthermore, the LSPR peaks of AgNPs became insignificant or disappeared after 48 hr possibly due to their salt-induced precipitation and/or dissolution as previously reported for commercially available AgNPs.[108] However, the formation of a protein corona in whole media seems to increase AgNP stability and thereby to counteract the salt effects at longer incubation times (24 hr) and higher salt concentrations (1x). For example, no major flocculation or dissolution was noticed after AgNPs' incubation for 24 hr with whole DMEM media (Figure 2.S4).

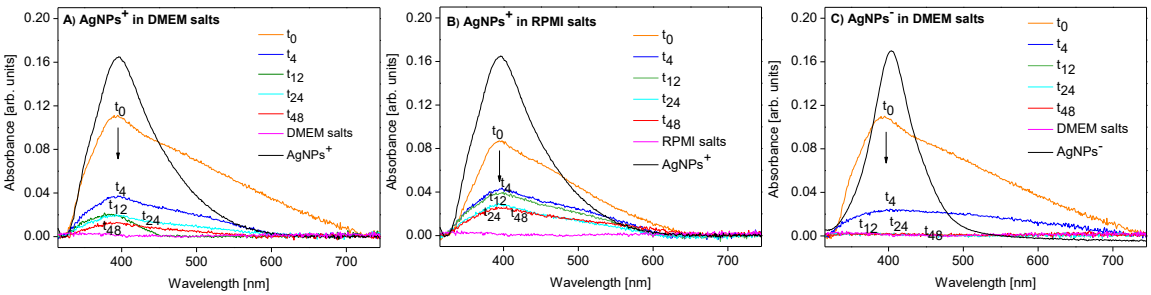

Figure 2.S5: UV-Vis absorption spectra of 10 µg mL^{-1} of AgNPs incubated with the salts present in the cell culture media (at the same concentration, 1x) as a function of time (0-48 hr). A) $AgNPs^{+}$ in DMEM salts ($CaCl_2$, KCl, $MgSO_4$, NaCl, and NaH_2PO_4 H_20), B) $AgNPs^{+}$ in RPMI salts (KCl, $MgSO_4$, NaCl, $NaHCO_3$, and NaH_2PO_4), and C) $AgNPs^{-}$ in DMEM salts.

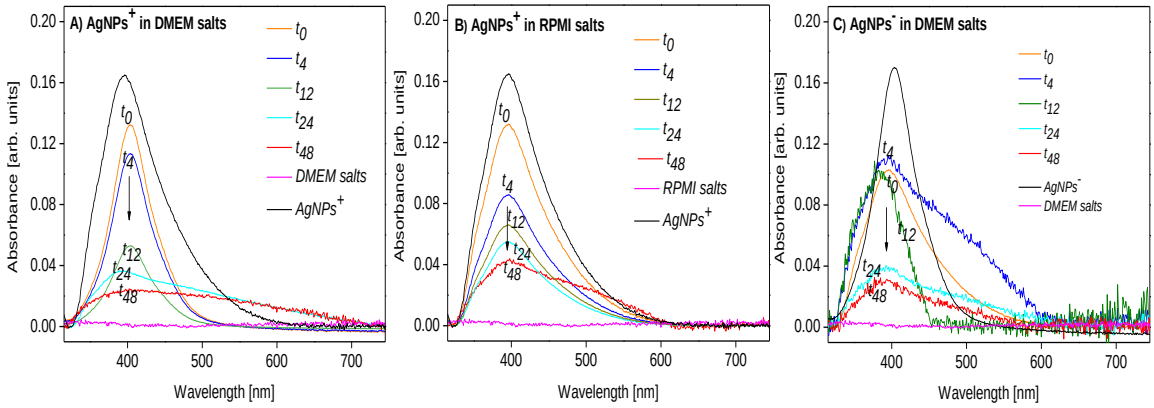

Figure 2.S6: UV-Vis absorption spectra of 10 µg mL^{-1} of AgNPs incubated with the salts present in the cell culture media (0.5x concentration) as a function of time (0-48 hr). A) $AgNPs^{+}$ in DMEM ($CaCl_2$, KCl, $MgSO_4$, NaCl, and NaH_2PO_4 H_20), B) $AgNPs^{+}$ in RPMI, and C) $AgNPs^{-}$ in DMEM (KCl, $MgSO_4$, NaCl, $NaHCO_3$, and NaH_2PO_4).

To understand the colloidal dispersity in cell culture media, the hydrodynamic diameters of AgNPs were measured by dynamic light scattering (DLS). The final concentration of $AgNPs^{+}$ and $AgNPs^{-}$ in DMEM and RPMI cell culture media was 10 µg mL^{-1} (Figure 2.S7). The hydrodynamic diameters of $AgNPs^{-}$ were found to experience an over 4-fold increase in cell culture media. In addition, the mixing of $AgNPs^{+}$ with DMEM and RPMI led to the appearance of a second, broad DLS peak in the 1240-3220 nm and 130-1290 nm size range, respectively. Thus, the UV-Vis absorption and DLS results suggest that in culture media, AgNP-agglomeration and –size increase dominate over the salt-induced AgNP dissolution, which previous studies considered an indicator of protein corona formation.[86,109]

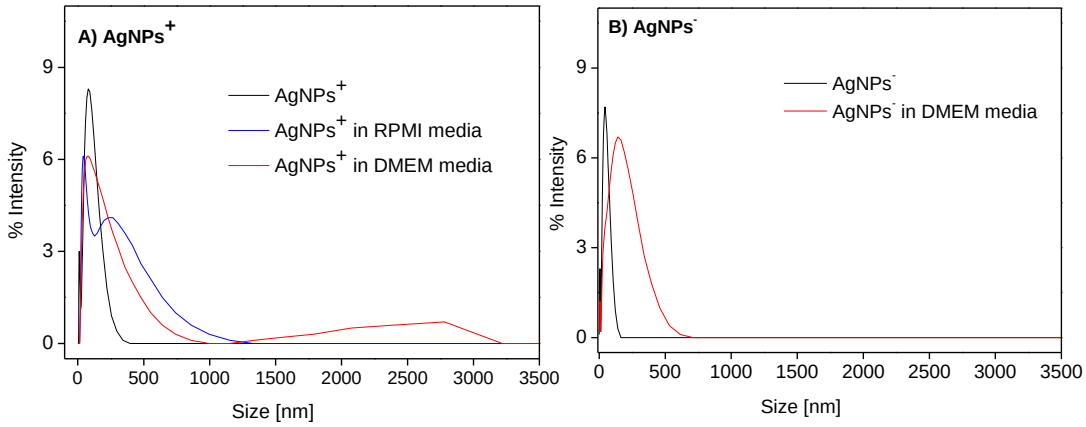

Figure 2.S7: Dynamic light scattering (DLS) results showing the intensity-based size distribution of AgNPs alone and in the cell culture media (DMEM and RPMI): A) $AgNPs^{+}$ and B) $AgNPs^{-}$. Each spectrum represents the average of N = 100 measurements.

TEM-EDX recordings on both AgNPs mixed with cell culture media further clarified these aspects (Figure 2.S8). The TEM-EDX data revealed: a) the agglomeration

of AgNPs around salt crystals (*e.g.*, Ag, Na, K, Ca, and Cl) and b) the formation of protein corona around AgNPs in different media, *i.e.*, DMEM and RPMI samples (*e.g.*, Ag, C, and O).

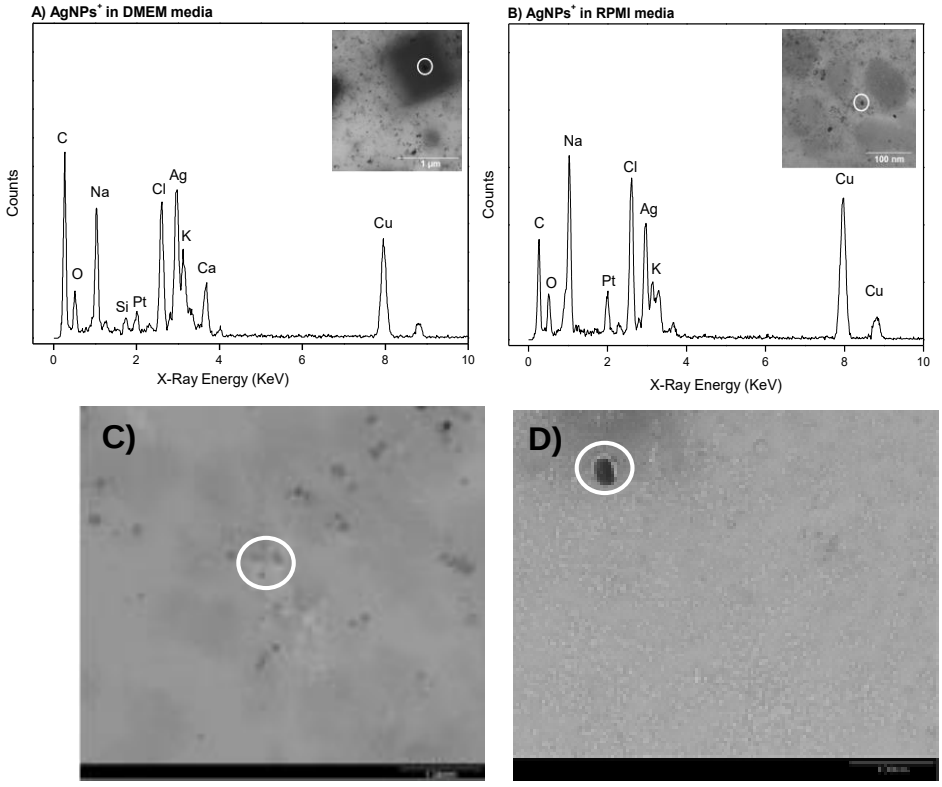

Figure 2.S8. TEM-EDX spectra of 10 µg mL^{-1} of $AgNPs^{+}$ incubated with A) DMEM and B) RPMI cell culture media for 1 hr. The insets display the TEM images from which spectra were acquired (white circle). The presence of C, Si, Pt, and Cu in the EDX spectra are from the TEM grids. C) and D) images illustrate the protein corona formation in DMEM and RPMI media, respectively (white circles). Scale bars are A) 1 µm and B), C, and D) 100 nm.

ADME of AgNPs

Absorption:

Vero 76 cells: ICP-OES measurements on the extracellular matrix (Figure 2.S9) revealed that 45-90% and 20-95% of the administered $AgNPs^{+}$ and $AgNPs^{-}$, respectively, were still present in the media after the cell harvest. As demonstrated by the SEM-EDX analysis of the cell culture plates, the remaining portion of AgNPs may have adsorbed on the walls of the cell plates (Figure S10).

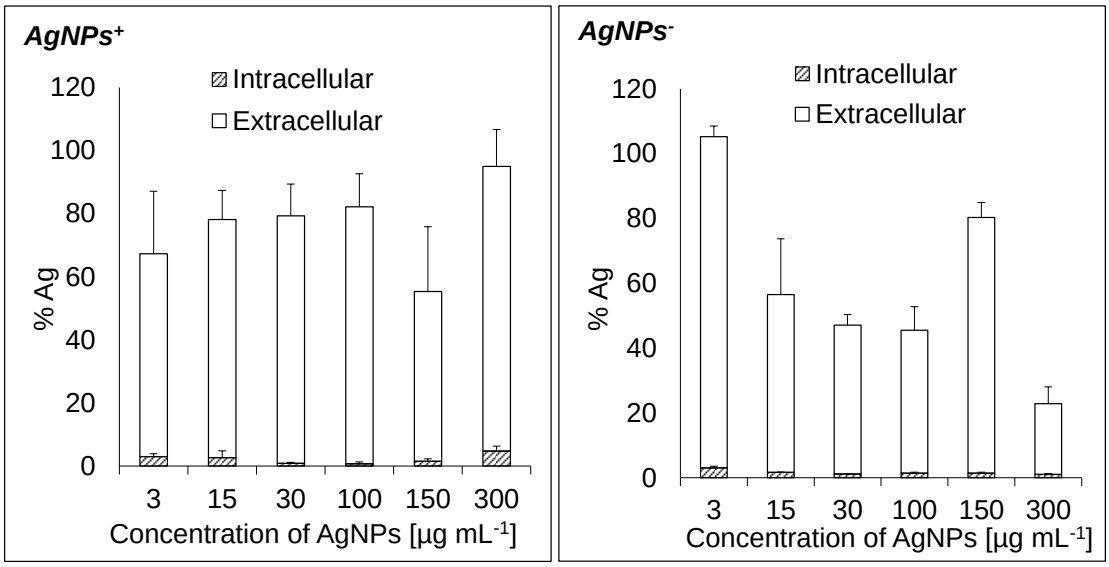

Figure 2.S9: Intracellular (cells) and extracellular (media and washes) accumulation of Ag post-24 hr exposure of cells to $AgNPs^{+}$ and $AgNPs^{-}$.

Scanning electron microscopy energy dispersive X-ray spectroscopy (SEM-EDX): The cell culture plates were examined by SEM-EDX after "cold" digestions and washes. Images were acquired with a FEI Quanta 650 FEG equipped with an X-ray microanalyzer (EDAX Octane Super). The following instrumental parameters were employed for measurements: backscattered electrons mode (BSE), 1,000–15,000 X magnification, 15

kV electron beam voltage, 30 mm work distance, 4-5 nm spot size, 0.95 Torr pressure, and 20 ºC temperature.

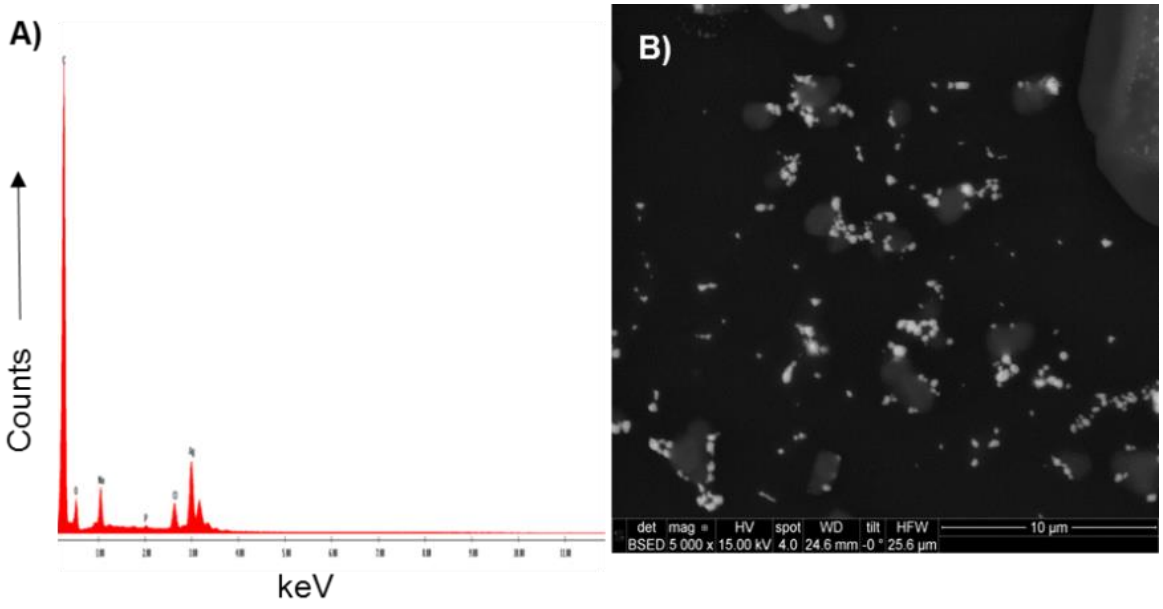

Figure 2.S10: SEM-EDX spectrum (A) and SEM image (B) of the cell culture plate post-exposure to 3 µg mL^{-1} of $AgNPs^{+}$ for 4 hr. The scale bar is 10 µm.

SEM-EDX measurements on these cell culture plates showed the presence of metallic Ag on their walls. An illustrative SEM-EDX graph and an optical image of the culture plate, in which cells were exposed to 3 µg mL^{-1} $AgNPs^{+}$ for 4 hr, are shown in Figure 2.S10. The SEM-EDX data indicated that in this case, ~10-20% of the administered AgNPs were retained on the culture plates.

HEK 293 cells: The absorption versus time curve of HEK 293 cells exposed to 20 µg mL^{-1} of $AgNPs^{+}$ for 4, 12, 24, and 48 hr are presented in Figure 2.S11. The ICP-OES results demonstrated that these cells followed non-linear absorption.

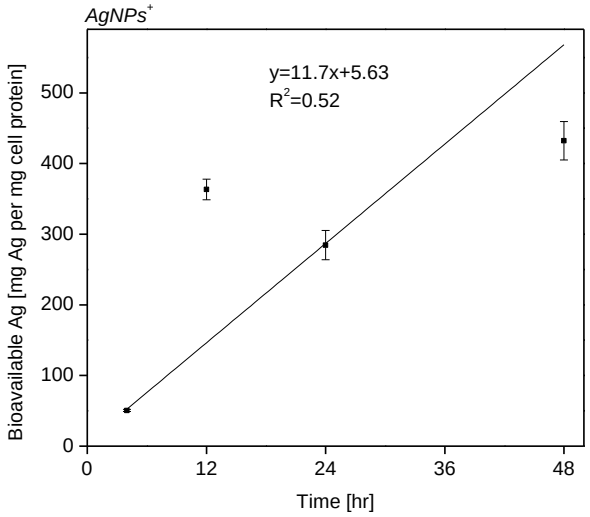

Figure 2.S11: Bioavailability of Ag in HEK 293 cells exposed to 20 µg $mL^{-1}$of $AgNPs^{+}$ for 4, 12, 24, and 48 hr. The error bars represent the standard error of $N = 3$ independent trials. Non-linear absorption was followed during the monitored time periods (4-48 hr).

Distribution:

***CHSI*:** Vero 76 cells exposed to 100 µg mL^{-1} of $AgNPs^{-}$ for ~ 4 hr were fixed and imaged for AgNP internalization. Figure 2.S12 shows the enhanced dark-field optical images of a single fixed cell along with the hyperspectral profile of extracellular and intracellular $AgNPs^{-}$.

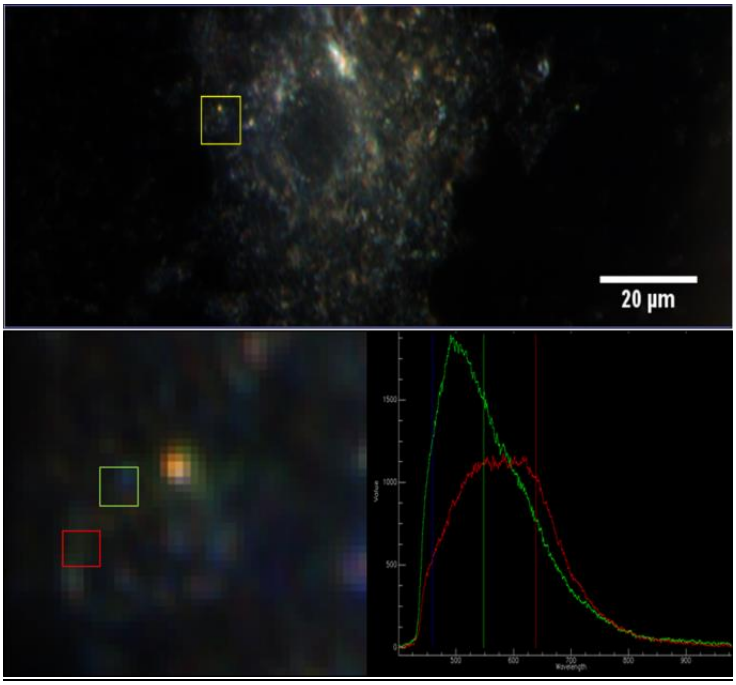

Figure 2.S12: *Top panel*: Enhanced dark-field microscopic image of a single, fixed Vero 76 cell that was exposed to 100 µg mL^{-1} of $AgNPs^{-}$ for ~ 4 hr. The yellow square encloses a cellular area that was further zoomed in. *Bottom left panel*: The optical image of the marked cellular area showing the presence of extracellular (red square) and intracellular (green square) $AgNPs^{-}$. *Bottom right panel:* Corresponding hyperspectral signatures of the marked areas that were similarly color coded to demonstrate the internalization of $AgNPs^{-}$.

HEK 293 cells were similarly exposed to 10 µg mL^{-1} of $AgNPs^{+}$ for ~ 24 hr. Pelleted cells were fixed and imaged for AgNP internalization. Figure 2.S13 shows the enhanced dark-field optical images of a fixed cell and the corresponding controls along with the mean hyperspectral signatures. In a nutshell, the CytoViva data showed that $AgNPs^{+}$ were widely distributed across the cells with distinct patterns of cellular

entry/exit (red spheres) and sub-cellular localization (blue and green spheres). Specifically, the majority of the red-colored particles were found to be on the cell membranes (Figure 2.S13 A). The corresponding hyperspectral signature indicated a ~130 nm red-shift in LSPR profile of these particles (Figure 2.S13 B) from $AgNPs^{+}$ control. Although both the green and blue spheres were visualized as internalized and/or close to the membrane, their hyperspectral profiles were different. Specifically, the spectra of green-colored particles was moderately red-shifted (~30 nm) with a ~104 nm increase in FWHM, while the blue spheres only exhibited a ~156 nm increase in FWHM. The changes in the LSPR profiles might be the result of the increase in AgNP diameters during protein corona formation (red-shifts) or the potential encapsulation of some AgNPs in endosomal or lysosomal compartments (red- and blue-shifts). While the formation of protein corona and the subsequent red-shifts in the LSPR peaks were also suggested by the collected TEM, DLS and absorption data, additional chemical and biological investigations are needed in order to confirm these explanations.

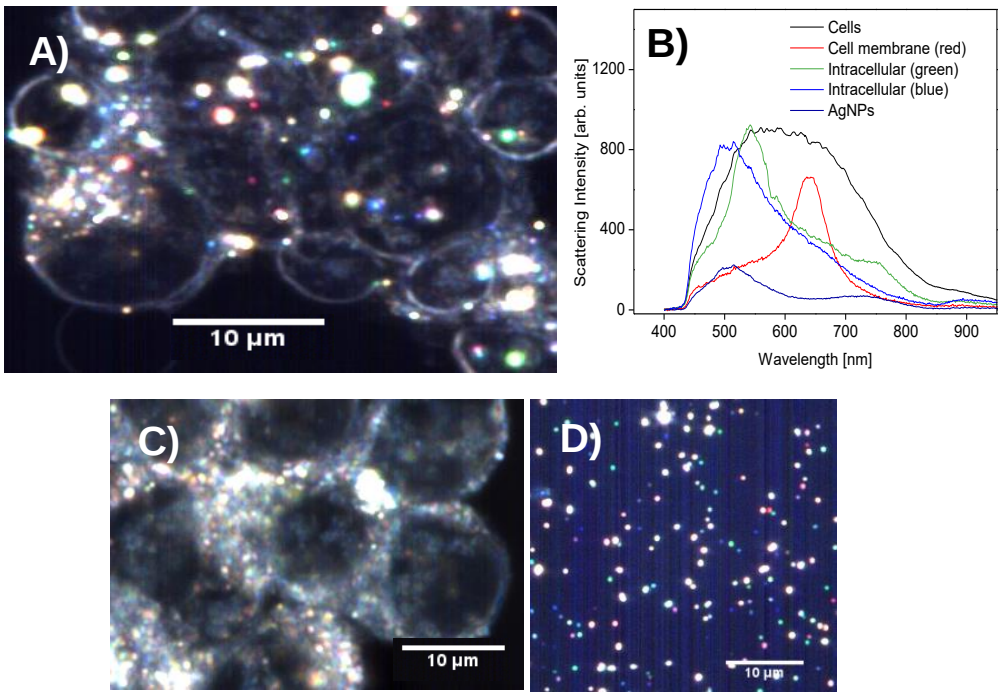

Figure 2.S13: A) CytoViva dark-field image (100x magnification) of fixed HEK 293 cells that were exposed to 10 µg mL^{-1} of $AgNPs^{+}$ for ~ 24 hr. Red, blue and green spherical particles indicate the distribution of $AgNPs^{+}$. B) Corresponding mean hyperspectral signatures (*N=10* particles) that were similarly color coded to demonstrate the cellular localization of $AgNPs^{+}$. Control images of C) cells alone and D) $AgNPs^{+}$ alone are also shown. The scale bar is 10 µm in all images.

RHSI: Raman maps of single Vero 76 cells (*N* = 3 cells for each condition, 15 x 15 µm regions) exposed to 100 µg mL^{-1} of $AgNPs^{+}$ for ~ 4 hr were acquired and an agglomerative hierarchical clustering analysis (AHCA) was performed on these maps. Figure 2.S14 (panels A and B) displays the optical image of a mapped cell exposed to $AgNPs^{+}$ and the pseudo-color cluster image (*N* =10 clusters) constructed from the Raman map of this cell. Table 2.S2 summarizes the tentative peak assignments of the AHCA

clusters of cells exposed to both $AgNPs^{+}$ and $AgNPs^{-}$ and their possible cellular location. Similarly, RHSI of fixed HEK 293 cells (10 x 10 µm regions) exposed to 10 µg mL^{-1} of $AgNPs^{+}$ for ~ 24 hr were obtained and AHCA was performed. The pseudo-color cluster image (*N* =10 clusters) constructed from the mapped cell and Raman spectra of cluster 2 are shown in Figure 2.S15.

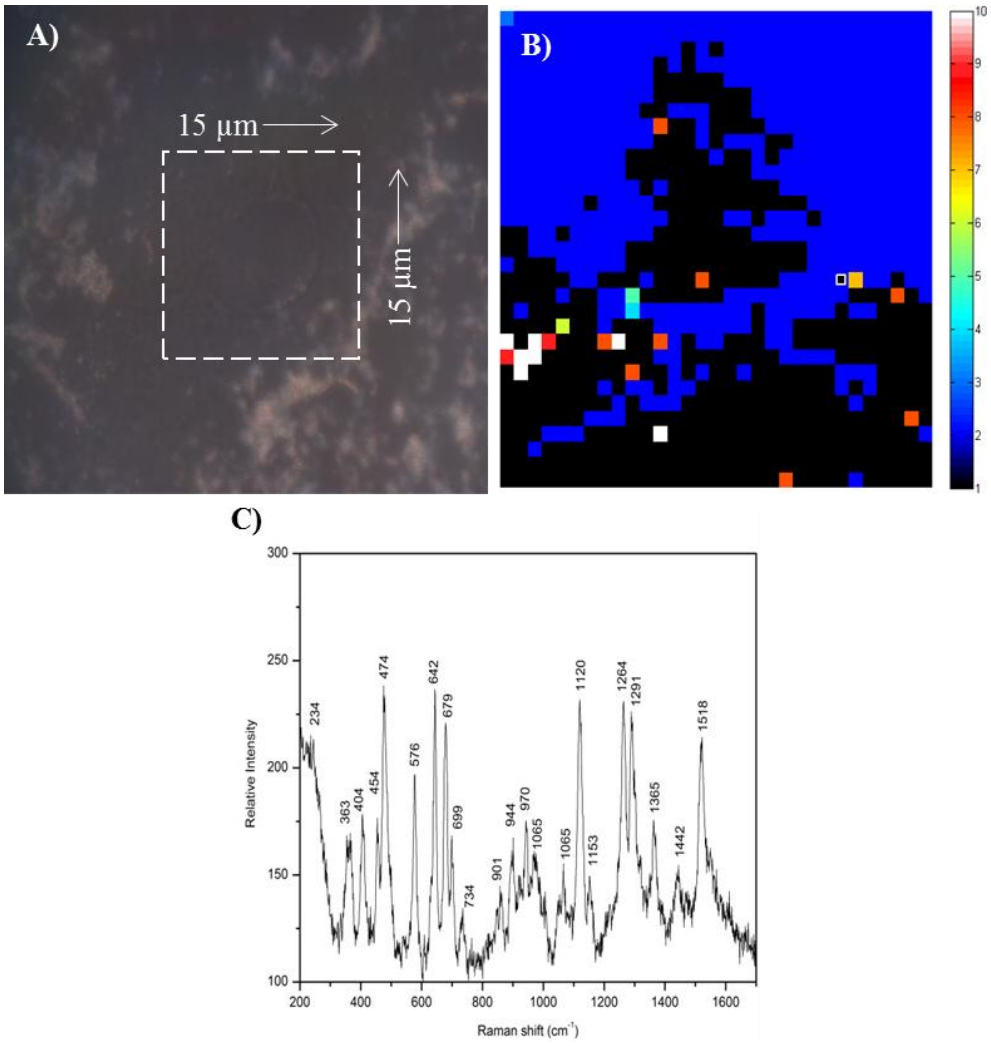

Figure 2.S14: A) Optical microscopic image of a single, fixed Vero 76 cell that was exposed to 100 µg mL^{-1} of $AgNPs^{+}$ for ~ 4 hr. The dotted white square encloses the cellular area that was mapped by Raman spectroscopy. (B) Pseudo-colored clustered

image in RGB scale (*N*= 10 clusters, > 90% data variance) of the mapped area by AHCA. Each cluster comprises spectral groups with similar distribution variance. C) Raman signatures of cluster 2 demonstrating $AgNP^{+}$ distribution.

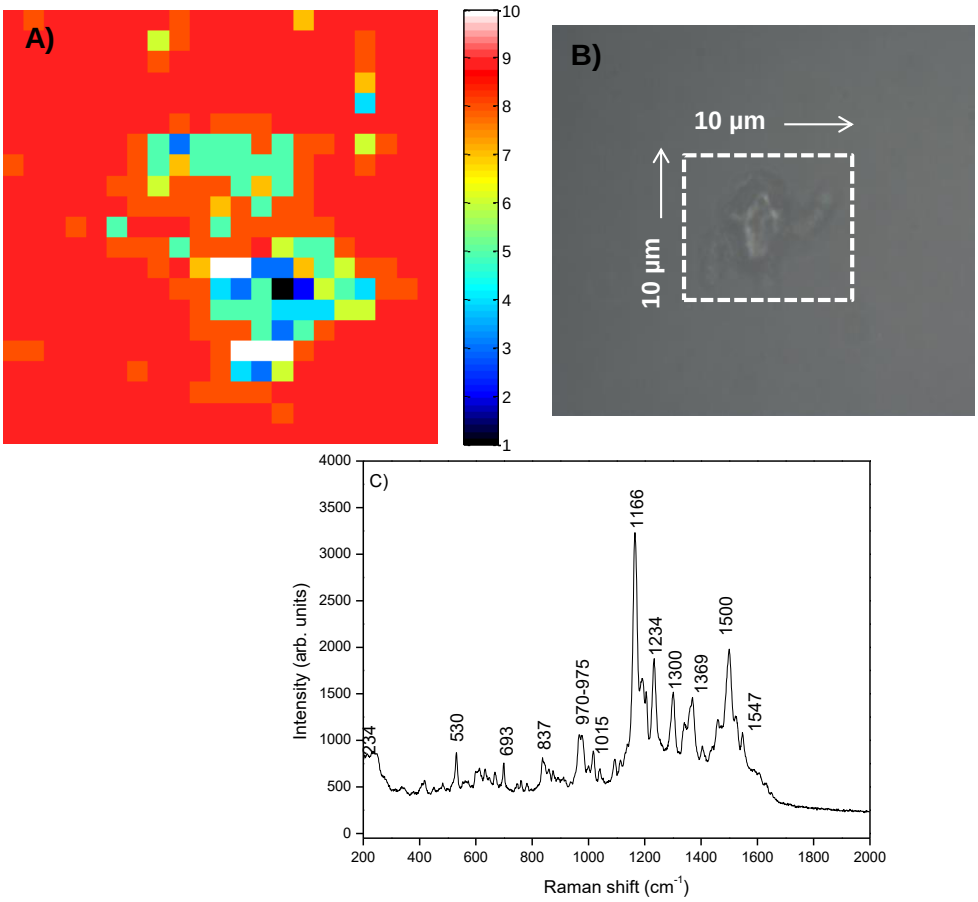

Figure 2.S15: (A) Pseudo-colored clustered image in RGB scale (*N*= 10 clusters, > 90% data variance) of the mapped area by AHCA. Each cluster comprises spectral groups with similar distribution variance. B) Optical microscopic image of a single, fixed HEK 293 cell that was exposed to 10 µg mL^{-1} of $AgNPs^{+}$ for ~ 24 hr. The dotted white square encloses the cellular area that was mapped by Raman spectroscopy. Each cluster

comprises spectral groups with similar distribution variance. C) Raman signatures of cluster 2 demonstrating $AgNP^{+}$ distribution.

Table 2.S2: Tentative peak assignments of AHCA clusters and the possible cellular locations of AgNPs in single cells (*N*=3 fixed cells exposed to 100 µg mL^{-1} of AgNPs for 4 hr).

Raman peak (cm^{-1})						**Tentative assignment**	**Possible cellular locations of AgNPs**
$AgNPs^{+}$		**$AgNPs^{-}$**					
C2	***C3***	***C1***	***C2***	***C5***	***C10***		
699						Phopholipids (cholesterol)	Cell membrane[110]
	713					Phospholipids head-groups, (phosphotidyl choline)	Cell membrane[110,111]
734, 970	735, 957-960	732				Phospholipids	Cell membrane[112]

		811	819			Phophotidyl esterases (RNA)	Cytoplasm[111]
				1318		Imidazole ring	Endosomes[113]
1264, 1442		1408, 1433		1447, 1657	1264	Lipid droplets	Cytoplasm[111,58,114]

Metabolism:

CPE-TFF was performed on HEK 293 cells exposed to 10 μg mL^{-1} of $AgNPs^{+}$ for 24 hr and the resultant Ag species (AgNPs and Ag^{+}) present in the cellular matrices were isolated and quantified by ICP-OES as shown in Figure 2.S16.

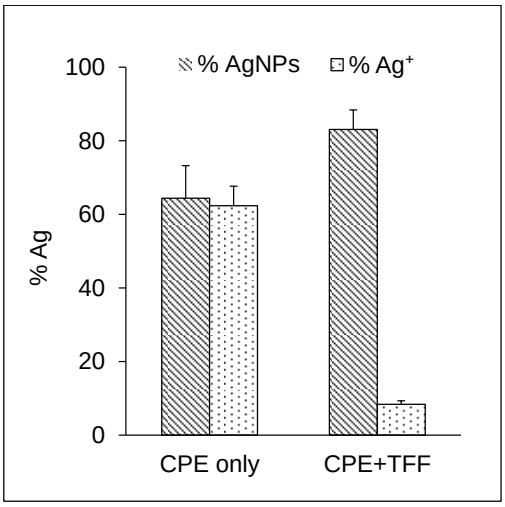

Figure 2.S16: A) Percentages of the two Ag species ($AgNPs^{+}$ and Ag^{+}) isolated *via* CPE alone and CPE in combination with a one-step TFF (1 kD filter) as quantified by ICP-OES in HEK 293 cells. All values were normalized to the total amount of Ag absorbed by cells prior to CPE. Error bars indicate the standard error of $N = 3$ independent trials.

Cytotoxicity

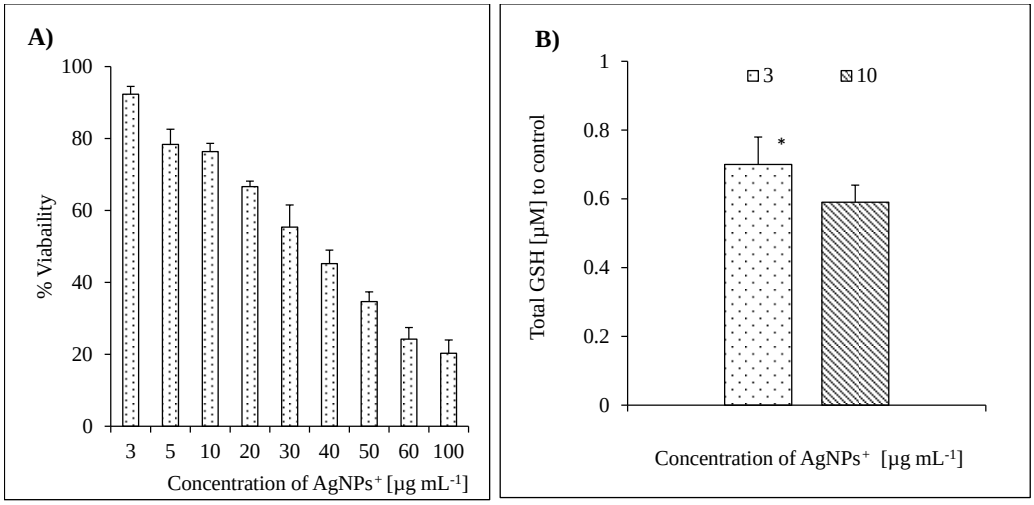

Figure 2.S17: A) Percentage viability of HEK 293 cells (~1 x 10^4 cells per well) exposed to various concentrations of $AgNPs^+$ for 24 hr *via* MTT assay. All results were plotted after subtracting the corresponding absorbance values of the blanks (media + $AgNPs^+$) and then normalizing to the absorbance of untreated cells. B) Total GSH levels in HEK 293 cells exposed to sub-lethal concentrations of $AgNPs^+$ (3 and 10 µg mL^{-1}) for 24 hr. All GSH results (µM) were normalized to the corresponding control cell values (untreated cells). '*' indicates the presence of statistical significance among the two concentrations of a specific Ag exposure ($p < 0.05$, 1-way ANOVA). In all plots, error bars indicate the standard error of $N = 3$ independent trials.

Elimination:

The total Ag cleared by HEK 293 cells that were exposed to 20 µg mL^{-1} of $AgNPs^+$ for 24 hr is shown in Figure 2.S18. ICP-OES results demonstrated that zeroth-order elimination was followed by the cells at the measured time periods of 1, 4, 12, and 24 hrs. The corresponding half-life ($t_{1/2}$) and zeroth-order elimination rate constant (k_0)

were 73 hr and a 0.057 µg /mg protein hr^{-1}, respectively. Although it is rarely seen, the half-lives of drugs that follow zero-order elimination increase with the administered dose. It can be recalled that there was non-linear absorption in HEK293 cells at same administered concentration. It is also possible that HEK293 cells might be saturated at this sub-lethal concentrations, thus exhibiting constant clearance at 20 µg mL^{-1} of $AgNPs^{+}$.[70]

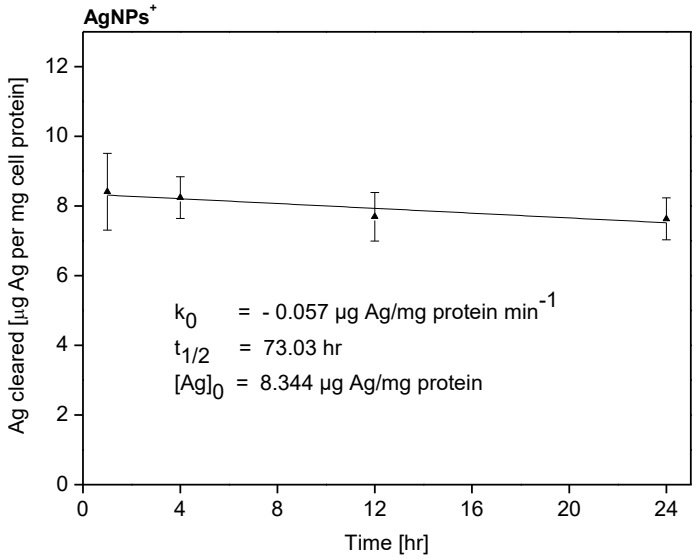

Figure 2.S18: Clearance of Ag (µg Ag per mg of protein) from HEK293 cells exposed to 20 µg mL^{-1} of $AgNPs^{+}$ for 24 hr. The ICP-OES measurements of total Ag were carried out at 1, 4, 12, and 24 hr after replenishing the media (no AgNPs). The bars represent the standard error of N =3 independent trials at each elimination time point.

CHAPTER 3

INTRODUCING "GREEN" AND "NON-GREEN" ASPECTS OF NOBLE METAL NANOPARTICLE SYNTHESIS: AN INQUIRY-BASED LABORATORY EXPERIMENT FOR CHEMISTRY AND ENGINEERING STUDENTS

Sesha L. A. Paluri, Michelle L. Edwards, Nhi H. Lam, Elizabeth M. Williams, Allie Meyerhoefer, and Ioana E. Pavel Sizemore

Department of Chemistry, Wright State University,

3640 Colonel Glenn Highway, Dayton, OH 45435-0001, United States

COPYRIGHT PERMISSION

SUMMARY OF INVOLVEMENT

Sesha L A Paluri was responsible for the drafting, editing the manuscript along with construction of figures and tables. She and the second author, Michelle Edwards, were instructors of this module and therefore were in-charge of: framing inquiry-based questionnaire, design and execution of laboratory sessions, data analysis including student assignments, assessments, pre- and post-evaluations.

GRAPHICAL ABSTRACT

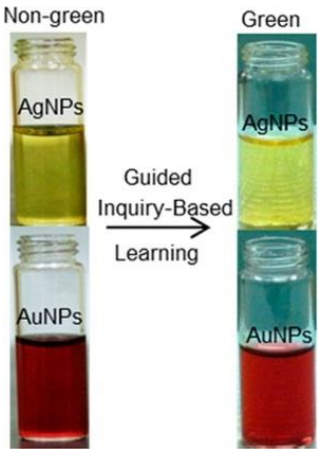

ABSTRACT

In recent years, nanoscience and nanotechnology have been drawing enormous attention due to the numerous applications of nanomaterials. In an attempt to nurture interest towards these areas in young minds and to develop the next generation of environmentally conscious scientists and engineers, this new laboratory module focuses on the green and nongreen aspects of noble metal nanoparticles (NPs) synthesis. The element of novelty is represented by the guided, inquiry-based exploration of alternative, green fabrication methods using environmentally friendly reducing agents (e.g., tea extracts, coffee, honey, coconut oil, and banana peel). The inquiry-based learning was developed according to the five essential features laid by the National Research Council (NRC), and was successfully implemented after science and engineering students gained theoretical knowledge and hands-on experience with conventional, nongreen fabrication methods of colloidal silver and gold NPs (i.e., the Lee-Meisel and Turkevich methods).

The student assignments and evaluations demonstrated that this inquiry-based laboratory increased students' interest in green nanochemistry, provided them with new laboratory skills, and stimulated their critical thinking.

KEYWORDS

Colloids; Environmental Chemistry; Graduate Education/Research; Green Chemistry; Hands-On Learning/Manipulatives; Inquiry-Based/Discovery Learning; Interdisciplinary/Multidisciplinary; Laboratory Instruction; Nanotechnology; Upper-Division Undergraduate

INTRODUCTION

Since the first recorded use of nanoscience in the 4th century, man has been intrigued with the unique properties of noble metal nanoparticles (NPs)[115]. By 2015, the nanoscience and nanotechnology sectors are expected to contribute over $2.4 trillion to the global economy and to impact our society, much like information technology has influenced the economy and the way we live[116]. This growth is related to the increased demand for nanotechnology-enabled products in the healthcare, electronic, semiconductor, chemical and automotive markets[116]. Thus, there is a great demand for qualified scientists, engineers and technicians in the field of nanoscience and nanotechnology[117]. In fact, a recent study by the National Science Foundation (NSF) indicated that by 2020, over six million nanotech employees will be needed worldwide, with over two million of jobs being located in the U.S. alone[118].

As of March 2013, the Nanotechnology Consumer Product Inventory comprised of 1,628 registered products or product lines[117]. Over 380 of these products contain silver nanoparticles (AgNPs) and around 19 gold nanoparticles (AuNPs). Generally, colloidal noble metal nanoparticles are synthesized in a non-green manner, by the reduction of a metallic salt[119]. For example, one of the most widely-used fabrication methods for colloidal AgNPs and AuNPs involves the high temperature, energy consuming reduction of silver nitrate (by Lee-Meisel[120,121]) and tetrachloroauric acid (by Turkevich[122,123]), respectively, by trisodium citrate. As an alternative, green fabrication methods have been raising increased research and environmental interest. To address this need, a few groups have proposed traditional, undergraduate laboratory experiments that focus on the fabrication of noble metal nanostructures using reducing agents of low environmental impact and enhanced biodegradability such as green tea[124]and plants[125]. Adding to the ongoing efforts, the main goal of this laboratory module is to help develop the next generation of environmentally conscious chemists and engineers by introducing them to both the green and non-green aspects of noble metal nanoparticle synthesis. In comparison to the previous nano-laboratory educational work[126-134], the proposed laboratory module brings an additional element of novelty by using guided, inquiry-based learning. Briefly, undergraduate and graduate students from multiple disciplines (chemistry, physics, mechanical and materials engineering, and environmental sciences) were given a common research problem and were allowed to come up with their own, educated solution. In the first segment of the laboratory activity, students enrolled in an *Experimental Nanomaterials and Nanoscience laboratory course* synthesized AgNPs and AuNPs using the non-green Lee-Meisel and Turkevich methods. In the second segment

of the laboratory activity, students were requested to identify and implement a green fabrication method based on their level of knowledge and experience.

The inquiry-based learning is a novel pedagogy that emphasizes students and teachers as learning partners[135]. In real scientific scenarios, a researcher is exposed to several unanswered issues, and needs to use his cognitive abilities and scientific reasoning to address the experimental questions. A mere knowledge from text books as traditionally taught in instructional classrooms may not be sufficient to master the technical field. The inquiry-based learning provides room for students to question themselves and to explore the given topic of interest. In the past decade, this educational approach has been successfully encompassed in several elementary and higher grade level schools[134-136], as well as in the undergraduate curriculum[128,137,138]. Thus, learning by guided scientific inquiry is expected to increase students' enthusiasm in nanochemistry as well as to broaden their understanding and acquisition abilities compared to conventional laboratory experiments.

MATERIALS AND METHODS

All the reagents utilized in the experiment were obtained from Fisher Scientific. High purity water (> 18 MΩ cm) was employed as solvent throughout the laboratory activity.

Non-green fabrication of colloidal AgNPs and AuNPs

In the first segment of the laboratory activity, students performed test tube level syntheses of colloidal AgNPs and AuNPs using the Lee Meisel[114] and Turkevich[122,126,139] methods, respectively. In this regard, a standard operating procedure (SOP) was prepared

and distributed to students beforehand. Briefly, 20 mL of silver nitrate ($AgNO_3$, 1 mM) and 20 mL of tetrachloroauric acid ($HauCl_4•3H_2O$, 1 mM) were added to pre-cleaned test tubes, which were labeled AgNPs and AuNPs, respectively. The test tubes were then placed in a hot water bath pre-heated to boiling for about 10 min. This was followed by the addition of 2 mL of trisodium citrate ($Na_3C_6H_5O_7•2H_2O$, 34 mM) in each of the noble metal salt solutions. Shortly after (~15 min), notable color changes were observed in the test tubes, namely wine red for AuNPs and dark yellow for AgNPs (Figure 3.1A). To ensure the completion of the reduction reaction, heating was continued for another 10-15 min. It should be noted that the original synthesis procedures from literature were scaled down and adapted to fit the allotted laboratory time and resources.

Green fabrication of colloidal AgNPs and AuNPs

In the second segment of the laboratory activity, students performed synthesis of colloidal AgNPs and AuNPs using a series of environmentally friendly reducing reagents (*e.g.*, phytochemicals in tea extracts[140,141], polyphenols in coffee[141], glucose in honey[142,143], triglycerides in coconut oil[144] and cellulose, pectin in banana peel[145]), while the noble metal salt was kept the same (*i.e.*, $AgNO_3$ or $HauCl_4•3H_2O$). The solvent of choice was in most cases water, and the reactions were performed in test tubes under the instructor's supervision. The above mentioned procedures were tested for reproducibility by the teaching assistants after the laboratory completion. Two sample procedures, which were adopted and employed by students for their inquiry-based learning assignment, are outlined below:

Natural honey-reduced AgNPs[143]: In this procedure, 1 mM of an aqueous $AgNO_3$ solution was reduced using a honey extract. The extract was prepared by dissolving 20 g

of honey in 80 mL of water. Twenty milliliters of the $AgNO_3$ solution were dispensed into 15 mL of the honey extract and were stirred well while heating at 80 ˚C for 10 min. The appearance of a stable, dark yellow color (in ~10 min) marked the formation of AgNPs (Figure 3.1B), and stirring was continued for another 30 min to ensure the completion of the reduction reaction.

***Lipton green tea-reduced* AuNPs**[124]: In this procedure, 100 mM of an aqueous $HauCl_4•3H_2O$ solution was reduced using a green tea extract. The tea extract was prepared by magnetically stirring 200 g of tea leaves in 12 mL of water for 15 min at room temperature. One hundred microliters of the $HauCl_4•3H_2O$ solution were added to 6 mL of the tea filtrate, and a wine red color characteristic to the formation of AuNPs was observed in ~10 min (Figure 3.1B). Stirring was continued for another 30 min to ensure the completion of the reduction reaction.

UV-Vis absorption spectrophotometry of colloidal AgNPs and AuNPs

To confirm the formation of NPs, small colloid aliquots were collected at the end of each synthesis for further characterization using a Cary 50 UV-Vis-NIR spectrophotometer (Varian Inc.), at 1 nm intervals. Prior to the UV-Vis measurements, samples were diluted with high purity water (1:10 volume ratio) in disposable cuvettes of a total volume of 3.0 mL and a path length of 10.0 mm (Fisher Scientific).

Hazards

Both $Na_3C_6H_5O_7•2H_2O$ and $AgNO_3$ (a strong oxidizer) have the potential to cause irritations upon contact with skin, eyes and respiratory tract. $HauCl_4•3H_2O$ is corrosive and can cause burns by all routes of exposure. All chemical reactions must be performed in a chemical safety hood. Personal protective equipment (PPE) must be worn at all times

during the course of the experiment (laboratory coats, ANSI-certified safety goggles and gloves).

RESULTS AND DISCUSSION

Guided Scientific Inquiry

This laboratory module was developed according to five essential features laid by the National Research Council (NRC) for inquiry-based teaching and learning.[146] In this approach, learners:

(1) *"Are engaged by scientifically oriented questions,*

(2) *Give priority to evidence, which allows them to develop and evaluate explanations that address scientifically oriented questions,*

(3) *Formulate explanations from evidence to address scientifically oriented questions,*

(4) *Evaluate their explanations in light of alternative explanations, particularly those reflecting scientific understanding, and*

(5) *Communicate and justify their proposed explanations".*[1146]

To incorporate these inquiry-based features into the proposed laboratory, the following steps were undertaken:

(1) *Students were posed a scientific problem, namely, the identification and implementation of a green fabrication method for colloidal AgNPs or AuNPs.*

(2) *To guide the selection process, a few examples of nongreen and green bottom-up*

approaches were carefully discussed during the recitation period of the first segment of the laboratory activity, and the process of performing a scientific literature search was demonstrated. This was in particular helpful to the students, who had no previous experience with inquiry-based learning. Afterward, students successfully synthesized colloidal AgNPs and AuNPs using "cook-book" procedures for the well-established Lee–Meisel and Turkevich methods, respectively.

(3) *During the second segment of the laboratory activity, students were requested to review the scientific literature in order to identify a method for the fabrication of green NPs. Graduate students and upper-level undergraduate students were also encouraged to explore new, creative routes of fabrication. Some students actually adapted methods to include the use of materials not listed in scientific literature. For example, several students attempted to synthesize AuNPs using multiple roasts of coffee or different types of tea from local grocery stores as green reducing agents.*

(4) *The selected green methods were then closely assessed and modified (if necessary) together with the instructor to ensure the successful completion of the reactions within the allocated time period and access to all needed resources. Building upon the laboratory experience gained through the nongreen syntheses, students implemented the proposed green syntheses, characterized the colloidal products by absorption spectroscopy, and carefully collected the experimental observations.*

(5) *Following the completion of the laboratory activities, students were invited to*

compare the results of the green and nongreen fabrication methods, and to justify their selection of a green method in a journal-article like laboratory report. Students were also encouraged to discuss the reactions involved in the reduction process and to provide future experimental measures for improving the green products.

Comparing the Optical Properties of Green and Nongreen Noble Metal NPs

A widely explored optical property of NPs, the localized surface plasmon resonance (LSPR), was utilized in this experiment to confirm the formation of AgNPs and AuNPs. LSPR arises from the collective oscillation of free electrons confined to the surface of nanomaterials (i.e., the so-called surface plasmons) upon the incidence of plane polarized light, at resonance wavelengths.[147] As a result, AgNPs and AuNPs exhibit characteristic LSPR peaks in the visible region of electromagnetic spectrum (Figure 3.1). The LSPR peaks and the colors exhibited by the colloidal NPs are interrelated: larger NPs exhibit red-shifted LSPR peaks. Representative UV–vis absorption spectra and the characteristic color of the colloidal NPs, which were fabricated by students using the nongreen and green methods, are shown in Figure 3.1. Stable AgNPs exhibited yellow color due to the absorption in the blue region corresponding to an LSPR peak at 420–440 nm. Similarly, AuNPs appeared wine red due to the absorption of green light corresponding to an LSPR maximum at 520–540 nm in the visible spectrum. The observed LSPR peaks were reproducible and were in good agreement with literature.[120,126]

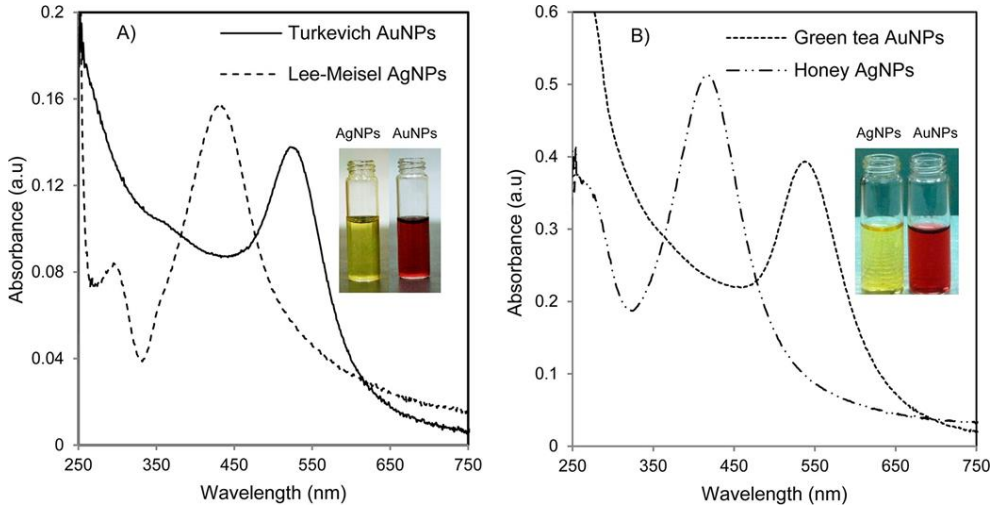

Figure 3.1: UV–vis absorption spectra and characteristic colors of the colloidal AgNPs and AuNPs synthesized by (A) nongreen and (B) green methods.

In-Class Assessments

To assess the overall comprehension of basic fabrication concepts and the correct execution of the experiments, a set of predefined laboratory skills (LS#1–4) were anonymously evaluated by the instructors (Table 3.1). These evaluations were based on the application of the theoretical knowledge and the experience gained through this laboratory. Table 3.1 shows that students completed the experiments with excellent laboratory practices and successfully applied the green chemistry principles underlying the proposed synthesis methods.

Table 3.1 Results of the Anonymous Assessments of Laboratory Skills

Laboratory Skill (LS)	**Assessment Results[a]**	
	Class Average (n = 15)	**Standard Deviation**
LS#1: Students were able to perform nongreen synthesis of NPs with the instructor's assistance.	1.1	0.2
LS#2: Students were able to independently extract the green reducing agent.	1.1	0.1
LS#3: Students were able to complete the green synthesis of NPs.	1.2	0.3
LS#4: Students were able to correctly collect the UV–vis absorption spectra on the diluted colloidal samples of NPs	1.1	0.2

a Laboratory skills were assessed on a three point system: 1, *Always performing the skill*; 2, *Sometimes performing the skill*; and 3, *Never performing the skill*.

Because this laboratory targeted a multidisciplinary audience of science and engineering students, a small set of multiple choice questions (Q#1–5) was posed to students during recitation to evaluate their understanding of basic nanoscience concepts prior to the laboratory. The questions interrogated the nanoscale dimensions (Q#1), the Tyndall effect (Q#2), the type of nanofabrication methods commonly utilized by chemists (Q#3) and engineers (Q#4), and the color of colloidal nanoparticles associated with the LSPR effect (Supporting Information). At the beginning of the first segment of the laboratory, students were invited to answer a similar set of questions. The student responses (Figure 3.2), which were recorded by means of Power Point polling (Turning

Point Clicker technology), demonstrated that the introductory recitation material improved students' basic understanding and acted as a bridge for the students from various disciplines. As an additional benefit, this activity also increased class interactivity and improved student engagement. The completion of laboratory experiments culminated with a written assignment, which required students to compare the advantages and disadvantages offered by the nongreen and green fabrication methods of noble metal NPs in a journal article-like laboratory report.

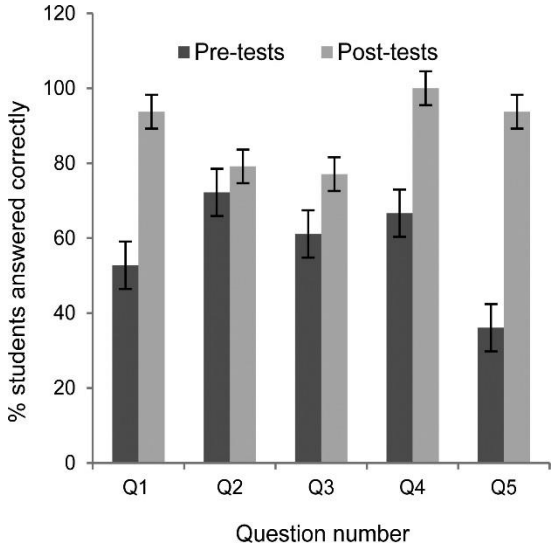

Figure 3.2. Histograms portraying the contribution of this laboratory module to the overall procurement of nanochemistry knowledge. Students (n = 15) volunteered to anonymously answer a set of scientific questions (Q#1–5) before and after the recitation period. For each question, the percentage of students that provided a correct answer was instantly evaluated by the Turning point software. Error bars represent the standard errors of the results.

Pre- and Post- laboratory Surveys

To ensure the overall success of the new laboratory experiment, anonymous surveys were administered to students. These evaluations were aimed at collecting feedback on the overall design of the laboratory, the students' interest and experience before and after the completion of the experiments (SQ#1–4). On a comparative scale of 1–10, with 1 being the lowest, the survey results (Table 3.2) showed that the overall interest in this experiment increased from a class average of 8.4 pre-laboratory to 9.7 post-laboratory. The comments from the post-surveys also showed that students' enthusiasm about nanoscience had increased. Here are a few examples of students' comments: "*This laboratory is interesting, I would like to pursue a career in nanotechnology*", "*Employing green methods to make nanoparticles is cool*", and "*This nanotechnology lab is awesome*".

Table 3.2 Results of the Anonymous, Pre- and Post-laboratory Student Surveys

Survey Question (SQ)	**Survey Results[a]**	
	Class Average (*n* = 15)	**Standard Deviation**
SQ#1: Overall interest in the proposed experiments pre-laboratory	8.4	2.4
SQ#2: Overall interest in the proposed experiments post-laboratory	9.7	0.5
SQ#3: Overall experience in this laboratory	9.4	0.6
SQ#4: Overall rating of the laboratory module	9.7	0.6

a Students' responses to the survey questions were evaluated on a 10 point scale, with 1 being the lowest and 10 being the highest.

CONCLUSIONS

The proposed laboratory module and the associated student assignments were successful in providing students of diverse academic backgrounds with hands-on experience and basic knowledge in the green and nongreen aspects of noble metal NP syntheses. Students' creativity and critical thinking were stimulated through a guided, inquiry-based learning approach. As a result, the overall interest and enthusiasm for green nanochemistry increased after the completion of the experiments as indicated by the student assignments and anonymous evaluations.

ACKNOWLEDGEMENTS

Financial support through the NSF-NUE in Engineering Program (Award No. EEC-1138235) and WSU start-up is highly acknowledged.

SUPPORTING INFORMATION

Additional material for students, instructors, and lesson plan recommendations are provided in supporting information.

Instructions for Students

Safety and Hazards

To ensure safety, all students should wear Personal Protective Equipment (PPE) throughout the laboratory session. PPE includes laboratory coat, gloves and ANSI-approved safety goggles. Upon the completion of experiment, care should be taken to collect the generated metal waste in properly labeled containers and to dispose it according to the Environmental Protection Agency's Resource and Recovery Act (EPA-RCRA).

Introduction

In recent years, nanotechnology and nanoscience have experienced significant progress due to the increasing number of nanoparticle (NP)-based applications in various sectors such as food, medicine, cosmetics, molecular machinery, and telecommunications[1]. Nanometer (nm) by definition, is one billionth (10^{-9}) of a meter, a dimension characteristic to many biological entities including DNA (diameter of 2.5 nm), viruses (10 to 60 nm), and bacteria (30 nm to 10 μm).[148]

Nanotechnology deals with the synthesis and fabrication of particles that have at least one dimension in the range of 1-100 nm and unique properties that emerge out of the nanoscale dimensions. Particularly, nanosized metals have been greatly explored over the recent years due to their special optical, catalytic, electromagnetic and mechanical properties. According to Consumer Product Inventory by the Project of Emerging Nanotechnologies[117], in 2013, 383 out of the 1,628 consumer products were based on silver nanoparticles (AgNPs), while 19 comprised gold nanoparticles (AuNPs). Besides the positive impact of NPs on diverse sectors, the human and environmental exposures to the hazardous chemicals employed during NPs fabrication have also increased. In addition, the toxicological effects associated with the human and animal exposure to AgNPs are still under investigation. As a result, many federal authorities like the United States Environmental Protection Agency and the Health & Consumer Protection Directorate of the European Commission began to exert regulations for the use of engineered NPs in food and consumer products[149]. Consequently, "green" fabrication methods of NPs emerged as great alternatives. As the name suggests, these methods utilize environment friendly or naturally available reducing agents, thus minimizing the use of harmful chemicals during the synthesis process. Examples of green reducing agents include banana peel[145a] and black pepper[150] for AgNPs and coriander leaf[151] and chitosan[152] for AuNPs.

In this laboratory, students will synthesize AgNPs and AuNPs using nongreen and green procedures and characterize the products using ultraviolet-visible (UV-Vis) absorption spectroscopy. Prior to the experiment, during the recitation period, students will be introduced to the basic concepts of nanofabrication, the optical properties of noble

metal NPs, the principles of green chemistry, and several green synthesis methods of noble metal NPs described in literature.

Experiment

This laboratory experiment will be performed in two segments. The first segment will be dedicated to the synthesis of colloidal AgNPs and AuNPs by well-established, nongreen methods. The second segment will focus on a guided, inquiry-based learning assignment for the fabrication of green colloidal AgNPs and AuNPs, which will be discussed later in this section. Graduate students are encouraged to work independently, while undergraduate students will be permitted to work in pairs.

1) <u>Nongreen fabrication of noble metal NPs: Well-established methods</u>

Nongreen AgNPs and AuNPs will be synthesized in test tubes using the widely-used Lee Meisel and Turkevich methods, respectively. Briefly, 20 mL solutions of a silver salt (1mM of silver nitrate) and gold salt (1 mM of tetrachloroauric acid) will be added to two pre-labelled test tubes and will be heated in a boiling water bath for ~10 min. This will be followed by the addition of 2 mL of reducing agent (34 mM of trisodium citrate) to both test tubes. Heating will be continued until a notable color change occurs (usually in ~15 min). Since AgNPs are light sensitive, it is extremely important to maintain a dark environment in the chemical fume hoods throughout the experiment.

Solutions of trisodium citrate (34 mM), silver nitrate (1mM), and tetrachloroauric acid (1mM) will be prepared according to the following procedures.

a) 34 mM of trisodium citrate solution: In a 100-mL volumetric flask, 1.000 g of trisodium citrate ($Na_3C_6H_5O_7 \cdot 2H_2O$) should be dissolved in 50.0 mL of high purity water. Water should be added to make up the volume to 100.0 mL, and the flask should be covered with parafilm. This solution should be stable for up to three months in the refrigerator.

b) 1 mM of silver nitrate solution: In a 100-mL volumetric flask, 1.700×10^{-2} g of silver salt ($AgNO_3$) should be dissolved in 50.0 mL of high purity water. Water should be added to make up the volume to 100.0 mL. The silver nitrate solution is light sensitive; thus, it should be transferred to a glass amber bottle or the flask should be covered with aluminum foil to prevent exposure to light. Under refrigeration, this solution is stable for up to two weeks.

c) 1 mM of tetrachloroauric acid solution: In a 100-mL volumetric flask, 2.000×10^{-2} g of gold salt ($HauCl_4 \cdot 3H_2O$) should be dissolved in 50.0 mL of high purity water. Water should be added to make up the volume to 100.0 mL, and the flask should be covered with parafilm. This solution should be stable for up to a month when stored in refrigerator.

Materials

Laboratory supplies

- 500-mL Erlenmeyer flasks or Amber glass bottles for storing the freshly synthesized NPs
- 50-mL Graduated cylinders to measure the desired volumes of solution
- Aluminum foil to wrap the glassware containing the colloidal NPs

- 250-mL Glass beakers for setting the water baths
- Disposable pipets
- Parafilm
- Hot-stir plates
- Magnetic stir bars
- Glass stir rods
- Test tubes of 20 mL volume or larger
- Test tube holders/racks
- Colored label tapes
- 3-mL Disposable cuvettes for absorption measurements
- Delicate wipes for cleaning the cuvettes
- Thermometers
- Gloves in all sizes

Reagents

- Silver nitrate ($AgNO_3$)
- Trisodium citrate ($Na_3C_6H_5O_7 \bullet 2H_2O$)
- Tetrachloroauric acid (HauCl4$\bullet 3H_2O$)
- High purity water (>18 MΩ cm)

2) <u>Green fabrication of noble metal NPs: A guided, inquiry-based learning assignment</u>

In this guided, inquiry-based learning assignment, students are encouraged to explore the scientific literature in order to identify a green reducing agent for the fabrication of noble metal NPs. The green procedure should be completed within the allocated time period of the second laboratory segment (3 hr) and should make use of the laboratory resources that are provided below in the Materials list. If necessary, the reaction volumes will be scaled down to fit the test tubes utilized during the first laboratory segment. The preparation of the selected green reducing agent and/or the green reaction conditions may require additional equipment that must be requested and discussed with the instructor beforehand.

Materials

Laboratory supplies

- Cheese cloth
- Blender
- UV lamp
- Test tubes
- Test tube racks/holders
- 250-mL Beakers
- 50-mL Graduated cylinders
- Hot-stir plates
- Magnetic stir bars
- 3-mL disposable cuvettes for absorption measurements
- Colored label tapes

- Delicate wipes for cleaning the cuvettes
- Thermometers
- Gloves in all sizes

Reagents

- Silver nitrate ($AgNO_3$)
- Trisodium citrate ($Na_3C_6H_5O_7 \bullet 2H_2O$)
- Tetrachloroauric acid ($HauCl_4 \bullet 3H_2O$)
- High purity water (>18 MΩ cm)

Students will prepare a brief, step wise procedure for the green fabrication of AgNPs or AuNPs by the reduction of the noble metal salt with the selected reducing agent. The proposed procedure, the corresponding journal article reference(s), and any additional request for supplies will be submitted in advance to the instructor for discussion and approval. Procedures that are considered not feasible will be amended or replaced together with the instructor. The green fabrication methods will then be carried out during the second segment of the laboratory activity. Students will characterize their final colloidal products using UV-Vis absorption spectroscopy and will note their experimental observations. After the completion of the experiment, students will submit a write-up on both segments of the laboratory in the form of a journal article.

<u>Important points about the write-up of the laboratory report</u>

- It should be in Journal Article format, and should follow the ACS guidelines.

- It should compare the advantages and disadvantages offered by the nongreen and green fabrication methods of noble metal NPs. More experienced students are encouraged to propose a possible reaction mechanism for the formation of the green noble metal NPs. This can be discussed in advance with the course instructor.
- The conclusion section should incorporate students' suggestions with respect to possible future improvements of the green method.

Notes for instructors

For a better overall productivity of the laboratory, it is suggested to divide the entire experiment into two separate segments dedicated to the nongreen and the green fabrication of noble metal NPs. In this work, the first segment of the laboratory activity focused on the nongreen synthesis of noble metals NPs in order to familiarize students with well-established methods and to provide them with sufficient preparation time for the green, inquiry-based learning assignment, during the second segment of the laboratory activity.

1) Nongreen fabrication of noble metal NPs: Well-established methods

- For laboratory segments shorter than 3 hrs, it is suggested to prepare all solutions in advance (*i.e.*, silver nitrate, tetrachloroauric acid, and trisodium citrate). All glassware and laboratory utensils should also be precleaned.

- For the successful completion of the proposed experiments, it is highly recommended to organize a 1-hr long recitation prior to the first laboratory segment. The recitation material should introduce students to the fabrication, properties, and current

applications of colloidal NPs, and should describe the relevance of green fabrication methods in nanoscience. A brief overview of the experiment should be provided, and the potential risks and corresponding safety precautions should also be discussed in great detail. The inquiry based learning assignment should be carefully addressed to ensure the correct understanding of the designated tasks.

2) **Green fabrication of noble metal NPs: A guided, inquiry-based learning assignment**

A set of instructions should be provided to students in advance and should be discussed during recitation. Instructors should verify the feasibility of the selected green procedure for the fabrication of noble metal NPs and modify it together with the students if necessary. Instructors should be open for consultation at each step of the inquiry-based assignment.

a) Guided literature search for a green fabrication method of NPs:

Students should perform a literature search in order to identify a green reducing agent for the provided noble metal salts (*i.e.,* silver nitrate and tetrachloroauric acid). To guide the scientific search, a few illustrative examples of green synthetic approaches should be discussed in advance with the students and possible, key words for search should be suggested (*e.g.*, green reducing agent, green synthesis of silver nanoparticles/gold nanoparticles, and so on). Students having more research experience and knowledge in the nanofabrication areas should be encouraged to explore a novel green fabrication method.

b) Adaptation of the identified green fabrication method of NPs:

In consultation with the instructors, students should make the necessary changes to the identified green procedures so that the methods can be carried out in a test tube similar to the nongreen synthesis.

c) Write-up of the identified green fabrication method of NPs:

Next, students should write a brief, step-wise procedure for that particular green method and should cite the used literature reference.

Sample of a green fabrication procedure proposed by a student pre-laboratory

The green fabrication procedure of colloidal AuNPs and the corresponding UV-Vis absorption spectrum (Figure 3.S1) are reproduced below with student's permission.

Green synthesis of gold nanoparticles (AuNPs)

"Procedure: Briefly, an aqueous solution of tetrachloroauric acid was reduced with polyphenols and various phytochemicals within tea extract. The tea extract was prepared by magnetically stirring tea leaves for 15 min, filtering, and adding a small volume of the gold solution to a diluted portion of the filtrate. Stirring continued for 15 min, then the stir bar was removed and the process was allowed to complete within 30 min. A purple-red color change is indicative of a successful synthesis, which can be confirmed with a UV-Vis absorbance around 530-560 nm.

Steps involved in the extraction:

- *Weigh 200 mg of tea leaves into a flask with 12mL of distilled water*
- *Add a stir bar and mix at room temperature for 15 minutes*
- *Filter the extract with filter paper No. 1 and collect the filtrate*
- *Add 6mL of this filtrate (or 6mL of the dilution) into a flask*
- *Prepare a 0.1M solution of HauCl4*
- *Pipette 100µL and slowly dispense into the filtrate, sit for 5 minutes*
- *Note color change and allow stirring for another 15 min.*
- *Remove the stir bar and let the forming colloid sit for a half hour*

Reference: Sharma, R. K.; Gulati, S.; Mehta, S. "Preparation of Gold Nanoparticles Using Tea: A Green Chemistry Experiment" J. Chem. Educ., 2012, 89 (10), pp 1316–1318."

The student has slightly modified the original procedure to fit the experimental requirements and additionally made the following observations:

"*Different concentrations (1, 5, and 10%) of the stock tea solution can be used in the same procedure. As the concentration of tea leaves decreases,* λ_{max} *changes from 530 to 563 nm".*

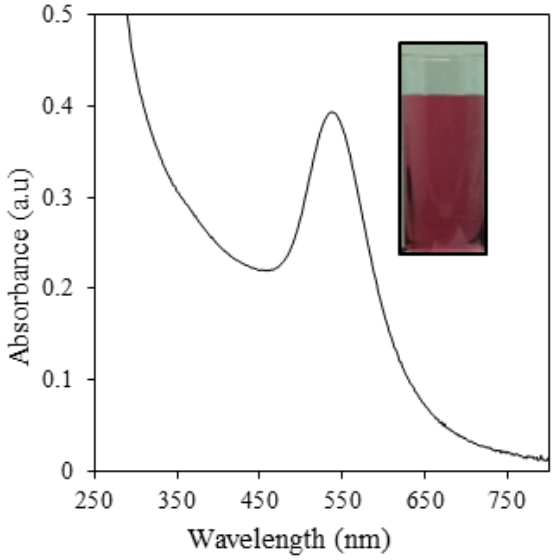

Figure 3.S1: UV-Vis absorption spectrum (λ_{max} at 537 nm) and visual image (wine red color) of green tea AuNPs.

Table 3.S1: Lesson plan and proposed time schedule for the two laboratory segments.

Laboratory components	**Time period[a]**
The first segment of the laboratory	3 hrs
➢ Recitation	30 hr
• Pretests using clicker-based technologies	10 min
• Introduction to proposed nanomaterial, the green chemistry principles and simple demos	25 min
• Introduction to the guided, inquiry-based learning assignment	25 min
➢ Laboratory experiments	2 hrs

• Posttests using clicker-based technologies
• Nongreen fabrication of NPs
  • Lee-Meisel AgNPs and
  • Turkevich AuNPs
• Introduction to UV-Vis absorption spectroscopy
• Collection of UV-Vis spectra for the nongreen NPs
	10 min
	
	60 min
	
	20 min
	
	30 min

*The second segment of the laboratory**	3 hrs
• Preparation of green reducing agent(s)	60 min
• Green fabrication of colloidal AgNPs or AuNPs	90 min
• Collection of UV-Vis spectra for the green NPs	30 min

[a]*The duration of the second laboratory segment may vary with the green synthesis procedure chosen by the student for the guided inquiry-based assignment.*

Turning Point clicker-based multiple choice questions

1) What is the size range of substances that can be classified as nanoparticles?

   a. 1-100 nm

   b. 100-1000 nm

   c. 0.001-1 nm

   d. None of these

2) If a mixture shows no settling but exhibits the Tyndall effect, it is classified as:

a. *Solution*

b. *Suspension*

c. *Colloid*

d. *None of these*

3) Chemists often use this type of approach to prepare colloidal nanoparticles:

a. *Top down*

b. *Bottom up*

c. *Neither of the above*

4) When engineers use lasers to make nanoparticles from bulk materials, the process is called as:

a. *Top down*

b. *Bottom up*

c. *Neither of the above*

5) What color do colloidal gold nanoparticles have in general?

a. *Gold*

b. *Silver*

c. *Light yellow*

d. *Red*

POGIL activity

An additional set of questions based on the Process Oriented Guided Inquiry Learning (**POGIL**) teaching approach was developed to be administered to our students during the recitation period. After becoming familiar with the surface plasmon resonance (SPR) concept of NPs and measuring it for the well-established Lee-Meisel silver nanoparticles (AgNPs) and Turkevich gold nanoparticles (AuNPs), students may be requested to explore new UV-Vis absorption data and to explain the observed spectral profiles. Student-student interactions should be encouraged in order to constructively stimulate the learning process of this essential SPR characterization process.

1. a) What are the similarities in the three absorption spectra shown below in Figure 3.S2A, 3.S2B, and 3.S2C?
   b) What do these similarities tell you about the type of nanoparticles that are produced?
2. a) How is the graph in Figure 3.S2C different from other two graphs in Figure 3.S2A and 3.S2B?
   b) What could be the reason behind the observed difference(s)?
   c) What does this difference(s) tell you about the type of nanoparticles that are produced?

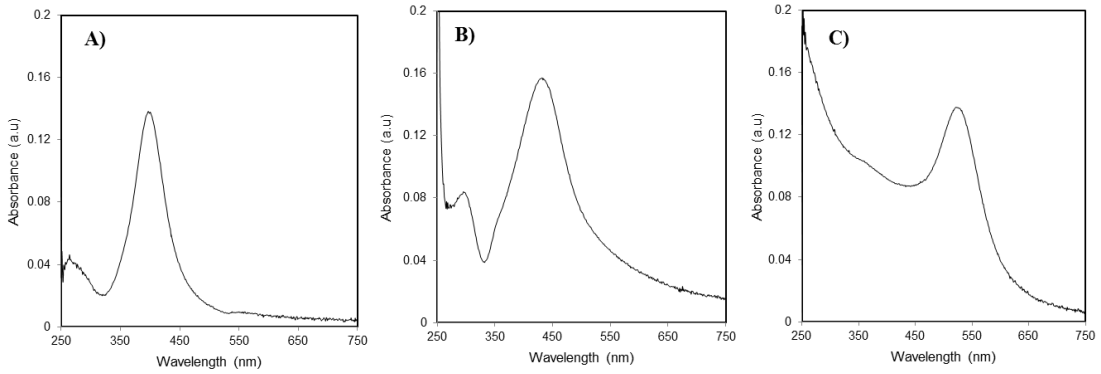

Figure 3.S2 UV-Vis absorption spectra of three types of colloidal NPs.

Evaluation of laboratory skills

Instructors may evaluate laboratory skills of students based on a three point system:

1 - Always performing the skill,

2 - Sometimes performing the skill, and

3 - Never performing the skill.

a) *Students were able to perform nongreen synthesis of NPs with the instructor's assistance.*
b) *Students were able to independently extract the green reducing agent.*
c) *Students were able to complete the green synthesis of NPs.*
d) *Students were able to correctly collect the UV-Vis absorption spectra on the diluted colloidal samples of NPs*

CHAPTER 4

CONCLUSIONS

The cross-disciplinary dynamics of nanoscientific research has offered overwhelming advantages that lead to an explosion of new products over the past five years. On the other hand, this tremendous prevalence of NPs is often concerning, as they are neither regulated nor always listed as an integral component of consumer products. Unlike pharmaceuticals, the risk assessments for AgNPs are not clearly defined. This could be due to the large variations in the physicochemical properties employed across the studies with limited knowledge on their biological fate. Although there is extensive nanotoxicological research with wide-variety of materials, most of the studies did not document the physicochemical properties of NPs. Moreover, there is no acceptable strategy to evaluate the ADMEs of NPs. In this context, it is essential to develop and validate standardized, reliable approaches to test the ADMEs of well-characterized NPs. Thus, the goal of this dissertation was to address these knowledge gaps in nanoscientific research and education.

Chapter 2 comprised of series of techniques such as: ICP-OES, CytoViva, Raman spectroscopy and CPE-TFF that were developed and tested to facilitate the assessment of ADMEs of two widely-employed AgNPs in two different cell lines. This new customized strategy paves way to analyze nanokinetics at the cellular level. In addition, this suite of analytical approaches will facilitate the testing of various nanomaterials and they can be further optimized for *in vivo* samples such as tissues (autopsies) or biological fluids. Chapter 3 described a newly developed inquiry-based teaching laboratory that utilized few of the above synthesis and characterization concepts, which was aimed at undergraduate and graduate students from multiple disciplines. The pedagogical approaches employed here introduced students to various concepts of nanochemistry

through previously reported macro-level examples. The in-class activities together with hands-on laboratory experience comprising different green and nongreen synthesis methods helped students understand how materials behave differently at nanoscale.

Due to the myriad possible forms and types of nanomaterials that currently exist, it is likely that humans and environment are at risk of their exposure. For instance, to design and optimize dose of any given nano-formulation or nano-carrier, it is critical to know: ***(A)*** *the actual concentration of NPs that reaches the target tissue or cell,* ***(D)*** *the preferential regions of NP accumulation,* ***(M)*** *the predominant chemical form,* ***(E)*** *the rate at which it NP gets cleared, half-life and elimination trends.* Therefore, to advance nanomedical research, reliable methods to evaluate the ADMEs of NPs while simultaneously accounting for their unique properties is a priority. The current study can provide a step-by-step guidance for studying i*n vitro* nanokinetics. Furthermore, the methods proposed here can be optimized to test biological fluid samples (*e.g.*, *blood*, gastric fluids, *etc.*,) or for analyzing samples during strategy-driven simulation studies (*e.g.*, blood-brain, placenta, *etc.*,), which can shed light on the *in vivo* nanokinetics.

As nanotechnology is already part of our routine life, besides understanding its toxicokinetics, providing basic knowledge about nanoscale behavior to younger generation is of paramount importance. To understand this extremely broad field that connects numerous conventional disciplines, future nano-education programs should incorporate inquiry-based learning laboratories at undergraduate and graduate levels.

FRESHWATER CRAYFISH: A POTENTIAL BENTHIC-ZONE INDICATOR OF NANOSILVER AND IONIC SILVER POLLUTION

Seth W. Brittle†, Sesha L. A. Paluri†, Daniel P. Foose†, Matthew T. Ruis‡, Matthew T. Amato‡, Nhi H. Lam†, Bryan Buttigieg‡, Zofia E. Gagnon‡, and Ioana E. Sizemore**

† Department of Chemistry, Wright State University, 3640 Colonel Glenn Hwy., Dayton, Ohio 45435, United States

‡ Department of Environmental Science, Marist College, 3399 North Road, Poughkeepsie, New York 12601, United States

SUMMARY OF INVOLVEMENT

Sesha L A Paluri is the second author of this manuscript. She helped with the harvest of crayfish tissues, and contributed to the digestions for ICP-OES measurements. She also contributed to the drafting and proof-reading of the manuscript

REFERENCES

1. Market report, National Science foundation. https://www.nsf.gov/news/news_summ.jsp?cntn_id=130586 (accessed, February 2017).
2. Outlook, Nanotechnology Market. http://www.prnewswire.com/news-releases/global-nanotechnology-market-outlook-2015-2020---industry-will-grow-to-reach-us-758-billion-507155671.html (accessed, February 2017).
3. Vance, M. E.; Kuiken, T.; Vejerano, E. P.; McGinnis, S. P.; Hochella, M. F., Jr.; Rejeski, D.; Hull, M. S., *Beilstein J. Nanotechnol.*, **2015**, *6*, 1769-1780
4. Barber, D. J.; Freestone, C. I., *Archaeometry*, **1990**, *32*, 1, 33-45.
5. Lee, P. C.; Meisel, D., *J. Phys. Chem.*, **1982**, *86*, 17, 3391-3395.
6. U.S. EPA. Nanomaterial Case Study: Nanoscale Silver in Disinfectant Spray (Final Report). U.S. Environmental Protection Agency, Washington, DC, EPA/600/R-10/081F, **2012**.
7. Reidy, B.; Haase, A.; Luch, A.; Dawson, K. A.; Lynch, I, *Materials*, **2013**. *6*, 6, 2295-2350.
8. Chaloupka, K.; Malam, Y.; Seifalian, A. M, *Trends in Biotechnol.* **2010,** *28*, 11, 580-588.
9. Lin, J.; Huang, Z.; Wu, H.; Zhou, W.; Jin, P.; Wei, P.; Zhang, Y.; Zheng, F.; Zhang, J.; Xu, J, *Autophagy*, **2014**, *10*, 2006.

10. Mori, Y.; Ono, T.; Miyahira, Y.; Nguyen, V. Q.; Matsui, T.; Ishihara, M, *Nanoscale Res. Lett.* **2013***, 8,* 1,1-6.

11. Evanoff, D. D.; Chumanov, G, *Chem.Phys.Chem.*, **2005**, *6,* 7, 1221-1231.

12. Saliminasab, M.; Bahrampour, A.; Zandi, M. H, *J. Optics*, **2012**, *14,* 12, 122301.

13. Andara, M.; Agarwal, A.; Scholvin, D.; Gerhardt, R. A.; Doraiswamy, A.; Jin, C., Lin, S, *Diamond and Relat. Mat.*, **2006**, *15*, 11, 1941-19483.

14. Seltenrich, N, *Environmental Health Perspect.*, **2013,** *12*, 7, A220-5.

15. Zhang, T.; Wang, L.; Chen, Q.; Chen, C, *Yonsei Med. J.*, **2014**, *55*, 2, 283-291.

16. Bedard, K.; Krause, K. H, *Physiol. Rev.*, **2007**, *87*, 1, 245-313.

17. Govender, R.; Phulukdaree, A.; Gengan, R.M.; Anand, K.; Chuturgoon, A.A, *J. Nanobiotechnol.* **2013,** *11*, 1, 5.

18. Ma, D. D; Yang, W. X, *Oncotarget*, **2016**, *7*, 26, 40882.

19. Arora, S.; Jain, J.; Rajwade, J. M.; Paknikar, K. M, *Toxicol. Lett*, **2008**, *179,* 2, 93-100.

20. Stoehr, L. C., Gonzalez, E., Stampfl, A., Casals, E., Duschl, A., Puntes, V., & Oostingh, G. J, *Part Fibre Toxicol.*, **2011**, *8,* 36, 3-15.

21. Oomen, A. G., Bos, P. M. J., Fernandes, T. F., Hund-Rinke, K., Boraschi, D., Byrne, H. J.; Landsiedel, R, *Nanotoxicol.*, **2014**, *8,* 3, 334–348.

22. Römer, I.; White, T. A.; Baalousha, M.; Chipman, K.; Viant, M. R.; Lead, J. R, *J. Chromat. A*, **2011**, *1218*, 27, 4226-4233

23. Park, J W.; Oh, J H.; Kim, W K.; Lee, S. K, *Environ. Contam. Toxicol.*, **2014**, *93*, 1, 53-59.

24. He, W.; Zhou, Y.; Wamer, W. G.; Boudreau, M. D.; Yin, J, *Biomaterials*, **2012** *33*, 30, 7547-7555.

25. Zolnik, B. S.; Sadrieh, N, *Adv. Drug Deliv. Rev.* **2009**, *61*, 422.

26. Savolainen, K.; Alenius, H.; Norppa, H.; Pylkkänen, L.; Tuomi, T.; Kasper, G, *Toxicology*, **2010**, *269*, 92.

27. Consumer Product Inventory, http://www.nanotechproject.org/cpi/about/analysis/, accessed: August, 2016.

28. Seltenrich, N, *Environ. Health Perspect.* **2013**, *121*, 220.

29. Ge, L.; Li, Q.; Wang, M.; Ouyang, J.; Li, X.; Xing, M. M, *Int. J. Nanomed.* **2014**, *9*, 2399.

30. Riehemann, K.; Schneider, S. W.; Luger, T. A.; Godin, B.; Ferrari, M.; Fuchs, H, *Angew. Chem.* **2009**, *121*, 886; *Angew. Chem., Int. Ed.* **2009**, *48*, 872.

31. Chaloupka, K.; Malam, Y.; Seifalian, A. M, *Trends. Biotechnol.* **2010**, *28*, 580.

32. Schluesener, J. K.; Schluesener, H. J, *Arch. Toxicol.* **2013**, *87*, 569.

33. Zhang, T.; Wang, L.; Chen, Q.; Chen, C, *Yonsei Med. J.* **2014**, *55*, 283.

34. Kawata, K.; Osawa, M.; Okabe, S, *Environ. Sci. Technol.* **2009**, *43*, 6046.

35. He, W.; Zhou, Y.; Wamer, W. G.; Boudreau, M. D.; Yin, J, *Biomaterials* **2012**, *33*, 7547.

36. Zolnik, B. S.; Sadrieh, N, *Adv. Drug Deliv. Rev.* **2009**, *61*, 422.

37. Savolainen, K.; Alenius, H.; Norppa, H.; Pylkkänen, L.; Tuomi, T.; Kasper, G, *Toxicology* **2010**, *269*, 92.

38. Ammerman, N. C.; Beier-Sexton, M.; Azad, A. F, *Curr. Protoc. Microbiol.* **2008**, A. 4E. 1.

39. Mori, Y.; Ono, T.; Miyahira, Y.; Nguyen, V. Q.; Matsui, T.; Ishihara, M, *Nanoscale Res. Lett.* **2013**, *8*, 1.

40. Khandelwal, N.; Kaur, G.; Kumar, N.; Tiwari, A, *Dig. J. Nanomater. Biostruct.* **2014**, *9*, *175*.

41. Lara, H. H.; Ayala-Nuñez, N. V.; Ixtepan-Turrent, L.; Rodriguez-Padilla, C, *J. Nanobiotechnol.* **2010**, *8*, 1.

42. Galdiero, S.; Falanga, A.; Vitiello, M.; Cantisani, M.; Marra, V.; Galdiero, M, *Molecules* **2011**, *16*, 8894.

43. Lu, L.; Sun, R.; Chen, R.; Hui, C.; Ho, C.; Luk, J. M.; Lau, G.; Che, C, *Antivir. Ther. (Lond)* **2008**, *13*, 253.

44. Orlowski, P.; Tomaszewska, E.; Gniadek, M.; Baska, P.; Nowakowska, J.; Sokolowska, J.; Nowak, Z.; Donten, M.; Celichowski, G.; Grobelny, J, *PloS one.* **2014**, *9*, e104113.

45. Asati A.; Santra S.; Kaittanis C.; Perez J. M, *ACS nano*. **2010,** *4*, 9, 5321-5331.

46. Reddy, A. R. N.; Reddy, Y. N.; Krishna, D. R.; Himabindu, V, *Toxicology*. **2010**, *272*, 1, 11-16.

47. Wang, F.; Gao, F.; Lan, M.; Yuan, H.; Huang, Y.; Liu, J, *Toxicol. In Vitro*, **2009**, *23*,5, 808-815.

48. Yu, S.; Chao, J.; Sun, J.; Yin, Y.; Liu, J.; Jiang, G, *Environ. Sci. Technol.* **2013**, *47*, 3268.

49. Jang, M.; Kim, W.; Lee, S.; Henry, T. B.; Park, J, *Environ. Sci. Technol.* **2014**, *48*, 11568.

50. Rezić, I, *Trends Anal. Chem.* **2011**, *30*, 1159.

51. Xu, H.; Shi, X.; Ma, H.; Lv, Y.; Zhang, L.; Mao, Z, *Appl. Surf. Sci.* **2011**, *257*, 6799.

52. Brittle, S. W.; Baker, J. D.; Dorney, K. M.; Dagher, J. M.; Ebrahimian, T.; Higgins, S. R.; Pavel Sizemore, I. E, *J. Chem. Educ.* **2015**, *92*, 1061.

53. EPA Method 6010C (SW-846): Inductively Coupled Plasma-Atomic Emission Spectrometry, Revision 3, *http://www.epa.gov/sites/production/files/2015-07/documents/epa-6010c.pdf*, accessed: September, 2016.

54. Peña, María Del Pilar Sosa; Gottipati, A.; Tahiliani, S.; Neu-Baker, N. M.; Frame, M. D.; Friedman, A. J.; Brenner, S. A, *Microsc. Res. Tech.* **2016,** *79*, 349.

55. Mortimer, M.; Gogos, A.; Bartolomé, N.; Kahru, A.; Bucheli, T. D.; Slaveykova, V. I, *Environ. Sci. Technol.* **2014**, *48*, 8760.

56. SoRelle, E. D.; Liba, O.; Campbell, J. L.; Dalal, R.; Zavaleta, C. L.; de la Zerda, A, *eLife* **2016**, *5*, e16352.

57. Klein, K.; Gigler, A. M.; Aschenbrenner, T.; Monetti, R.; Bunk, W.; Jamitzky, F.; Morfill, G.; Stark, R. W.; Schlegel, J, *Biophys. J.* **2012**, *102*, 360.

58. Matthäus, C.; Chernenko, T.; Newmark, J. A.; Warner, C. M.; Diem, M, *Biophys. J.* **2007**, *93*, 668.

59. Chao, J.; Liu, J.; Yu, S.; Feng, Y.; Tan, Z.; Liu, R.; Yin, Y, *Anal. Chem.* **2011**, *83*, 6875.

60. Yin, L.; Cheng, Y.; Espinasse, B.; Colman, B. P.; Auffan, M.; Wiesner, M.; Rose, J.; Liu, J.; Bernhardt, E. S, *Environ. Sci. Technol.* **2011**, *45*, 2360.

61. Dorney, K. M.; Baker, J. D.; Edwards, M. L.; Kanel, S. R.; O'Malley, M.; Pavel Sizemore, I. E, *J. Chem. Educ.* **2014**, *91*, 1044.

62. Trefry, J. C.; Monahan, J. L.; Weaver, K. M.; Meyerhoefer, A. J.; Markopolous, M. M.; Arnold, Z. S.; Wooley, D. P.; Pavel, I. E., *J. Am. Chem. Soc.* **2010**, *132*, 10970.

63. Anders, C. B.; Baker, J. D.; Stahler, A. C.; Williams, A. J.; Sisco, J. N.; Trefry, J. C.; Wooley, D. P.; Pavel Sizemore, I. E., *J. Vis. Exp.* **2012**, *68*, 4167.

64. Van der Zande, M.; Vandebriel, R. J.; Van Doren, E.; Kramer, E.; Herrera Rivera, Z.; Serrano-Rojero, C. S.; Gremmer, E. R.; Mast, J.; Peters, R. J.; Hollman, P. C, *ACS Nano* **2012**, *6*, 7427.

65. Minimum Information for Nanomaterial Characterization Initiative, The Parameters List, https://characterizationmatters.wordpress.com/parameters/, accessed: August, 2016.

66. Sun, L.; Song, Y.; Wang, L.; Guo, C.; Sun, Y.; Liu, Z.; Li, Z, *J. Phys. Chem. C* **2008**, *112*, 1415.

67. Creighton, J. A.; Blatchford, C. G.; Albrecht, M. G, *J. Chem. Soc., Faraday Trans.* **1979**, *75*, 790.

68. Spectrumlabs, Poresize chart, *http://www.spectrumlabs.com/filtration/PoreSize.html*, accessed: August, 2016.

69. Schafer, R. W, *IEEE Signal Process. Mag.* **2011**, *28*, 111.

70. Shargel, L.; Wu-Pong, S.; Yu, A. B, *Applied Biopharmaceutics & Pharmacokinetics*, McGraw-Hill, New York, **2007**,.pp. 159-181.

71. U.S. EPA. Nanomaterial Case Study: Nanoscale Silver in Disinfectant Spray (Final Report). U.S. Environmental Protection Agency, Washington, DC, EPA/600/R-10/081F, 2012.

72. Tak, Y. K.; Pal, S.; Naoghare, P. K.; Rangasamy, S.; Song, J. M, *Sci. Rep.* **2015**, *5*, 16908.

73. El Badawy, A. M.; Silva, R. G.; Morris, B.; Scheckel, K. G.; Suidan, M. T.; Tolaymat, T. M, *Environ. Sci. Technol.* **2010**, *45*, 283.

74. Park, Y, *Toxicol. Res.* **2014**, *30*, 169.

75. Pavel, I. E.; Alnajjar, K. S.; Monahan, J. L.; Stahler, A.; Hunter, N. E.; Weaver, K. M.; Baker, J. D.; Meyerhoefer, A. J.; Dolson, D. A, *J. Chem. Educ.* **2011**, *89*, 286.

76. Nanomedicine and Nano Device Pipeline Surges 68%, NanoBiotech News-NanoTechWire.com, http://www.nanotechwire.com/news.asp?nid=2743, accessed: August, 2016.

77. Powers, M. Nanomedicine, Device & Diagnostics Report, Nanomedicine and nano device pipeline surges 68%. *NanoBiotech News* **2006**, *68*, 1.

78. Sriram, M. I.; Kanth, S. B.; Kalishwaralal, K.; Gurunathan, S, *Int. J. Nanomed.* **2010**, *5*, 753.

79. Mollick, M. M. R.; Rana, D.; Dash, S. K.; Chattopadhyay, S.; Bhowmick, B.; Maity, D.; Mondal, D.; Pattanayak, S.; Roy, S.; Chakraborty, M, *Arabian J. Chem.* in press, http://dx.doi.org/10.1016/j.arabjc.2015.04.033.

80. Lin, J.; Huang, Z.; Wu, H.; Zhou, W.; Jin, P.; Wei, P.; Zhang, Y.; Zheng, F.; Zhang, J.; Xu, J, *Autophagy* **2014**, *10*, 2006.

81. U.S. Food and Drug Administration. Guidance for Industry: Safety of Nanomaterials in Cosmetic Products, *http://www.fda.gov/Cosmetics/GuidanceRegulation/GuidanceDocuments/ucm300886.htm*, accessed: August, 2015.

82. Schmid, S. L.; Carter, L. L, *J. Cell Biol.* **1990**, *111*, 2307.

83. Oh, N.; Park, J, *Int. J. Nanomed.* **2014**, *9*, 51.

84. Verma, A.; Stellacci, F, *Small* **2010**, *6*, 12.

85. Jurašin, D. D.; Ćurlin, M.; Capjak, I.; Crnković, T.; Lovrić, M.; Babič, M.; Horák, D.; Vrček, I. V.; Gajović, S, *Beilstein J. Nanotechnol.* **2016**, *7*, 246.

86. Shannahan, J. H.; Lai, X.; Ke, P. C.; Podila, R.; Brown, J. M.; Witzmann, F. A, *PLoS One* **2013**, *8*, e74001.

87. Sabuncu, A. C.; Grubbs, J.; Qian, S.; Abdel-Fattah, T. M.; Stacey, M. W.; Beskok, A, *Colloids Surf., B.* **2012**, *95*, 96.

88. Arora, S.; Jain, J.; Rajwade, J. M.; Paknikar, K. M, *Toxicol. Lett.* **2008**, *179*, 93.

89. Zhang, X.; Choi, Y.; Han, J. W.; Kim, E.; Park, J. H.; Gurunathan, S.; Kim, J, *Int. J. Nanomed.* **2015**, *10*, 1335.

90. Meyer, J. N.; Lord, C. A.; Yang, X. Y.; Turner, E. A.; Badireddy, A. R.; Marinakos, S. M.; Chilkoti, A.; Wiesner, M. R.; Auffan, M, *Aquat. Toxicol.* **2010**, *100*, 140.

91. Ito, S, *Paediatr. Child. Health.* **2011**, *16*, 535.

92. Hagens, W. I.; Oomen, A. G.; de Jong, W. H.; Cassee, F. R.; Sips, A. J, *Regul. Toxicol. Pharmacol.* **2007**, *49*, 217.

93. Jenkins, S. V.; Qu, H.; Mudalige, T.; Ingle, T. M.; Wang, R.; Wang, F.; Howard, P. C.; Chen, J.; Zhang, Y, *Biomaterials* **2015**, *51*, 226.

94. Ye, S.; Wu, Y.; Zhang, W.; Li, N.; Tang, B, *Chem. Commun.* **2014**, *50*, 9409.

95. Cho, H.; Lee, B.; Liu, G. L.; Agarwal, A.; Lee, L. P, *Lab on a Chip* **2009**, *9*, 3360.

96. Kneipp, K.; Wang, Y.; Kneipp, H.; Perelman, L. T.; Itzkan, I.; Dasari, R. R.; Feld, M. S., *Phys. Rev. Lett.* **1997**, *78*, 1667.

97. Berridge, M. V.; Herst, P. M.; Tan, A. S, *Biotechnol. Annu. Rev.* **2005**, *11*, 127.

98. Riss, T. L.; Moravec, R. A.; Niles, A. L.; Benink, H. A.; Worzella, T. J.; Minor, L. In *Cell Viability Assays;* Sittampalam, G. S., Coussens, N. P., Nelson, H., Arkin, M., Auld, D., Austin, C., Bejcek, B., Glicksman, M., Inglese, J., Iversen, P. W., Li, Z., McGee, J., McManus, O., Minor, L., Napper, A., Peltier, J. M., Riss, T., Trask OJ, J. and Weidner, J., Eds.; Assay Guidance Manual; Bethesda (MD), 2004.

99. Siemen, D.Ziemer, M, *IUBMB Life* **2013**, *65*, 255.

100. Newsholme, P.; Rebelato, E.; Abdulkader, F.; Krause, M.; Carpinelli, A.; Curi, R, *J. Endocrinol.* **2012**, *214*, 11.

101. Fang, R. H.; Hu, C. J.; Zhang, L, *Expert Opin. Biol. Ther.* **2012**, *12*, 385.

102. Sakhtianchi, R.; Minchin, R. F.; Lee, K.; Alkilany, A. M.; Serpooshan, V.; Mahmoudi, M, *Adv. Colloid Interface Sci.* **2013**, *201*, 18.

103. Teuscher, N, Calculation of Elimination rate constant, *http://www.certara.com/2015/02/02/calculating-the-elimination-rate-constant/*, accessed: August, 2016.

104. EPA Method 6010C (SW-846): Inductively Coupled Plasma-Atomic Emission Spectrometry, Revision 3, *http://www.epa.gov/sites/production/files/2015-07/documents/epa-6010c.pdf*, accessed: September, 2016.

105. Dorney, K. M, M.S. Thesis, Wright State University, Dayton, OH, 2014.

106. Sabella, S.; Carney, R. P.; Brunetti, V.; Malvindi, M. A.; Al-Juffali, N.; Vecchio, G.; Janes, S. M.; Bakr, O. M.; Cingolani, R.; Stellacci, F, *Nanoscale* **2014**, *6*, 7052.

107. Maiorano, G.; Sabella, S.; Sorce, B.; Brunetti, V.; Malvindi, M. A.; Cingolani, R.; Pompa, P. P, *ACS Nano* **2010**, *4*, 7481.

108. Wasmuth C.; Rüdel H.; Düring R. A.; Klawonn T, *Chemosphere* **2016**, *144*, 2018.

109. Miclăuş, T.; Beer, C.; Chevallier, J.; Scavenius, C.; Bochenkov, V.E.; Enghild, J. J.; Sutherland, D. S, *Nat. Commun.* **2016**, *7*.

110. Applications of Raman Spectroscopy to Biology: From Basic Studies to Disease Diagnosis [Online]; Ghomi, M., Ed.; IOS Press: Amsterdam, 2012; Vol. 5. ISSN 1875-0656.

111. Notingher, I, *Sensors* 2007, 7, 1343.

112. Procházka, M. Raman and surface-enhanced Raman scattering (SERS) Biosensing. Proc. SPIE 8774, Optical Sensors 2013, 877409, Prague, Czech Republic, May 3, 2013. doi:10.1117/12.2021555.

113. Huefner, A.; Kuan, W.; Müller, K. H.; Skepper, J. N.; Barker, R. A.; Mahajan, S, *ACS Nano* **2015**, *10*, 307.

114. Smith, R.; Wright, K.; Ashton, L, *The Analyst* **2016,** *141*, 3590.

115. National Nanotechnology Initiative. http://www.nano.gov (accessed September 29, **2013**).

116. Century Market Research. *Global Nanotechnology Industry Output Expected to Reach $.2.4 Trillion by 2015*; News room: Marketwire: New York, November **2011**. http://www.marketwired.com/press-release/global-nanotechnology-industry-output-expected-to-reach-24-trillion-by-2015-otcbb-apnt-1588327.htm (accessed January 11, **2014**).

117. Consumer Products Inventory: The Project of Emerging Nanotechnologies. http://www.nanotechproject.org/cpi/about/analysis/ (accessed May 30, **2014**).

118. Roco, M, *J. Nanopart. Res.* **2001**, *3*, 353– 360.

119. Sau, T. K.; Murphy, C. J, *J. Am. Chem. Soc.* **2004**, *126*, 8648– 8649.

120. Lee, P. C.; Meisel, D, *J. Phys. Chem.* **1982**, *86*, 3391– 3395.

121. Evanoff, D. D., Jr.; Chumanov, G, *Chem. Phys. Chem.* **2005**, *6*, 7, 1221– 1231.

122. Kimling, J.; Maier, M.; Okenve, B.; Kotaidis, V.; Ballot, H.; Plech, A, *J. Phys. Chem. B* **2006**, *110*, 32, 15700– 15707.

123. Jana, N. R.; Gearheart, L.; Murphy, C. J, *Chem. Mater.* **2001**, *13*, 7, 2313– 2322.

124. Sharma, R. K.; Gulati, S.; Mehta, S, *J. Chem. Educ.* **2012**, *89*, 1316– 1318.

125. Siavesh, I, *Green Chem.* **2011**, *13*, 2638–2650.

126. McFarland, A. D.; Haynes, C. L.; Mirkin, C. A.; Van Duyne, R. P.; Godwin, H. A, *J. Chem. Educ.* **2004**, *81*, 4, 544A– 544B.

127. Dungey, K. E.; Muller, D. P.; Gunter, T, *J. Chem. Educ.***2005**, *82*, 5, 769– 770.

128. Frank, A. J.; Cathcart, N.; Maly, K. E.; Kitaev, V, *J. Chem. Educ.* **2012**, *87*, 10, 1098– 1101.

129. Guedens, W. J.; Reynders, M.; Van den Rul, H.; Elen, K.; Hardy, A.; Van Bael, M. K, *J. Chem. Educ.* **2013**, *91*, 259– 263.

130. Metz, K. M.; Sanders, S. E.; Miller, A. K.; French, K. R , *J. Chem. Educ.* **2013**, 91, 264– 268.

131. Mulfinger, L.; Solomon, S.D.; Bahadory, M.; Jeyarajasingam, A. V.; Rutkowsky, S. A.; Boritz, C.Synthesis and Study of Silver Nanoparticles *J. Chem. Educ.* **2007**, *84*, 2, 322– 325.

132. Njagi, J.; Warner, J.; Andreescu, S.A, *J. Chem. Educ.* **2007**, *84*, 7, 1180– 1182.

133. Sereda, G.; Rajpara, V, J *Chem. Educ.* **2010**, 87 (9) 978– 980.

134. VanDorn, D.; Ravalli, M. T.; Small, M. M.; Hillery, B.; Andreescu, S, *J. Chem. Educ.* **2011**, *88*, 1119– 1122.

135. Fullan, M.; Langworthy, M. *Towards a New End: New Pedagogies for Deep Learning*; Collaborative Impact: Seattle, WA, **2013**.

136. Criswell, B. Framing *J. Chem. Educ.* **2011**, *89*, 199– 205.

137. Apedoe, X. S, *Sci. Educ.* **2008**, *92*, 4, 631– 663.

138. Bruck, L. B.; Towns, M. H, *J. Chem. Educ.* **2009**, *86*, 7 820– 822.

139. Turkevich, J.; Stevenson, P. C.; Hillier, J. A, *Discuss. Faraday Soc.* **1951**, *11*, 55– 75.

140. Nune, S.K.; Chanda, N.; Shukla, R.; Katti, K.; Kulkarni, R. R.; Thilakavathy, S.; Mekapothula, S.; Kannan, R.; Katti, K. V.; *J. Mater. Chem.* **2009**, *19*, 2912– 2920.

141. Nadagouda, M. N.; Varma, R. S, *Green Chem.* **2008**, *10*, 859– 862.

142. Sreelakshmi, C.; Datta, K. K. R.; Yadav, J. S.; Reddy, B. V, *J. Nanosci. Nanotechnol.* **2011**, 11, 6995– 7000.

143. Philip, D, *Spectrochim. Acta, Part A*, **2010**, *75*, 1078– 1081.

144. Zamiri, R.; Azmi, B.; Sadrolhosseini, A.; Ahangar, H.; Zaidan, A.; Mahdi, M, *Int. J. Nanomed.* **2011**, *6*, 71– 5.

145. (a) Bankar, A.; Joshi, B.; Kumar, A. R.; Zinjarde, S, *Colloids Surf., A* **2010**, *368*, 58– 63 (b) Bankar, A.; Joshi, B.; Kumar, A. R.; Zinjarde, S, *Colloids Surf., B* **2010**, *80*, 45– 50.

146. Olson, S.; Loucks-Horsley, S., Eds.; *National Academy Press*: Washington, DC, **2000**.

147. Hong, Y.; Huh, Y.; Yoon, D. S.; Yang, J, *J. Nanomater.* **2012**, *11*, 1– 13.

148. Ostiguy, C.; Roberge, B.; Woods, C.; Soucy, B, Engineered Nanoparticles: Current Knowledge About OHS Risks and Prevention Measures. Montreal, QC: *Institut de recherche Robert-Sauvé en santé et en sécurité du travail (IRSST),* July **2010.**

149. Bashaw, J.; Regulation of Nanoparticles: Trying to Keep Pace with a Scientific Revolution. **2009,** *6*, 4, 475-482.

150. Augustine, R.; Kalarikkal, N.; Thomas, S. A Facile and Rapid Method for the Black Pepper Leaf Mediated Green Synthesis of Silver Nanoparticles and the Antimicrobial Study. *Appl. Nanosci*. **2013**, 1-10.

151. Narayanan, K. B.; Sakthivel, N. Coriander Leaf Mediated Biosynthesis of Gold Nanoparticles. *Mater. Lett.* **2008**, *62*, 4588-4590.

152. Huang, H.; Yang, X. Synthesis of Chitosan-Stabilized Gold Nanoparticles in the Absence/Presence of Tripolyphosphate. Biomacromolecules, **2004**, *5*, 6, 2340-2346.